DESIGN AND CHARACTERIZATION OF MATERIALS AND PROCESSES FOR AREA SELECTIVE ATOMIC LAYER DEPOSITION

A Dissertation
Presented to
The Academic Faculty

By

Ashwini Kumar Sinha

In Partial Fulfillment
Of the Requirements for the Degree of
Doctor of Philosophy in Chemical Engineering

Georgia Institute of Technology
December 2006

DESIGN AND CHARACTERIZATION OF MATERIALS AND PROCESSES FOR AREA SELECTIVE ATOMIC LAYER DEPOSITION

Approved by:

Dr. Clifford L. Henderson
School of Chemical & Biomolecular Engineering
Georgia Institute of Technology

Dr. Dennis W. Hess
School of Chemical & Biomolecular Engineering
Georgia Institute of Technology

Dr. Martha A. Gallivan
School of Chemical & Biomolecular Engineering
Georgia Institute of Technology

Dr. Christopher J. Summers
School of Materials Science and Engineering
Georgia Institute of Technology

Dr. Laren M. Tolbert
School of Chemistry & Biochemistry
Georgia Institute of Technology

October 20, 2006

ACKNOWLEDGEMENTS

I would like to express my sincerest gratitude to my advisors Dr. Cliff Henderson and Dr. Dennis Hess for taking me as their student and extending continuous encouragement, support and guidance during this research. Their support has been instrumental in keeping me motivated during the moments of failure. I also want to thank Dr. Martha Gallivan, Dr. Chris Summers and Dr. Laren Tolbert for serving on my committee and providing valuable suggestions during this work. Many thanks are due to Applied Materials Inc. for providing financial support through their Graduate Fellowship award.

I want to thank every member, present and past, of Dr. Henderson's and Hess's research group for helping me with ideas and making life at graduate school a very enjoyable and memorable experience. In particular, many thanks to Cheng-Tsung Lee for performing e-beam patterning, Yueming Hua for his assistance in AFM, NMR and TGA studies and polymer synthesis, Mike Romeo and Guoan Wang for fabricating capacitors for electrical characterization, Shantanu Pathak for his assistance in performing oxygen plasma and Will Reed for providing resources and expertise in drilling holes through metal sheets during setup of QCM experiments. In addition, members from other research group have also extended enormous support during my research. I would like to express my thanks to Yeny Hudiono and Sanjoy Mukherjee from Nair's research group for their help in AFM and x-ray reflectivity experiments respectively, Jason Hicks/Rebecca Shiels/Mike Mckittrick/Joe Nguyen from Jones's research group for their assistance in using glove box and Preeti Chandra from Koros research group for valuable discussions with her on sorption experiments. I cannot forget

mentioning Ingu Song and Dr. Qian Luo for assisting me in maintaining the XPS system and Dr. Galit Levitin who has served as a mentor as well as colleague during my graduate study. I am highly grateful to Jeff Andrew and Bradley Parker from ChBE machine shop for their help during fabrication of the experimental apparatus. This work would not have been complete without their help.

I want to thank my friends: Suchitra Konduri, Niket Kaisare, Gracy Wingkono, Krishna Bharath, Venkatesh Krishnan, Rajat Dua, Sourabh Ravindran, Niranjan Balwalli Shabbir Husain, Neil Mukherjee and Murali Padala for providing me a great company during my stay in Atlanta. My special thanks to Manish Gupta for his tremendous help during first two years here and Preeti Chandra for being my greatest friend. Finally, I want to thank my family. The most important support has come from my parents, who have always stood beside me in difficult times. I am also thankful to my grandparents for their blessings and my sisters (Didiya and Shishi) for their constant encouragement. I have received moral support and constant encouragement from every member of my family; they have always had great faith in me and have supported me during every step of my life.

TABLE OF CONTENTS

ACKNOWLEDGEMENTS iii

LIST OF TABLES ix

LIST OF FIGURES x

SUMMARY xiv

CHAPTER 1: INTRODUCTION AND BACKGROUND 1

1.1 INTRODUCTION TO ATOMIC LAYER DEPOSITION (ALD) 1

1.1.1 HISTORY OF ALD 1

1.1.2 BASIC PRINCIPLES OF ALD 4

1.2 TRADITIONAL MATERIAL PATTERNING: BASIC PROCESS SCHEME 9

1.3 DIRECT MATERIAL PATTERNING 14

1.3.1 AREA SELECTIVE ATOMIC LAYER DEPOSITION TECHNIQUE (ASALDT) 15

1.4 ORGANIZATION OF THESIS 20

1.5 REFERENCES 22

CHAPTER 2: DESIGN OF ATOMIC LAYER DEPOSITION REACTOR 26

2.1 ATOMIC LAYER DEPOSITION REACTOR 26

2.1.1 REACTION CHAMBER 27

2.1.2 SUBSTRATE HOLDER AND SUBSTRATE TEMPERATURE CONTROL SYSTEM 30

2.1.3 PRECURSOR DELIVERY SYSTEM AND PRECURSOR PULSING MECHANISM 32

2.1.4 EXHAUST SYSTEM 34

2.2 TIO_2 ALD USING $TICL_4$ AND H_2O 35

2.2.1 ALD PROCEDURE 35

2.2.2 FILM CHARACTERIZATION 36

2.2.3 VERIFICATION OF ALD GROWTH MODE 42

2.3 CONCLUSIONS 45

2.4 REFERENCES 46

CHAPTER 3: SELECTIVE ALD USING SELF ASSEMBLED MONOLAYER AS MASKING LAYER 47

3.1 INTRODUCTION 47

3.2 SELF ASSEMBLED MONOLAYERS 48

3.3 MATERIAL SELECTION 50

3.4 SILANIZATION PROCEDURE 52

3.5 CHARACTERIZATION OF SAMS 53

3.6 ALD STUDIES ON SAM SURFACES 55

3.6.1 EFFECT OF ANCHORING GROUP 55

3.6.2 EFFECT OF TAIL GROUP 61

3.7 CONCLUSIONS 62

3.8 REFERENCES 63

CHAPTER 4: AREA SELECTIVE ATOMIC LAYER DEPOSITION: USE OF POLYMER FILM BASED MASKING LAYERS 66

4.1 INTRODUCTION 66

4.2 MATERIALS AND METHODS 69

4.2.1 PREPARATION OF POLYMER FILM 69

4.2.2 FILM THICKNESS MEASUREMENT 70

4.2.3 X-RAY PHOTOELECTRON SPECTROSCOPY (XPS) FOR FILM COMPOSITION 71

4.3 ALD GROWTH STUDIES ON POLYMER FILMS 72

4.3.1 CHEMICAL FUNCTIONALITY AND REACTIVITY OF THE POLYMER 72

4.3.2 EFFECT OF REMNANT WATER IN THE POLYMER FILM 75

4.3.3 THICKNESS OF THE MASKING LAYER 77

4.4 DEPOSITION OF PATTERNED FILM 81

4.5 CONCLUSIONS.. 84

4.6 REFERENCES 85

CHAPTER 5: AREA SELECTIVE ATOMIC LAYER DEPOSITION OF TITANIUM DIOXIDE: EFFECT OF PRECURSOR CHEMISTRY 86

5.1 INTRODUCTION 86

5.2 EXPERIMENTAL APPARATUS & PROCEDURE...................................... 87

5.3 DEPOSITION ON SILICON SUSBTRATE 88

5.4 ALD GROWTH STUDIES ON POLYMER FILMS...................................... 91

5.5 CONCLUSIONS... 103

5.6 REFERENCES 105

CHAPTER 6: A NOVEL TOP SURFACE IMAGING METHOD USING AREA SELECTIVE ATOMIC LAYER DEPOSITION ON CHEMICALLY AMPLIFIED POLYMER PHOTORESIST FILMS 107

6.1 INTRODUCTION 107

6.2 EXPERIMENTAL PROCEDURE AND RESULTS 113

6.3 FUNDAMENTAL BEHAVIOR OF ASALD-TSI PROCESS 119

6.4 CONCLUSIONS... 126

6.5 REFERENCES 126

CHAPTER 7: TRANSPORT BEHAVIOR OF ALD-PRECURSORS THROUGH POLYMER MASKING LAYERS ... 129

7.1 INTRODUCTION ... 129

7.2 BACKGROUND ... 130

7.2.1 FUNDAMENTALS OF MASS TRANSPORT ... 130

7.2.2 QUARTZ CRYSTAL MICROBALANCE ... 132

7.3 EXPERIMENTAL ... 135

7.3.1 EXPERIMENTAL APPARATUS ... 135

7.3.2 MATERIALS AND SAMPLE PREPARATION ... 137

7.3.3 FILM THICKNESS MEASUREMENTS ... 138

7.3.4 SORPTION/DESORPTION MEASUREMENTS ... 138

7.4 WATER SORPTION STUDIES ... 140

7.5 TITANIUM ISOPROPOXIDE AND TITANIUM TETRACHLORIDE SORPTION STUDIES ... 144

7.6 CONCLUSIONS ... 152

7.7 REFERENCES ... 153

CHAPTER 8: SUMMARY AND RECOMMENDATIONS FOR FUTURE WORK. 155

8.1 SUMMARY ... 155

8.2 RECOMMENDATIONS FOR FUTURE WORK ... 160

8.3 REFERENCES ... 163

LIST OF TABLES

Table 1-1: Characteristic features of ALD with resulting implications for the process and practical advantages 8

Table 1-2: Area selective ALD: Summary of previous studies 18

Table 7-1: Estimated heat of sorption of water in PHOST, HFA-PNB and PMMA 142

Table 7-2: Estimated solubility of water in PHOST, HFA-PNB and PMMA under different conditions 143

LIST OF FIGURES

Figure 1-1: (a) Cross-sectional TEM image of a MOSFET showing different possible application areas for ALD. (b) FIB cross-section through a 6-layer Cu/low-k dielectric interconnect structure where metal nitride barrier layers and seed layers for Cu electroplating are deposited via ALD.[10] 4

Figure 1-2: ALD processes for a two precursor system 6

Figure 1-3: Traditional material patterning process........ 9

Figure 1-4: (a) Schematic representation of an area selective ALD (ASALD), (b) Resulting structure after the ASALD process if starting substrate does not allow ALD nucleation........ 17

Figure 2-1: Schematic of the ALD reactor system 27

Figure 2-2: Images of samples obtained from initial reactor design 29

Figure 2-3: Detailed schematic illustrating the substrate holder 32

Figure 2-4: Samples obtained after ALD using the reactor configuration (a) without a metering valve (cycle sequence: 2.5s-10s-2.5s-10s), (b) with a metering valve (cycle sequence: 2.5s-10s-2.5s-10s), (c) with a metering valve (cycle sequence: 2.5s-17s-2.5s-17s)........ 34

Figure 2-5: XPS spectra of a representative TiO_2 film deposited using $TiCl_4$-H_2O ALD 38

Figure 2-6: AFM image of a scan on 14 nm thick film deposited using $TiCl_4$-H_2O ALD39

Figure 2-7: Parallel plate capacitor structure used for electrical characterization........ 40

Figure 2-8: (a) I-V characteristic of the parallel plate capacitors (with different electrode size) with ALD titania as the dielectric layer (b) Current (area normalized) versus voltage characteristic 41

Figure 2-9: C-V plots of the parallel plate capacitors (with different electrode size) made with ALD titania as dielectric layer. Measured capacitance of 50 μm square electrode is plotted on secondary Y-axis for clearer presentation of data. 42

Figure 2-10: Thickness grown per ALD cycle versus exposure time for one of the precursors. The legend format refers to the time duration of each step in the ALD cycle. For example, “X-20-2.5-20” refers to an ALD sequence of (1) X seconds exposure of $TiCl_4$, (2) 20 seconds N_2 purge, (3) 2.5 seconds exposure to water, and (4) 20 seconds N_2 purge. The two different data sets are for varying the (□) water exposure time and the (◊) $TiCl_4$ exposure time. 44

Figure 2-11: Thickness of the TiO_2 film as a function of number of ALD cycles. The linear growth with number of cycles is indicative of an ALD process............................ 45

Figure 3-1: Different formation mechanism and structure of OTS SAMs on SiO_2 substrate. a) Sagiv and Maoz; b) Ansgt and Simmons; c) Silberzan et al. 50

Figure 3-2: Ti atomic% on various SAM surfaces after 100 ALD cycles........................ 56

Figure 3-3: Ti2p peak intensity from scans on a bare Si substrate and an OTS-SAM coated substrate after different numbers of ALD cycles. 57

Figure 3-4: AFM images of OTS-SAM surfaces (a) before annealing (b) after annealing. 60

Figure 3-5: AFM image of a F-silane SAM surface... 62

Figure 4-1: Schematic illustration of polymer masking based ASALDT......................... 68

Figure 4-2: Ti atomic % on different polymers after 100 cycles, the pulse sequence is 2s-25s-1s-60s 74

Figure 4-3: Ti atomic % on different polymers at different purge time after water pulse and for $TiCl_4$ only case; pulse sequence is, diagonal stripes: -2s-25s-1s-60s-, grey: -2s-25s-1s-120s-, black: -2s-25s-.. 77

Figure 4-4: XPS spectra showing Ti2p peak on the substrate for different initial thickness of PMMA film. The scans are taken after the PMMA film is removed from the Si wafer. a: 32 nm, b: 56 nm, c: 103 nm, d: 180 nm, e: 420 nm. The spectra have been relatively shifted along the Y axis for clearer representation. 81

Figure 4-5: XPS scan showing Ti2p peak in different region after stripping the PMMA film. Open area: regions which were not covered with polymer film. Masked area: regions which were initially covered with the polymer film 83

Figure 4-6: Optical micrographs of different size TiO_2 patterns fabricated via area selective ALD. 83

Figure 5-1: Thickness grown per ALD cycle versus exposure time for one of the ALD precursors. The legend format refers to the time duration of each step in the ALD cycle. For example, “X-25-2.0-30” refers to an ALD sequence of (1) X seconds exposure of $Ti(OCH(CH_3)_2)_4$, (2) 25 seconds N_2 purge, (3) 2.0 seconds exposure to water, and (4) 30 seconds N_2 purge. The two different data sets are represent variations in the (□)$Ti(OCH(CH_3)_2)_4$ exposure time and the (◊) water exposure time. 89

Figure 5-2: Thickness of the TiO_2 film as a function of number of ALD cycles. The linear growth with number of cycles is indicative of an ALD process............................ 90

Figure 5-3: C1s and Ti2p spectra as obtained from XPS scans on PMMA film post 400 ALD cycles for $TiCl_4$ process 94

Figure 5-4: C1s and Ti2p spectra as obtained from XPS scans on a PMMA film after 500 ALD cycles for the $Ti(OCH(CH_3)_2)_4$ process 94

Figure 5-5: Comparison of XPS spectra showing the Ti2p peak on a silicon substrate surface after 500 ALD cycles using the TiIP-H2O precursor system for surface areas that were covered by a 100 nm PMMA film, and for surface areas that were open directly to the ALD atmosphere. Deposition of titania occurred on the open surface while no visible deposition of Ti or titania occurred under the PMMA masked areas. Optical micrographs displaying different size titania patterns deposited using TiIP-H_2O/PMMA ASALDT are also shown. 96

Figure 5-6: Comparison of Ti at. % on PHOST and HFA-PNB; (a) After 100 ALD cycles, cycle sequence is $TiCl_4$-H_2O: 2s-25s-1s-60s, TiIP-H_2O: 2s-25s-1.5s-60s; (b) After 150 cycles of $TiCl_4$ (-2s-25s-) and TiIP (-2s-25s-) 99

Figure 6-1: Schematic of the new top surface imaging approach which utilizes area selective atomic layer deposition in conjunction with a radiation sensitive reactive polymer film to achieve direct patterned deposition of an etch barrier film. 113

Figure 6-2: Representative FTIR spectra of the PtBMA polymer used as the reactive imaging film in this work both before exposure and after exposure and post-exposure bake (PEB). 115

Figure 6-3: XPS spectra comparing the surface composition of the unexposed and exposed regions of the PtBMA polymer after exposure, PEB, and ALD. (A) C1s spectra and (B) Ti2P spectra. 117

Figure 6-4: Cross-section SEM image showing conformal TiO_2 layer grown on PtBMA film after UV exposure and PEB baking. 117

Figure 6-5: Optical micrographs showing different size and shape patterns obtained after completion of the four step process illustrated in Figure 6-1. 118

Figure 6-6: Silylation contrast plot for tBOC-PHOST [4] 119

Figure 6-7: ALD deposition contrast for an ASALD-TSI process (Δ – 50 cycles, ◊ - 100 cycles, □ – 150 cycles, ○ – 250 cycles, ▲ – 250 cycles (DBU loaded)) 121

Figure 6-8: Reaction scheme for chemical derivatization of carboxylic group using TFE[20] 122

Figure 6-9: Semi-quantitative estimation of active sites: F/O at. % ratio obtained from XPS of samples exposed to different exposure doses and chemically derivatized 123

Figure 7-1: Schematic of the 1-D geometry used in this study 131

Figure 7-2: Schematic of the QCM apparatus 136

Figure 7-3: Van't Hoff plots for water sorption in PHOST (7-3a), PMMA (7-3b) and HFA-PNB(7-3c) films 141

Figure 7-4: Sorption kinetics for titanium isopropoxide in PMMA at 160 ^{o}C. P = 3.8 Torr, film thickness = 805 nm.. 145

Figure 7-5: Van't Hoff plot for titanium isopropoxide sorption in PMMA 146

Figure 7-6: Diffusion coefficient of titanium isopropoxide in PMMA at different temperatures.. 146

Figure 7-7: Sorption kinetics of $TiCl_4$ in PMMA at 160 ^{o}C. P = 1.4 Torr, Film thickness: 748 nm 148

Figure 7-8: Estimation of diffusion coefficient of $TiCl_4$ in PMMA at 160 ^{o}C using the initial portion of the sorption curve 148

Figure 8-1: ALD growth of film on two different surfaces 162

SUMMARY

Atomic layer deposition (ALD) is of much interest for the deposition of high quality ultra-thin films. In ALD, film growth depends critically on the chemistry of the surface upon which deposition occurs. As a result, it should be possible to chemically tailor a surface to achieve area selective deposition. Achievement of area selective ALD (ASALD) requires that designated areas of the surface be "protected" to prevent the ALD reactions from occurring in those areas so that the ALD film nucleates and grows only on the "unprotected" regions. One obvious advantage of such an area selective, additive deposition process is the ability to directly grow patterns, thus eliminating the need for etching and associated cleaning steps. Elimination of these steps can greatly simplify the overall deposition and patterning process, reduce unintended (plasma) damage to substrates and devices, and aid in the integration and patterning of new materials that are difficult to etch.

The critical challenge in achieving ASALD is the development of materials and process sequences that modify selected regions of a film/substrate to prevent ALD reactions and thus prevent film growth. This work focused on designing materials and processes and developing methodologies to perform ASALD. TiO_2 was been chosen as a model system and the ALD precursors included $TiCl_4$/$Ti[OCH(CH_3)_2]_4$ (TiIP) and DI water. First investigation of masking approach involved the use of self assembled monolayers (SAMs) of alkyl or fluorinated-alkyl silanes to block the active nucleation sites on the substrate and thus prevent ALD growth. The results indicated that it is extremely challenging to obtain a pinhole free SAM layer and hence its successful implementation is difficult. Polymer films can be easily spin coated to produce defect

free film and can offer better alternative to SAM based masking approach. Thus, we introduced the use of polymer thin films as alternate masking scheme for ASALD. A number of factors that must be considered in designing a successful ASALD process based on polymer films were identified. These include: reactivity of polymer with ALD precursor, diffusion of ALD precursors through polymer mask and remnant precursor content in the polymer film during ALD cycling. Effect of all these parameters have been investigated in some detail. It was encouraging to observe that poly(methylmethacrylate) PMMA demonstrated low reactivity towards $TiCl_4$ and direct pattern deposition on lithographically defined PMMA demonstrated as a proof of concept for the polymer based masking approach for selective ALD. However, several limitations of this ASALD process were identified which were due to a combination of the intrinsic reactivity of PMMA with $TiCl_4$ and the diffusion of $TiCl_4$ through the PMMA film. These issues were addressed by using TiIP as an alternate metal precursor.

A novel method for performing top surface imaging (TSI) using ASALD on selectively exposed polymeric photoresist film was developed. In this method, exposure of the polymer thin film created reactive sites on the film surface in the exposed areas that subsequently serve as nucleation and growth sites for deposition of TiO_2 features using ASALD process. Subsequent oxygen plasma exposure yielded effective pattern transfer into the polymer film. Specifically, it was shown that titanium isopropoxide and water can be used as ALD precursors in conjunction with a chemically amplified photoresist film, formulated using a protected polymer (poly-tertbutylmethacrylate) and a photoacid generator (triphenylsulfonium tris(perfluoromethanesulfonyl) methide), to successfully perform such an ASALD-TSI process.

CHAPTER 1

INTRODUCTION AND BACKGROUND

1.1 INTRODUCTION TO ATOMIC LAYER DEPOSITION (ALD)

1.1.1 HISTORY OF ALD

The actual date of birth of ALD is somewhat controversial: depending upon the source, the credit for its development has been linked to different groups. According to the more commonly acknowledged origin, ALD was developed and introduced with a name of atomic layer epitaxy in the late 1970s by Suntola and coworkers in Finland[1]. The less commonly acknowledged origin of ALD dates back to the 1960s, when work conducted by Soviet researcher Aleskoviskii was presented at a conference[2]. The Soviet group described the $TiCl_4$-H_2O process to grow TiO_2 and $GeCl_4$-H_2O process to grow GeO_2 using a process they reported as "molecular layering". In fact, already in the 1960s a series of articles on "molecular layering reactions" was published by Aleskoviskii and co-workers. Unfortunately, I do not have access to the original paper (all publications in Russian journals) and am thus not aware of the particular details of their work. I have included a reference to their work in order to apprise the reader of the correct history of the development of ALD; in addition, mention should be made of a review[3] published recently by Puurunen where a complete list of references to the Soviet work and further details regarding this historical mistake are discussed.

However, the motivation behind the development of ALD by the Finnish group was a desire to make thin film electroluminescent (TFEL) flat panel displays, where high breakdown voltage (~2-3 megavolts/cm) dielectrics are required[4, 5]. ALD was successful in meeting the requirements of high dielectric strength, low pinhole density and uniformity over large-area substrates, and has been employed in TFEL production since the 1980s. Soon after the successful introduction of ALD, its application to epitaxial growth of compound semiconductors was demonstrated by several groups[6-8]. Since then semiconductors, especially III-V compounds, have been the most extensively investigated materials using ALD. Despite reports of a few outstanding results achieved with ALD of III-V compounds, the overall success has been limited, with little or no commercial application because of several processing challenges[9, 10]. The challenges mostly include (a) preferential aggregation of Ga atoms to previously formed Ga islands than adhesion to As surface, (b) high carbon contamination during the use of metal-organic precursors of group III, and (c) very narrow operating temperature differences between desirable surface reaction and undesirable precursor decomposition for most group III precursors. Halide precursors such as GaCl could be a potential solution to above challenges; however, incorporation of Cl still appeared to limit successful application[5, 9]. These issues have been discussed in greater detail in references 5, 9 and 10.

A renewed interest in ALD arose in the mid 1990s in the area of silicon-based microelectronic devices and integrated circuits. This interest was a direct consequence of the continuous shrinkage of device dimensions and increasing aspect ratio. The miniaturization of device dimensions has led to a reduction in the thickness of a variety

of films present on devices as well as the need to integrate new materials into semiconductor devices. For example, the gate dielectric, which is a key component in a CMOS transistor must be thinned to 1.2 nm at the 65 nm technology node in order to continue to use SiO_2 as the gate dielectric[11]. The problem of electron tunneling demanded the introduction of high dielectric constant (k) materials such as HfO_2 and ZrO_2, so that thicker dielectric layers, and thus lower leakage currents could be achieved. Nevertheless, the required thickness of the dielectric layer still remained on the order of ~5-7 nm. In addition, film quality requirements including defect density, surface smoothness and conformality have become increasingly stringent[12]. Achievement of these dielectric film requirements with excellent thickness control was easier to obtain with SiO_2 since it could be grown easily on a Si substrate via thermal oxidation. However, introduction of newer (high k) materials demanded alternative deposition techniques. Conventional film deposition techniques such as chemical vapor deposition (CVD) or physical vapor deposition (PVD) failed to meet the requirements of film quality for such low thickness regime. Furthermore, the advent of copper as an interconnect material required the integration of very thin, conformal and pin-hole free diffusion barrier layers (usually metal nitrides) to avoid diffusion of copper through interlevel dielectrics. These trends in microelectronic devices caused ALD to become essentially the only appropriate film deposition technique for a variety of films used in semiconductor device fabrication. At present, ALD is widely employed for gate dielectric deposition, diffusion barrier layers, high-k DRAM capacitors and seed layers for copper electrodeposition and tungsten-CVD. Figure 1-1a and 1-1b illustrate the above mentioned applications of ALD in current microelectronic devices.

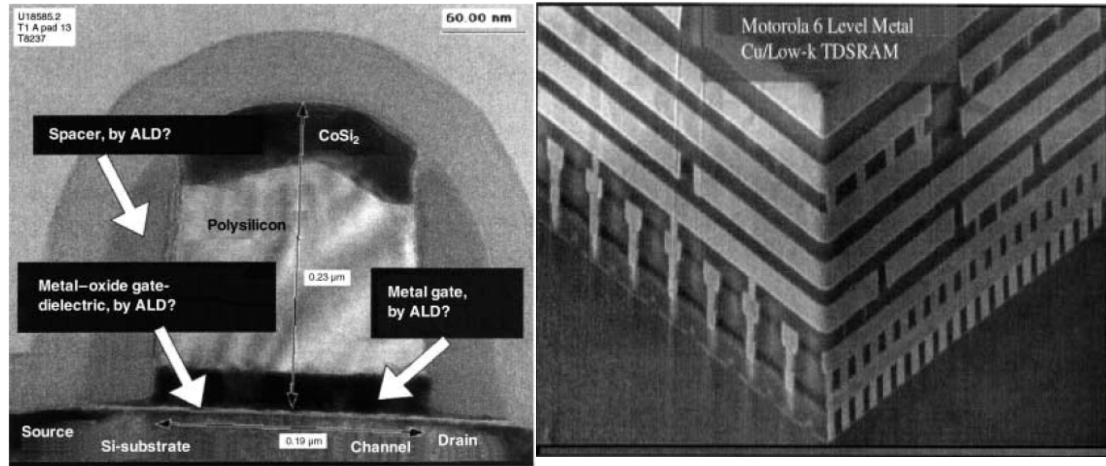

Figure 1-1: (a) Cross-sectional TEM image of a MOSFET showing different possible application areas for ALD. (b) FIB cross-section through a 6-layer Cu/low-k dielectric interconnect structure where metal nitride barrier layers and seed layers for Cu electroplating are deposited via ALD.[10]

1.1.2 BASIC PRINCIPLES OF ALD

Atomic layer deposition (ALD) is a chemical vapor deposition (CVD) method for thin films based on alternative saturative surface reactions; as such, the technique can be regarded as a special modification of CVD. It consists of the introduction of two or more precursors in an alternating manner spaced by a purge step. Figure 1-2 presents the sequence scheme for a simple two precursor system. Titanium dioxide (TiO_2) deposition using $TiCl_4$ and H_2O has been chosen because this is one of the precursor combinations used in the studies described in this thesis. The process consists of four major steps (1) precursor A ($TiCl_4$) exposure; (2) purging of reaction product (HCl) and extra reactant; (3) precursor B (H_2O) exposure and (4) purging of reaction product and extra reactant. To further illustrate the process, during the first step of a cycle, $TiCl_4$ vapor is exposed to a

surface terminated with surface hydroxyl groups. Exchange reactions of Cl ligands with these surface sites produce Cl-Ti-O bonds on the surface. HCl is produced as a byproduct which is purged away along with any extra reactant leaving a Cl terminated surface at the end of step 2. The second precursor, H_2O, is then introduced which goes through similar exchange reaction and byproduct (HCl) and extra water is purged away during step 4. At the conclusion of step 4 a TiO_2 monolayer (or a partial monolayer) with a hydroxyl terminated surface very similar to the original surface at the start of step 1 is formed; this surface can undergo a similar sequence of steps to form another layer on top of the existing layer. Thus, the sequence consisting of 2 precursor pulses and 2 purge steps is termed one "cycle". The cycle is repeated in a sequential manner allowing layer by layer film growth. In addition, it is not necessary for the precursors to chemisorb on the surface via exchange reaction only. The precursor can also associate/dissociate on the surface, thereby causing attachment as shown in scheme 2 of figure 1-2 where a $TiCl_4$ adsorption mechanism for such a scenario is described. In fact, this is usually the dominant reaction pathway at higher temperature where the surface is less hydrated so that fewer OH moieties are available[13-15].

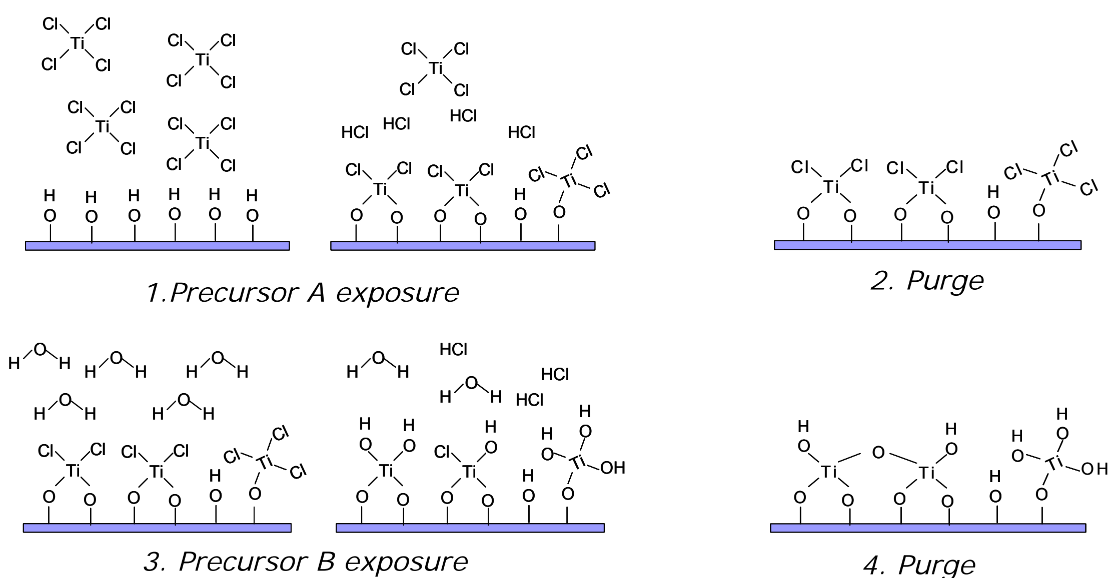

Scheme 1

Scheme 2

Figure 1-2: ALD processes for a two precursor system

The most important requirement during precursor exposure is to ensure sufficient flux of reactant so that deposition is limited by adsorption/reaction of precursor at surface sites instead of being limited by mass transfer of precursor molecules to surface sites. However, the purge sequence must ensure removal of products and reactant to eliminate the possibility of gas phase reactions. In an ideal ALD process, the precursor cannot

adsorb on an already existing precursor layer. Thus, during a precursor exposure step, after either all active sites available for exchange reaction/association/dissociation have been reacted or are inaccessible (due to steric hindrance), no further addition of mass on the substrate surface can occur even if the precursor exposure duration is extended. In other words, the adsorption/reaction step shows a self-saturative or self-limiting nature. This self saturative nature of the precursor exposure step represents the primary advantage of an ALD process- material growth is dependent only on the number of cycles, thereby ensuring atomic level control over the film thickness deposited. However, it must be recognized that during the initial cycles when the substrate surface is being covered by film material, the surface density of the chemisorption sites and accordingly the growth rate may change. Also, since the growth is not limited by mass transport of the precursor to any specific location (provided that sufficient flux exists to ensure a self saturated chemisorbed layer), the deposition rate is constant over the entire surface. This fact leads to high surface smoothness, step coverage and improved conformality of surface topology. The self limiting growth mechanism also ensures good reproducibility and relatively predictable scale-up.

A common misconception is that ALD growth always proceeds in a full monolayer-by-monolayer manner; this is generally not the case as only a fraction of monolayer (15-40 %) is typically deposited in each cycle. Reasons for the partial monolayer growth include the limited number of surface sites and the steric hindrance between bulky ligands. In certain instances, reaction products can re-adsorb onto the surface, thereby indirectly reducing the available surface sites. This scenario can occur during TiO_2 deposition using $TiCl_4$ and H_2O where HCl re-adsorbs on the titania layer at relatively

higher temperatures[15] . Table 1-1 lists some of the major characteristics of ALD, the resulting implications for film deposition and the practical advantages that can be realized with this film deposition method.

Table 1-1: Characteristic features of ALD with resulting implications for the process and practical advantages

Characteristic feature of ALD	Inherent implication on film deposition	Practical advantage
Alternate dosing of precursors	No gas phase reaction	Favors precursors that display high reactivity
	Sufficient time for completion of reaction step	Low defect and high quality material obtained even at low deposition temperature
Self limiting growth process	Film thickness is dependent only on number of deposition cycles	Accurate thickness control
	No need for reactant flux uniformity	Excellent surface area coverage Excellent conformality No limitations from use of solid precursor (uncontrolled vaporization rate)
	Layer by layer growth	Low roughness Low defect level
	Atomic level control of material composition	Sharp interfaces
Above two characteristic combined	***Deposition rely on reactions with active surface sites***	***Possibility of Selective deposition***

1.2 TRADITIONAL MATERIAL PATTERNING: BASIC PROCESS SCHEME

In addition to the self limited surface reaction controlled nature of the ALD process which offers the potential of selective deposition, challenges associated with traditional material patterning processes have also been an important driver for this work. Figure 1-3 presents a simple flow diagram describing the steps involved in producing a film pattern.

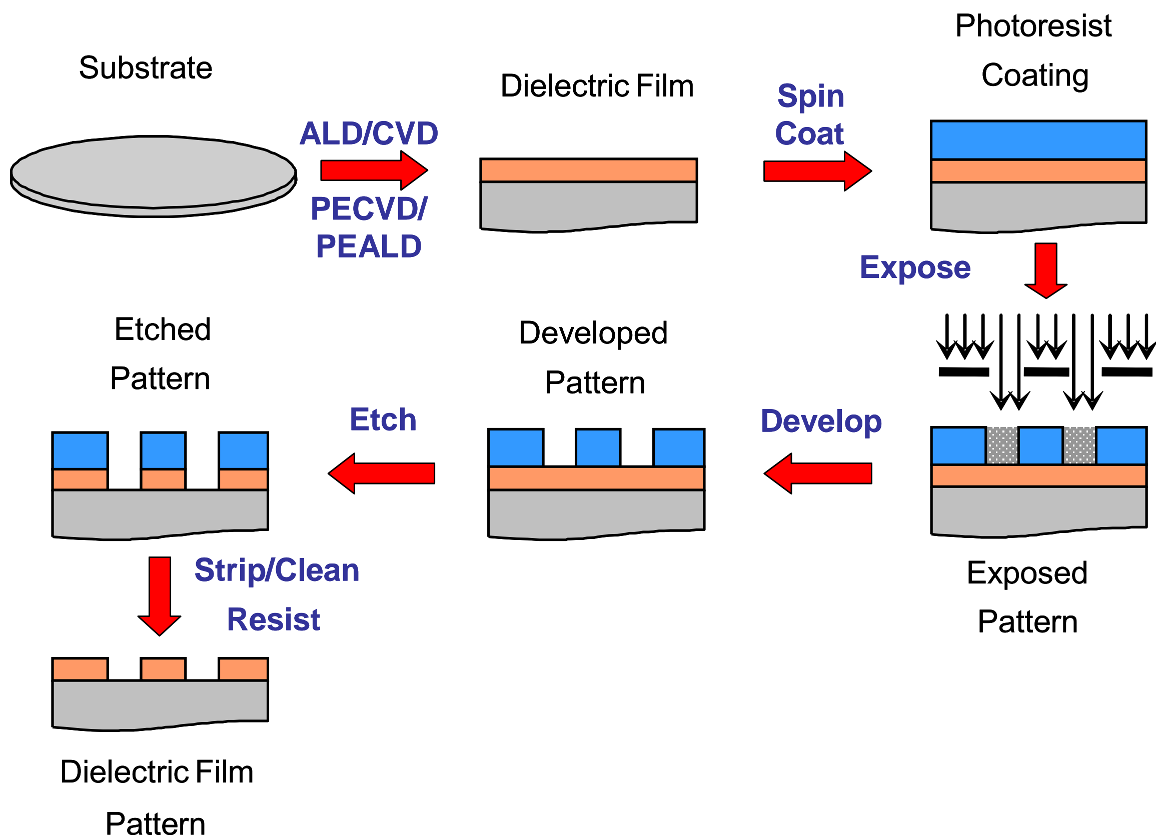

Figure 1-3: Traditional material patterning process

The major steps involved are:

1. Deposition of film to be patterned: The material (material A) whose patterned film is desired is first blanket coated on a substrate. A variety of deposition techniques including chemical vapor deposition, plasma enhanced-chemical vapor deposition, atomic layer deposition, plasma enhanced-atomic layer deposition, physical vapor deposition etc. have been employed to perform this task. The range of deposited film thickness may vary from several nanometers to several hundred nanometers depending upon the application. Clearly, the choice of deposition technique is dependent upon the required thickness and the quality of the desired material. If the desired thickness is of the order of 10-100 of nanometers, then a CVD-based technique is desirable primarily due to the significantly higher deposition rate relative to ALD. However, as discussed earlier, for thinner films with high quality, ALD is gaining significant popularity. During plasma enhanced deposition processes, precursor molecules are dissociated and ionized into free radicals and ions that are usually more reactive than the parent molecules. The increased reactivity of chemical species in such deposition schemes allows lowering of deposition temperature. Thus, where there is a limit on the maximum allowed processing temperature, plasma enhanced processes offer definite adavantages. However, highly energetic ions generated during plasma can induce damage to the substrate and thus may not be ideal where loss of device performance due to substrate damage is possible.

2. Lithography: This is the first active step of patterning where a photosensitive polymer (photoresist) is coated onto the deposited film. The photoresist is then selectively exposed

to a light source through a mask with the desired pattern. Under the action of light, the exposed areas undergo chemical change such that the resulting material has different solubility characteristics than those in the unexposed regions. The unexposed or exposed region is then selectively washed away in a developing solution depending upon photoresist tone (positive tone: exposed regions more soluble in developer solution; negative tone: unexposed regions more soluble in developer solution). This produces the desired pattern in the photoresist film. At present, most patterning is performed using 365 nm, 248 nm or 193 nm UV light sources. Examples of current resist chemistries include: Diazonaphthoquinone-Novolak based (365 nm, positive tone only), polyhydroxystyrene based (248 nm, positive and negative), and hexafluoroisopropyl-polynorbornene based (193 nm, positive and negative), acrylate based (e-beam).

3. Etching: The relief image in the photoresist is then transferred to the underlying film (material A) deposited during step 1 via an etching process. Etching can be performed under dry (vapor) or wet (liquid) conditions. In wet etching, the film material exposed in the open regions of the resist layer is dissolved when immersed in a chemical solution, whereas the resist material is expected to show inactivity towards the chemical solution to prevent underlying material from being exposed to the etching solution. However, due to the isotropic nature of this method, its application is only limited to low resolution patterning generally encountered in MEMS devices. The other form, termed dry etching, which for IC processing almost exclusively means a plasma-based etch, can give anisotropic etch profiles and is therefore more widely employed for high resolution patterning. Dry etching is conducted in a vacuum environment and uses a plasma of

reactive chemicals where the resulting fragments generated by the plasma react with the film material to produce volatile etch products. The key point to mention is that reactive etching is also isotropic in nature and usually a negative bias is induced to the substrate to achieve anisotropic etching. The reactive ions that generally carry a positive charge, accelerate into the (relatively) negative surface in a directional manner which imparts anisotropic nature to the etch process. Etching chamber is maintained at low pressure so that ions under go minimal collision to avoid losing their momentum and Ar is usually added which helps in producing ions at the start of the process. However, the biggest drawback of this scheme is that the energetic and directional ions that impart etch directionality also collide with the underlying substrate, transfer their momentum, and thus can inflict significant damage to the substrate. Plasma induced damage has been shown to adversely affect substrate properties by defect creation and can cause device failure, leakage currents, and/or reduced performance[16-18]. Plasma induced damage can take place in several forms:

a. Energetic ion bombardment can create lattice defects or dislocations, form dangling bonds on the surface, or implant ions from the plasma atmosphere. These defects often act as deep level states and produce compensation, trapping, or recombination of carriers in the semiconductor material. Damage as deep as 1000 Å has been reported in GaAs[19].

b. Hydrogen is often present during the etch process due to either its use in the plasma chemistry, residual water vapor in the chamber, or erosion of the photoresist mask, and can unintentionally passivate dopants present in the semiconductor material up to depths of several thousand angstroms. Polymer deposition may occur when using

plasma chemistries containing CH_x radicals or as a result of plasma-assisted reaction with or ablation of the photoresist mask.

c. Nonstoichiometric surfaces may be formed due to preferential loss of one of the lattice constituents[20]. This is often attributed to either preferential sputter desorption of the lighter element in the film or large differences in the volatility of the respective etch products. Nonstoichiometric depths are typically ~100 Å.

4. Strip and clean: After etching, the final pattern is obtained by removing the photoresist layer. Although this should be a relatively simple procedure, the actual process is quite complicated and requires close control, in part because of changes to the photoresist and residue generation from the preceding etch step. During etching the photoresist layer chemically reacts and can be sputtered by etching plasma. Etch products, polymeric residues and photoresist can deposit on the etching surface as well as on the side wall of pattern generated. The etch gas mixture frequently employs fluorine-based chemistries (e.g., CF_4), and thus the surface 'crust' that forms has a fluorocarbon chemical structure. In addition, etched material A can also redeposit on the side wall and on the top of the resist film. Due to the continuous reduction in feature sizes, it has become increasingly challenging to strip and clean the post etch residue for narrow trenches and vias. The problem is compounded by the fact that the solubility of etch residue in common solvents is low due to their heavily cross-linked and fluorocarbon nature. Efficient and effective removal often requires the use of highly aggressive chemistries containing fluoride ions, which etch the underlying substrate or attack the substrate-residue interface to aid in removal by a lift-off mechanism[21].

1.3 DIRECT MATERIAL PATTERNING

The various challenges described previously that result from the etching step in traditional material patterning schemes makes the idea of direct material patterning without need for an etch step attractive. A direct patterning approach will completely eliminate the associated plasma-induced damage, simplify the overall process flow and reduce device manufacturing costs. In addition to these benefits, such a scheme also facilitates the integration of materials (such as $BaSrTiO_3$) that are difficult to etch due to inability to form volatile etch products[22, 23].

Direct patterned deposition of Cu using single precursor CVD has been reported previously.[24-26] Jeon et al.[24] demonstrated the formation of patterned structures of Cu using (hexafluoroacetylacetonato)(vinyltrimethylsilane)copper(I) as the source gas on a variety of substrates (Al/Al_2O_3, Si/SiO_2, TiN/TiO_2, glass) that were partially masked using self assembled monolayers (SAMs) of octadecyltrichlorosilane (OTS). Other studies[25, 26] used a similar strategy of a masked Si substrate; however, these investigations invoked AZ5214 photoresist or polymethylmethacrylate as the mask material, and the source gas was 1,5-cyclooctadiene-Cu(I)-hexafluoroacetylacetonate. In large part, selective CVD approaches for Cu deposition are successful because they rely on single precursor CVD. Selective CVD of metal oxides is more challenging since deposition requires two precursors: a metal and an oxygen source, which can react in the gas phase and nucleate on masked regions. One interesting approach to perform direct patterned deposition of metal oxide films via photosensitive metallorganic precursors was recently demonstrated by Barstow et al[22]. In this technique, a solution containing 1:1:2 Ba(2-

ethylhexanoate), Sr(2-ethylhexanoate) and Ti-(diisopropoxide) (bis-acetylacetonoate) in methylisobutylketone was spin-coated onto a Si substrate. After a soft baking step, the films were selectively exposed to a DUV light source using an optical mask. A photochemical reaction results in fragmentation and volatilization of carboxylate linkages resulting in the complete loss of organic ligands attached to the metal center and produces a mixed oxide structure in the exposed region. The patterns are then developed by washing the unconverted precursor (i.e. unexposed) in a developer solvent mixture of IPA:MIBK (20:1). This approach clearly offers a very simple route to produce patterned metal oxide structures at ambient temperatures and pressures and does not require an etch step. However, since it relies on spin coating to produce the initial film, it is challenging to obtain very thin (<10 nm) films free of pinholes. Thus, this approach is not appropriate for applications requiring films of the order of 5-10 nm. In addition, the resulting films are amorphous which limits the achievable electrical properties such as dielectric constant (k); for example, the k value for TiO_2 films obtained in this manner was only ~30.

1.3.1 AREA SELECTIVE ATOMIC LAYER DEPOSITION TECHNIQUE (ASALDT)

The attributes of ALD suggest that it can play a major role in current and future selective film deposition processes because it can easily form thin films with excellent quality as discussed in the previous section. More importantly, we have already observed that during ALD, film growth occurs only via reactions with the sites on the surface upon which deposition occurs. Thus, if we can chemically block or physically mask those

active sites we should be able to prevent the nucleation of ALD films on those modified/protected areas, thereby ensuring that the ALD film nucleates and grows only on the desired unprotected regions. Such an approach should permit the direct patterned deposition of thin films of extremely high quality. A brief schematic illustrating the concept of area selective ALD technique (ASALDT) is presented in figure 1-4a. In this scheme we assume that the starting substrate has active sites on the surface on which an ALD film can nucleate. If this is not the case, then the substrate surface can be selectively modified to allow nucleation on the modified regions instead. Figure 1-4b shows the final structure that is obtained from this alternate scheme.

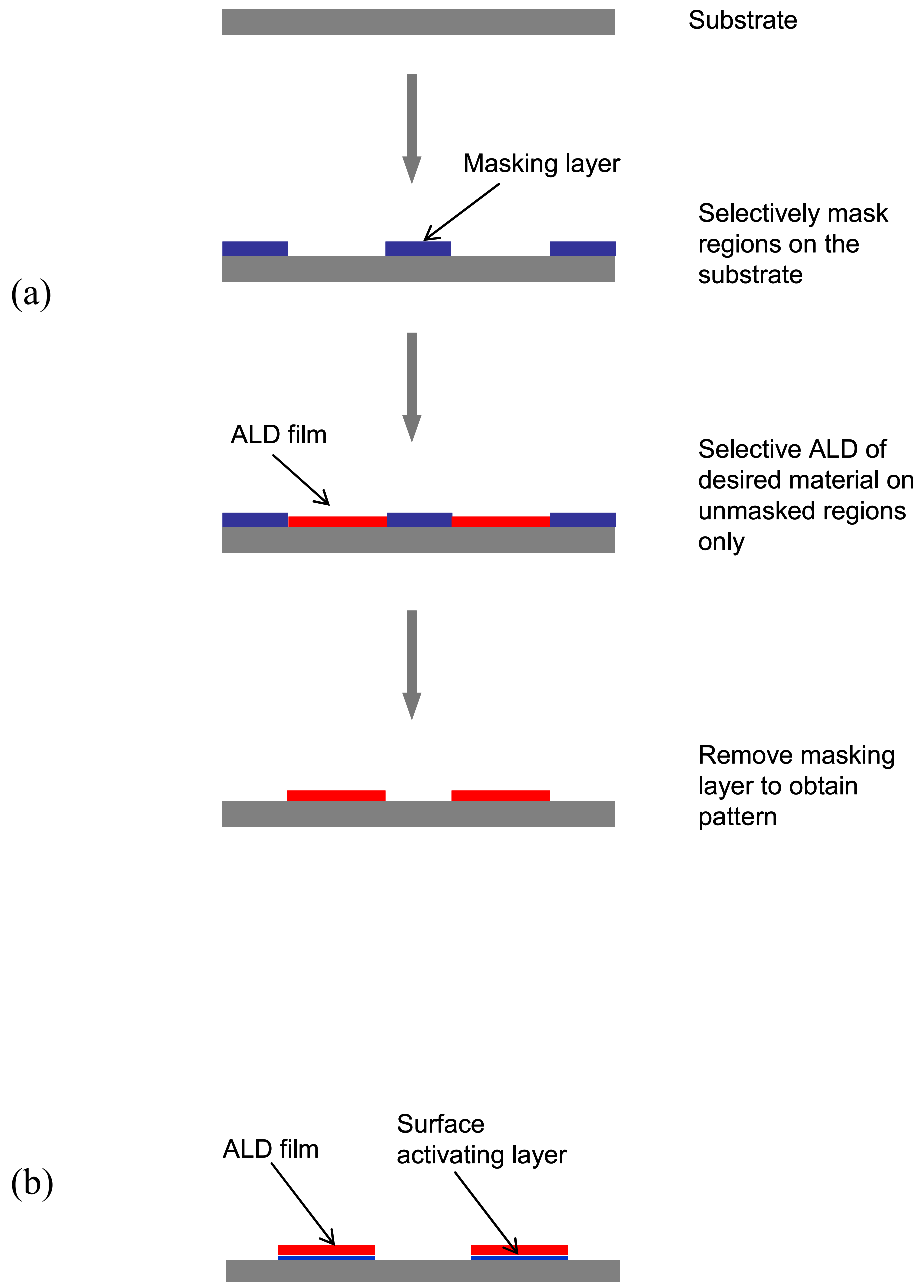

Figure 1-4: (a) Schematic representation of an area selective ALD (ASALD), (b) Resulting structure after the ASALD process if starting substrate does not allow ALD nucleation

The possibility of performing selective ALD has been pursued extensively in recent years. Table 1-2 summarizes the previous/current studies reporting area selective ALD of a variety of films on different substrates.

Table 1-2: Area selective ALD: Summary of previous studies

Researcher	**Precursors/ ALD film**	**Masking layer and patterning scheme**
Yan et al. (2001)[27]	$Zn(CH_3)_2$-H_2O/ ZnO	$CH_3(CH_2)_{21}SiCl_3$ / Microcontact printing (μcp)
Lee and Sung (2004)[28]	$Zr(OC(CH_3)_3)_4$-H_2O/ ZrO_2	$CH_3(CH_2)_{17}SiCl_3$ / Photocatalytic Lithography
Park et al. (2004)[29]	$Ti(OCH(CH_3)_2)_4$-H_2O/ TiO_2	$CH_3(CH_2)_{17}SiCl_3$ / Microcontact printing (μcp)
Seo et al. (2004)[30]	$Ti(OCH(CH_3)_2)_4$-H_2O/ TiO_2	$CH_3(CH_2)_{17}SiCl_3$ / Microcontact printing (μcp)
Chen et al. (2005)[31]	$Hf(N(CH_3)_2)_4$-H_2O/ HfO_2	$CH_3(CH_2)_{17}SiCl_3$ / Solution dip of a prepatterned substrate
Park et al. (2005)[32]	$(C_5H_5)_2Ru$-O_2/ Ru	$CH_3(CH_2)_{17}SiCl_3$ / Microcontact printing (μcp)
Chen et al. (2006)[33]	$CH_3C_5H_4Pt(CH_3)_3$-O_2/ Pt	$CH_3(CH_2)_{15}CHCH_2$ / Solution dip of a prepatterned substrate

It is evident from table 1-2 that all the early ASALDT approaches involved the use of long chain alkyl silanes with a reactive end group that serves as a masking agent (which will subsequently be referred to as a SAM (self assembled monolayer) based approach). All these SAM-based approaches rely on the chemical conversion of sites on the substrate surface which would be reactive toward the ALD precursors into a non-reactive form, thus preventing ALD nucleation and growth, and thereby achieving

selective ALD on unprotected regions only. Yan et al[27]. and Park et al.[29] used a simple microcontact printing technique to selectively block active silanol (Si-OH) sites on a Si substrate. A polydimethylsiloxane (PDMS) stamp inked with a solution containing the desired silane was placed onto a Si wafer. The Si-OH sites in contact with the stamp react with -$SiCl_3$ groups to form siloxane (-Si-O-Si) linkages having a long chain alkyl tail, whereas the non contact regions retain reactive silanol sites on which ALD nucleation can occur. Later, Lee and Sung[28] employed an interesting methodology of patterning a silanized surface via photocatalytic lithography[34, 35]. A quartz plate coated with patterned TiO_2 was brought into contact with an octadecyltrichlorosilane (OTS) SAM coated Si substrate. The SAM coated Si substrate was then exposed for 2 min to a 254 nm UV light source through a patterned TiO_2 coated quartz plate. Upon UV irradiation at 254 nm, the semiconductor TiO_2 generates electron-hole pairs, and subsequently produces highly reactive oxygen species (e.g., OH, O_2 radicals) via electron scavenging by adsorbed O_2 and hole trapping by the surface OH or adsorbed H_2O[35, 36]. These radicals oxidized and decomposed the organic SAM and thus exposed the protected Si-OH in the regions in close proximity to the TiO_2 patterns.

In comparison, the studies performed by Chen et al.[31, 33] employed a more complex scheme to create patterns of unprotected/protected regions on a substrate. A patterned SiO_2 substrate was first fabricated using thermal oxide growth and conventional lithography-etching steps. These patterned samples were then given a Piranha treatment followed by a 2 min dilute HF etch. This treatment removed the native oxide from the "bare" silicon, replacing it with hydride termination (Si–H), leaving hydroxylated SiO_2 in the SiO_2-patterned regions. Immediately after HF treatment, the samples were immersed

in a dilute OTS solution for 48 hrs to selectively link the OTS SAM layer onto the hydroxyl terminated SiO_2 patterned regions only. In their second study, these authors used octadecene which undergoes a hydrosilylation reaction with an Si-H surface to selectively produce a similar SAM structure on those surfaces only. All the studies discussed above generally utilize the masking scheme proposed in figure 1-4a, where active sites on a substrate are selectively masked and ALD occurs on the unprotected regions. The masking scheme described in figure 1-4b has not been investigated extensively and only one study employing such a scheme has been published[30]. In that study, a Au surface was activated by employing a SAM of mercaptandecanol, which generated OH sites on the SAM covered region and facilitated nucleation of ALD TiO_2 on those regions.

1.4 ORGANIZATION OF THESIS

Studies presented in table 1-2 have shown that substrate surfaces can be successfully tailored to deactivate/activate reaction sites in order to perform selective ALD in desired regions. The chronology of successful attempts on performing selective ALD indicates that most of the reported studies are very recent with only a single published report until the start of this work. Driven by the promise of an ASALDT-based direct patterning approach, we initiated our investigations into selective ALD techniques. A custom-designed ALD reactor system was built in house specifically for our studies; the setup and design of the system is discussed in Chapter 2. In order to develop methodology for selective deposition, a model system is required for the experimental

investigation. Titanium dioxide is one of the most widely studied oxides because of its interesting optical and electrical properties. These characteristics make TiO_2 useful in a variety of applications including antireflective coatings, chemical sensors and high-k dielectrics. Due to the numerous potential applications and abundant literature available on TiO_2, it has been selected as the material for investigation in this work. Specifically, $TiCl_4$ and DI water have been initially chosen as precursors to investigate the area selective ALD of titanium dioxide films. $TiCl_4$ has a very high reactivity towards hydroxyl bonds and thus the $TiCl_4$-H_2O ALD system offers highly sensitive system to evaluate the success of any masking methodology that we develop. One segment of our initial studies investigated the use of SAM-based approaches to perform ASALDT and the results are presented in Chapter 3. A more critical analysis of previous SAM-based approaches noted in section 1.3.1 above is also included in that chapter. During the course of our studies we observed certain challenges associated with SAM-based ASALDT (Chapter 3) and thus we proposed the use of polymer thin films as masking layers. In Chapter 4 we develop a methodology to perform area selective ALD using polymer-based masking approaches. In addition, various parameters that affect the success of a polymer-based masking approach have been identified and have been investigated in detail. Intrinsic reactivity of $TiCl_4$ with the polymer mask and diffusion through the masking layer appear to be the critical challenges for the polymer films-based masking approach and these challenges have been overcome by selecting an alternate metal precursor (Titanium isopropoxide). A comparative study on ALD and ASALD between titanium tetrachloride and titanium isopropoxide is presented in Chapter 5. During the studies on ALD on polymer films we observed that when ALD layers are able

to nucleate on polymer film surfaces, they form a very conformal film on the top of polymer surface which can act as etch barrier in oxygen plasma. We have exploited this characteristic to develop a novel top-surface imaging technique that uses area selective ALD on a chemically amplified resist. Chapter 6 includes a description of the development of this method. As part of this thesis, a quartz crystal microbalance (QCM) study was performed to measure diffusion coefficients of reactants through polymer thin films. Sorption/desorption experiments have been conducted to estimate the diffusion coefficients and equilibrium uptake of ALD precursors in polymer masks. The design of the QCM system and experimental results are discussed in Chapter 7. The thesis concludes by summarizing the contributions of this research and proposing future work in this area.

1.5 REFERENCES

1. Suntola, T. and Aston, J., US Patent# 4058,430. **1977**.

2. Aleskovskii, V. B.; Shevjakov, A. M.; Kuznetsova, G. N. In Chemistry of high-temperature materials, Proceendings of the second USSR conference on high-temperature chemistry of oxides, Leningrad, 1965; Leningrad, 1965; pp 149-155.

3. Puurunen, R. L., Surface chemistry of atomic layer deposition: A case study for the trimethylaluminum/water process. *Journal of Applied Physics* **2005,** 97, (12), 121301-1-121301-52

4. Suntola, T.; Hyvaerinen, J., Atomic layer epitaxy. *Annual Review of Materials Science* **1985,** 15, 177-95.

5. Suntola, T., Atomic layer epitaxy. *Thin Solid Films* **1992,** 216, (1), 84-9.

6. Nishizawa, J.; Abe, H.; Kurabayashi, T., Molecular layer epitaxy. *Journal of the Electrochemical Society* **1985,** 132, (5), 1197-200.

7. Bedair, S. M.; Tischler, M. A.; Katsuyama, T.; El-Masry, N. A., Atomic layer epitaxy of III-V binary compounds. *Applied Physics Letters* **1985,** 47, (1), 51-3.

8. Usui, A.; Sunakawa, H., GaAs Atomic Layer Epitaxy by Hydride VPE. *Japanese Journal of Applied Physics Part 2-Letters* **1986,** 25, (3), L212-L214.

9. Usui, A., Atomic Layer Epitaxy of III-V Compounds - Chemistry and Applications. *Proceedings of the Ieee* **1992,** 80, (10), 1641-1653.

10. Leskela, M.; Ritala, M., Atomic layer deposition chemistry: recent developments and future challenges. *Angewandte Chemie, International Edition* **2003,** 42, (45), 5548-5554.

11. Wilk, G. D.; Wallace, R. M.; Anthony, J. M., High-kappa gate dielectrics: Current status and materials properties considerations. *Journal of Applied Physics* **2001,** 89, (10), 5243-5275.

12. International Technology Roadmap for Semiconductors. **2003**.

13. Rahtu, A.; Ritala, M., Reaction mechanism studies on titanium isopropoxide-water atomic layer deposition process. *Chemical Vapor Deposition* **2002,** 8, (1), 21-28.

14. Aarik, J.; Aidla, A.; Sammelselg, V.; Siimon, H.; Uustare, T., Control of thin film structure by reactant pressure in atomic layer deposition of TiO2. *Journal of Crystal Growth* **1996,** 169, (3), 496-502.

15. Puurunen, R. L., Formation of metal oxide particles in atomic layer deposition during the chemisorption of metal chlorides. A review. *Chemical Vapor Deposition* **2005,** 11, (2), 79-90.

16. Jiang, J.; Awadelkarim, O. O.; Werking, J., Gate leakage current: A sensitive characterization parameter for plasma-induced damage detection in ultrathin oxide submicron transistors. *Journal of Vacuum Science & Technology, A: Vacuum, Surfaces, and Films* **1998,** 16, (3, Pt. 2), 1664-1669.

17. Karzhavin, Y.; Wu, W., Overview of plasma induced damage after dry etch processing. *IEEE/SEMI Advanced Semiconductor Manufacturing Conference and Workshop, 9th, Boston, Sept. 23-25, 1998* **1998**, 320-326.

18. Shul, R. J.; Zhang, L.; Baca, A. G.; Willison, C. G.; Han, J.; Pearton, S. J.; Lee, K. P.; Ren, F., Inductively coupled high-density plasma-induced etch damage of GaN MESFETs. *Solid-State Electronics* **2001,** 45, (1), 13-17.

19. Pearton, S. J., Characterization of damage in electron cyclotron resonance plasma etched compound semiconductors. *Applied Surface Science* **1997,** 117, 597-604.

20. Pang, S. W., Surface Damage on GaAs Induced by Reactive Ion Etching and Sputter Etching. *Journal of the Electrochemical Society* **1986,** 133, (4), 784-787.

21. Louveau, O.; Louis, D.; Assous, M.; Blanc, R.; Brun, P.; Lamy, S.; Lajoinie, E., Challenge of ashing and cleaning on SiOC-H dielectric: characterization and main issues. *Microelectronic Engineering* **2002,** 61-2, 867-874.

22. Barstow, S. J.; Jeyakumar, A.; Roman, P. J.; Henderson, C. L., Direct photopatterning of metal oxide structures using photosensitive metallorganics. *Journal of the Electrochemical Society* **2004,** 151, (10), F235-F241.

23. Choi, S. K.; Kim, D. P.; Kim, C. I.; Chang, E. G., Damage in etching of (Ba,Sr)TiO3 thin films using inductively coupled plasma. *Journal of Vacuum Science & Technology A* **2001,** 19, (4), 1063-1067.

24. Jeon, N. L.; Nuzzo, R. G.; Xia, Y. N.; Mrksich, M.; Whitesides, G. M., Patterned Self-Assembled Monolayers Formed by Microcontact Printing Direct Selective Metalization by Chemical-Vapor-Deposition on Planar and Nonplanar Substrates. *Langmuir* **1995,** 11, (8), 3024-3026.

25. Davazoglou, D.; Raptis, I.; Gleizes, A.; Vasilopoulou, M., Fabrication of very fine copper lines on silicon substrates patterned with poly(methylmethacrylate) via selective chemical vapor deposition. *Journal of Vacuum Science & Technology B* **2004,** 22, (2), 859-860.

26. Davazoglou, D.; Vidal, S.; Gleizes, A., Selective chemical vapor deposition of copper on AZ 5214 (TM)-patterned silicon substrates. *Journal of Vacuum Science & Technology B* **2001,** 19, (3), 759-761.

27. Yan, M.; Koide, Y.; Babcock, J. R.; Markworth, P. R.; Belot, J. A.; Marks, T. J.; Chang, R. P. H., Selective-area atomic layer epitaxy growth of ZnO features on soft lithography-patterned substrates. *Applied Physics Letters* **2001,** 79, (11), 1709-1711.

28. Lee, J. P.; Sung, M. M., A new patterning method using photocatalytic lithography and selective atomic layer deposition. *Journal of the American Chemical Society* **2004,** 126, (1), 28-29.

29. Park, M. H.; Jang, Y. J.; Sung-Suh, H. M.; Sung, M. M., Selective Atomic Layer Deposition of Titanium Oxide on Patterned Self-Assembled Monolayers Formed by Microcontact Printing. *Langmuir* **2004,** 20, (6), 2257-2260.

30. Seo, E. K.; Lee, J. W.; Sung-Suh, H. M.; Sung, M. M., Atomic layer deposition of titanium oxide on self-assembled-monolayer-coated gold. *Chemistry of Materials* **2004,** 16, (10), 1878-1883.

31. Chen, R.; Kim, H.; McIntyre, P. C.; Porter, D. W.; Bent, S. F., Achieving area-selective atomic layer deposition on patterned substrates by selective surface modification. *Applied Physics Letters* **2005,** 86, (19), 191910/1-191910/3.

32. Park, K. J.; Doub, J. M.; Gougousi, T.; Parsons, G. N., Microcontact patterning of ruthenium gate electrodes by selective area atomic layer deposition. *Applied Physics Letters* **2005,** 86, (5), 051903/1-051903/3.

33. Chen, R.; Bent, S. F., Chemistry for positive pattern transfer using area-selective atomic layer deposition. *Advanced Materials* **2006,** 18, (8), 1086-+.

34. Haick, H.; Paz, Y., "Dark" photocatalysis: The degradation of organic molecules anchored to dark microdomains of titanium dioxide. *Chemphyschem* **2003,** 4, (6), 617-620.

35. Tatsuma, T.; Kubo, W.; Fujishima, A., Patterning of solid surfaces by photocatalytic lithography based on the remote oxidation effect of TiO2. *Langmuir* **2002,** 18, (25), 9632-9634.

36. Ishibashi, K.; Nosaka, Y.; Hashimoto, K.; Fujishima, A., Time-dependent behavior of active oxygen species formed on photoirradiated TiO2 films in air. *Journal of Physical Chemistry B* **1998,** 102, (12), 2117-2120.

CHAPTER 2

DESIGN OF ATOMIC LAYER DEPOSITION REACTOR

The first step towards accomplishing the objectives of this work includes the design and fabrication of an ALD reactor system and the establishment of operating conditions to achieve deposition in an ALD mode. This chapter discusses the ALD reactor system design in some detail; particular attention is given to discussing the criteria or observed experimental results which influenced several design decisions. In addition, chemical, physical and electrical characterization of the TiO_2 ALD films has been performed and the results are included in this chapter.

2.1 ATOMIC LAYER DEPOSITION REACTOR

Figure 2-1 presents a schematic of our ALD reactor. The reactor consists of the following primary components:

1) Reaction chamber
2) Substrate holder and substrate temperature control system
3) Precursor delivery system including precursor pulsing
4) Vacuum pump

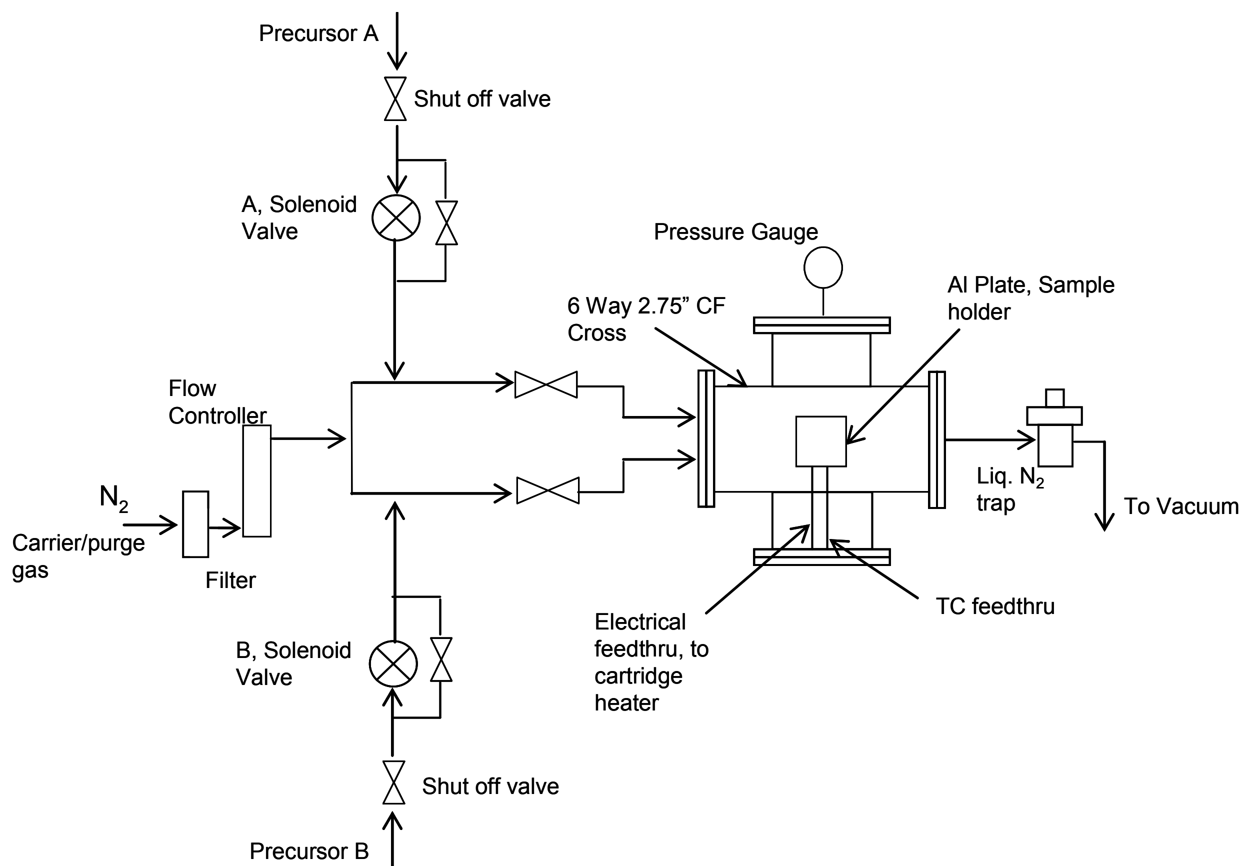

Figure 2-1: Schematic of the ALD reactor system

2.1.1 Reaction Chamber

Analogous to CVD, ALD processes can be performed in different types of reactors over a wide pressure range from atmospheric to ultrahigh vacuum. The reactor type can be divided into two groups: inert gas flow reactors operating under viscous or transition flow conditions at pressures higher than or equal to 100 mTorr, and high or ultrahigh vacuum reactors operating under molecular flow conditions. The former resembles CVD type reactors while the latter are similar to molecular beam epitaxy reactors. From the viewpoint of cost effectiveness of the process, flow reactors operating under viscous flow

are more popular. This is primarily due to: (1) purging of a properly designed flow reactor is much more rapid than evacuation of a high vacuum chamber, thus reducing the process time, and (2) operating a UHV system is significantly costlier and challenging than low vacuum systems.

Thus a flow type reactor system was chosen for our studies. A tubular shape for a reaction chamber (with flow direction parallel to the circular axis) is preferable since the fluid motion is essentially plug flow, thereby allowing the shortest purge time. The initial reactor was built using a 6-3/4" (ID: 5") conflate (CF) nipple which also serves as a tubular reactor. Unfortunately, even at the maximum conductance for the vacuum pump, the linear velocity of carrier gas was only 3.3 cm/s. This small bulk flow velocity in the flow direction allowed significant diffusive flux in all directions and so that the reactor behaved more like a mixed flow system, requiring longer purge duration. If the system is not sufficiently purged, gas phase reactions become significant, thus obviating the ALD growth mode. In fact, even with 60s purge duration, we observed nonuniform growth, excessive particle formation on substrates and visibly poor film quality. An image of ALD samples deposited using this reactor setup is shown in figure 2-2.

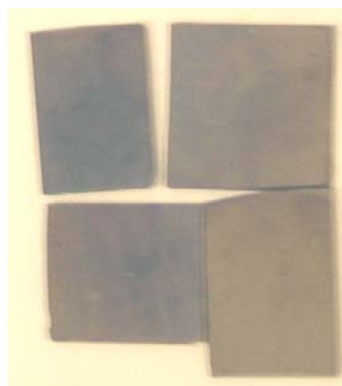

Figure 2-2: Images of samples obtained from initial reactor design

Increasing the pumping speed by employing a higher conductance vacuum pump correlated directly to increased cost. However, a less expensive solution was to use a reaction chamber with a smaller radial dimension. Although this approach reduced the size of substrate that could be processed, the focus of our studies was the generation of fundamental information regarding area selective ALD, so sample size was immaterial. As a result, the reaction chamber was downsized to a 2-3/4" (ID: 1.73") CF 6-way cross. With the same vacuum pump operating at maximum conductance, a purge gas flow rate of 78 sccm was achieved which translates to a linear velocity of 124.7 cm/s. Depositions conducted with new reactor configuration (after few more alterations in the overall system, discussed later) produced excellent quality films. No particulates were observed during or after deposition, at least with 10s of purge (experimental data were not collected below 10s); however, the duration of the purge step had to be increased to 20s in order to achieve uniform deposition rates over the entire substrate area. More discussion of these particular experiments is presented later. Nevertheless, comparison of the two different reactor configurations investigated indicated that a higher flow velocity

is preferable and it is important to size the dimensions of reaction chamber based upon maximum pumping capacity of the exhaust system.

2.1.2 SUBSTRATE HOLDER AND SUBSTRATE TEMPERATURE CONTROL SYSTEM

Figure 2-3 shows a detailed schematic illustrating the sample holder configuration for the reactor system. The holder consisted of cylindrical aluminum plate (1in dia × 1in height) with a recessed platform to place the sample on. The recessed platform prevented sample movement by convection from the purge gas flow. The holder was heated using a CSH series cartridge heater (Omega) and the temperature was read using a K-type thermocouple (Omega); the cartridge heater was placed in the center of the holder which resulted in a uniform temperature profile over the top surface of the plate. At a deposition temperature of 160 ^{o}C, the temperature variation on the plate surface was less than 0.5 ^{o}C at any two contact points.

Choice of deposition temperature was influenced by a number of issues. Previous studies reported that the reaction of $TiCl_4$ on oxide surfaces demonstrate saturation within the range of 150 ^{o}C – 500 ^{o}C.[1-3] In addition, since we intended to use SAMs of OTS as masking layers, their thermal stability must be taken into account when deciding the operating temperature for our studies. Previous investigations on the thermal stability of OTS SAMs reported changes in surface morphology after the SAM coated substrates were annealed above 175 ^{o}C.[4] Thus, 160 ^{o}C was chosen as the deposition temperature for our experiments so that we could safely perform deposition in an ALD mode and still

operate in a thermally stable region for SAM covered surfaces during our selective ALD studies.

It is important to note that this reactor system is a cold wall reactor since the substrate is heated to deposition temperature by resistively heating the substrate holder. On the other hand, in a hot wall configuration, the sample is radiatively heated to the desired temperature by heating the reactor wall to that temperature. From a process viewpoint, cold wall reactors are less preferable in cases where water is used as a reactant. During the water pulse, the cold walls of a reaction chamber can adsorb significant amounts of water which can desorb during the following purge step and can extend the required duration of the purge step. At elevated wall temperatures, physisorption of water is severely reduced which practically eliminates this issue. However, from a reactor construction viewpoint, a hot wall reactor is more cumbersome to build since the entire reactor configuration must be installed inside an oven/furnace. In our case, the challenges of a cold wall system are addressed by maintaining the reaction chamber wall and reactant flow lines at elevated temperature (~105°C) by wrapping them with heating tape.

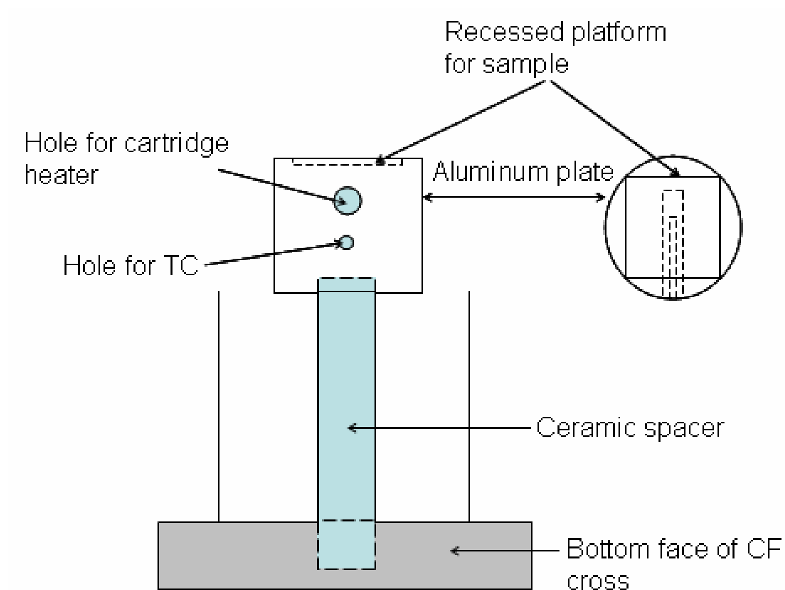

Figure 2-3: Detailed schematic illustrating the substrate holder

2.1.3 PRECURSOR DELIVERY SYSTEM AND PRECURSOR PULSING MECHANISM

Since ALD relies on a reaction sequence which reaches surface saturation at each step, the design of precursor delivery systems for ALD reactors is simpler than that of CVD systems where precise control of precursor delivery to maintain a uniform flux is required. For liquid precursors, two options (1) delivery via carrier gas and (2) delivery via precursor volatilization are common. In our reaction scheme, both $TiCl_4$ and H_2O have sufficient vapor pressure (13 Torr and 22 Torr respectively) at room temperature, and the operating chamber pressure is only 1 Torr. Thus, adopting option 2 was a natural choice, since precursors can be easily introduced into the reaction chamber via pressure differential driven flow. In addition, the N_2 purge gas line was connected immediately downstream of each solenoid valve. Thus, during the precursor exposure step, N_2 served

as a carrier gas to assist transport of precursor vapors to the reaction chamber. When titanium isopropoxide (TiIP) was used as a reactant/precursor, the source was heated to 83-85 ^{o}C which generated a vapor pressure of 3.8 Torr and thus TiIP could also be introduced in a similar manner. In addition, for TiIP, all the flow lines carrying isopropoxide precursor were heated to at least 85°C to avoid vapor condensation.

Alternate pulsing of precursors was achieved using pneumatically actuated solenoid valves (part no.: SS-42S4-31CD and response time: < 100 ms) which were installed between the precursor source and the reaction chamber; solenoid valve operation was controlled using a LabView program. A metering valve was also attached immediately upstream of each solenoid valve to control the total precursor flow. Incorporation of metering valves greatly improved control of the film quality. Figure 2-4 shows samples obtained after 250 ALD cycles (using $TiCl_4$ and water, exposure sequence: 2.5s – 10s – 2.5s – 10s) with and without the presence of metering valve. In addition, picture of a sample obtained after ALD with longer purge duration (17 s) is also presented. As is evident from the pictures, the films obtained from the reactor configuration without metering valves showed striated patterns suggesting significant differences in film thickness across the substrate area. The reason for such nonuniformities is that the excess precursor dose at each exposure was not completely removed during the purge step. Although increased purge duration could alleviate this problem, the dose was sufficiently high to generate a significant pressure spike within the chamber that even resulted in a change in the operating sound of the vacuum pump. In addition to wasting precursor materials, this approach would likely damage the vacuum pump.

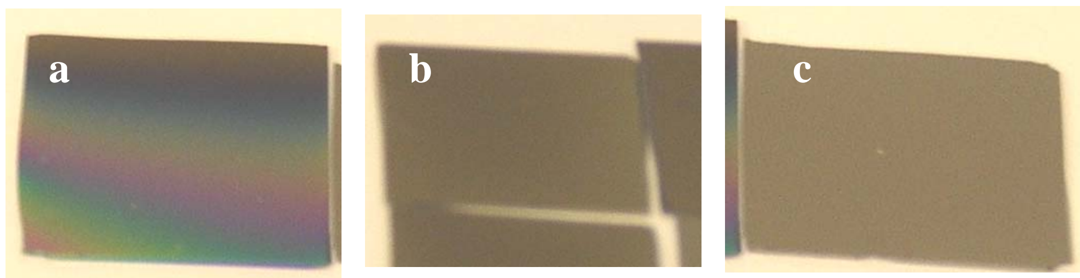

Figure 2-4: Samples obtained after ALD using the reactor configuration (a) without a metering valve (cycle sequence: 2.5s-10s-2.5s-10s), (b) with a metering valve (cycle sequence: 2.5s-10s-2.5s-10s), (c) with a metering valve (cycle sequence: 2.5s-17s-2.5s-17s)

Installation of a metering valve controlled the total flowrate of precursor and significantly improved the film quality as shown in figure 2-4. However, the film deposition rate was still not uniform, as indicated from the color gradient observed. In this regard, it should be mentioned the 6-way cross is not an ideal tubular reactor configuration. The regions near the side arm disrupt linear flow and can create a dead zone in that region where the flow velocity is less than that at the center of the reactor; a longer time is thus needed to purge those regions. Indeed, a minimum purge duration of 17s was required to obtain a uniform deposition rate across the entire substrate. As a result, for all subsequent experiments a purge duration of at least 20s was employed after each exposure pulse.

2.1.4 EXHAUST SYSTEM

An Alcatel 2021SD rotary vane mechanical pump was used to evacuate the reaction chamber. The pump was always operated at full conductance which gave a purge gas

(N_2) flow rate of 78 sccm. At this flowrate, the pressure inside the reaction chamber was maintained at 1 Torr. Ultra high purity nitrogen was used as purge gas; the N_2 flow line to the rotameter was equipped with a Matheson gas purifier (type 451) to trap moisture, oil and particulates (above 12 micron size) present in N_2. A liquid nitrogen trap was placed between the chamber and vacuum pump in order to prevent unreacted precursors and products from entering the pump.

To summarize our efforts in ALD reactor design, our observations indicate that a reactor configuration that offers proper provisions for purging the reactants after each precursor exposure is the most critical aspect in the successful design of ALD reactors.

2.2 TIO$_2$ ALD USING TICL$_4$ AND H$_2$O

2.2.1 ALD PROCEDURE

Blanket film depositions were initially conducted in order to investigate system behavior and determine the operating conditions (cycle sequence) required to perform ALD using titanium tetrachloride and water as precursors for the deposition of TiO_2. Titanium tetrachloride (99.9%) was purchased from Sigma-Aldrich and used as received for the titanium precursor source while deionized (DI) water was used as the oxygen precursor source. Both precursors were maintained at room temperature where the vapor pressures of $TiCl_4$ and H_2O are 13 torr and 23 torr, respectively. All depositions were conducted at a substrate temperature of 160 ^{o}C and 1 torr chamber pressure. p-type silicon <100> wafers were used as substrates. Prior to film deposition, wafers were thoroughly rinsed

with acetone, methanol, iso-propanol and DI water to remove surface organics and then immersed in 2 M HNO_3 for 2 hours to increase the surface hydroxyl concentration before ALD[5]. After removal from the HNO_3 solution, the wafers were rinsed again with DI water and dried under nitrogen before being loaded into the ALD chamber. The chamber was evacuated to a base pressure of 20mTorr and the substrates held at this pressure for 2 hours; during this time, the reactor walls were heated to ~ 105 ^{o}C. Subsequently, an N_2 flow was initiated until the chamber pressure reached 1 torr, after which the substrate holder was heated to the desired deposition temperature (160 ^{o}C). After an additional 5-10 min time period, ALD cycles were started. The ALD deposition cycle consisted of: (1) $TiCl_4$ pulse, (2) N_2 purge, (3) H_2O pulse, and (4) N_2 purge.

2.2.2 FILM CHARACTERIZATION

Film thickness measurements: Film thicknesses were measured using both spectroscopic ellipsometry and x-ray reflectivity. Spectroscopic ellipsometry measurements were performed with an M-2000 ellipsometer (J.A. Woollam Co. Inc.). Ellipsometry data were collected over a wavelength range from 400 to 1000 nm at angles of 65°, 70° and 75° (with respect to the substrate plane normal). Data were analyzed and fit to determine film thickness and refractive index using the WVASE-32 software package (J.A. Woollam Co.) by employing a Cauchy model for the films and using a standard silicon substrate library data file. In addition, a 1.8 nm thick layer of SiO_2 layer between Si substrate and TiO_2 film was also included in the film stack model to account for the native oxide present on the Si substrate. X-ray reflectivity measurements were

performed using a X'pertPRO XRD system (PANalytical Inc.). For x-ray reflectivity experiments, copper radiation with a wavelength of 1.54 Å was used with the x-ray source generator tension and current set at 45 kV and 40 mA respectively. Samples were scanned at low incident angles from 0° to 3.0^o with a step size of 0.005^o and a time per step of 0.1 s. Data were analyzed using the X'pert reflectivity software which calculates the film thickness from the relative distance in angular position of the fringes in the reflectivity scans. Thicknesses measured using both techniques generally agreed to within ± 0.2 nm. Refractive index (RI) (at 580 nm) of the films as obtained from ellipsometry data ranged between 2.15-2.30, which is consistent with RI data reported for amorphous titania (2.2-2.4 at 580 nm).[6]

<u>*Chemical analysis:*</u> Chemical analysis of the films and surfaces was performed using x-ray photoelectron spectroscopy (XPS). XPS spectra were collected using a Physical Electronics (PHI) Model 1600 XPS system equipped with a monochromator. The system used an Al Kα source (hν = 1486.8 eV) operating at 350 W beam power. Ejected photoelectrons were detected by a hemispherical analyzer that provided both high sensitivity and resolution. The operating pressure in the sampling chamber was below 5×10^{-9} Torr. Samples were aligned in the beam by maximizing photoelectron counts corresponding to the primary C1s peak in C—C bonds located at a binding energy of 284.8 eV. A neutralizer beam was used during XPS measurements to compensate for peak shifting which occurs due to charging of samples during x-ray exposure. All high resolution spectra were collected using a pass energy of 46.95 eV. The step size and time per step were chosen to be 0.025 eV and 100 ms, respectively. Atomic concentrations of different elements were calculated based on the photoelectron intensities of each element

and the elemental sensitivity factors provided by the instrument manufacturer. Peak intensities and compositions at different locations were compared to assess uniformity of film composition across the sample surface. Figure 2-5 shows a representative XPS spectrum of deposited TiO_2 films. XPS spectra showed that the deposited films are generally free of contaminants to the level of XPS detectability (~0.1 atomic %). The position of Ti2p3 peak is located at a binding energy of 258.8 eV, which is characteristic of Ti in TiO_2.[7] Also, the atomic concentration table showed O/Ti ratio of 2.07 confirming that deposited films are stoichiometrically close to TiO_2.

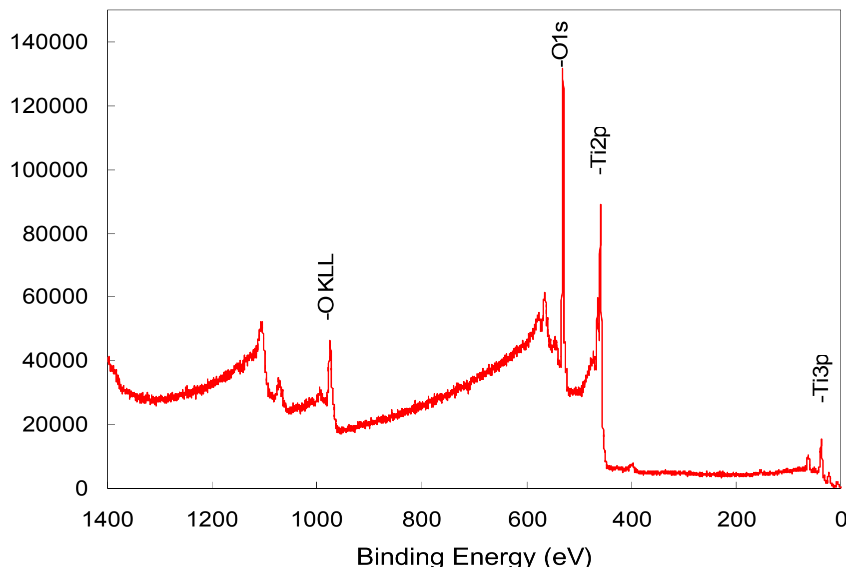

Figure 2-5: XPS spectra of a representative TiO_2 film deposited using $TiCl_4$-H_2O ALD

<u>*Surface roughness:*</u> Atomic force microscopy (AFM) was used to examine the surface roughness of the deposited films using a PicoPlus AFM (Molecular Imaging) operating in tapping mode with a 3-axis closed loop scanner. AFM scans indicated that the deposited films were smooth with an RMS roughness of 0.18 – 0.41 nm. Figure 2-6 shows a

microimage of a surface scan on a 14 nm titania film. Smoothness of film can easily be assessed by looking at a horizontal section-analysis on the surface.

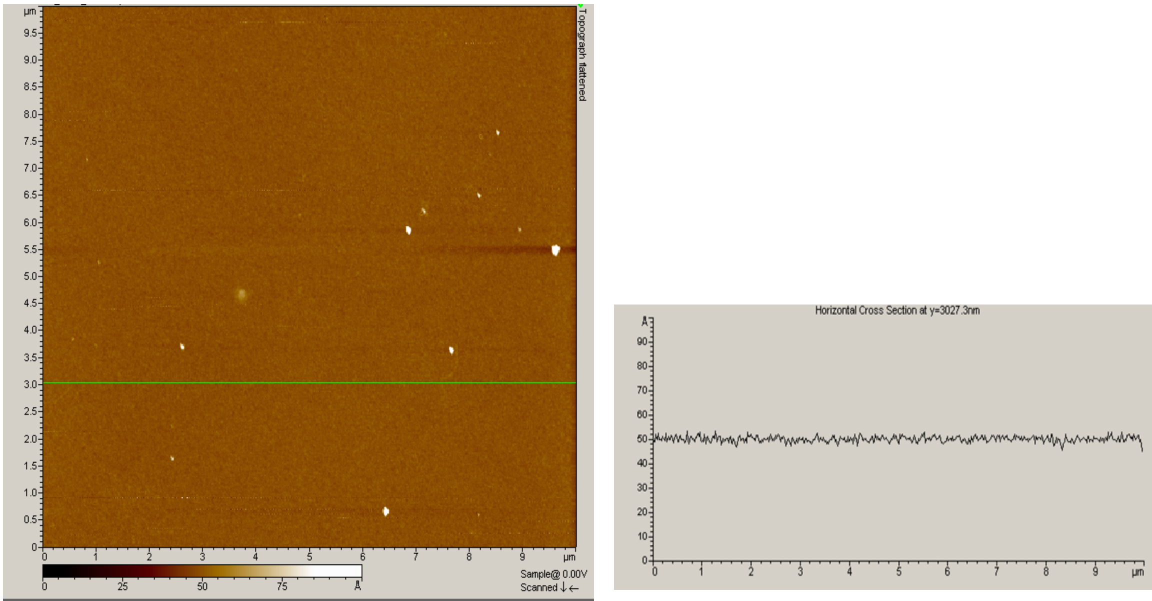

Figure 2-6: AFM image of a scan on 14 nm thick film deposited using $TiCl_4$-H_2O ALD

<u>*Electrical Characterization:*</u> Capacitance-voltage (C-V) and current-voltage (I-V) measurements were performed on the deposited films to estimate the dielectric constant and breakdown voltage of ALD titania films using metal-insulator-metal (MIM) capacitors. These were fabricated by first depositing a 20/500 nm thick Ti/Al film onto the Si substrate by DC sputtering. Al acted as bottom electrode of the capacitor, whereas the Ti film served as an adhesion promoter between the Si substrate and the Al film. Then, TiO_2 of thickness 30 nm was deposited using the ALD process described in section 2.2.1. Au (thickness 300 nm), which was e-beam evaporated on the oxide film and

patterned using a lift off technique, served as the top electrode. This generated MIM parallel plate capacitor structures with electrodes ranging from 25-500 micron squares.

I-V measurements were performed using an HP-4156 Precision Semiconductor Parameter Analyzer and C-V analyses were conducted using a Keithly 550 CV analyzer. The C-V and I-V characteristics of the titania layer were examined by contacting two capacitor top electrodes (of the same size) and using the underlying continuous Al film as a common ground plane. This essentially created a circuit having two capacitors in series as illustrated in figure 2-7.

Figure 2-7: Parallel plate capacitor structure used for electrical characterization

Figures 2-8 and 2-9 show the I-V and C-V plots obtained from measurements on capacitors of different electrode sizes. The combined breakdown voltage was estimated to be 3V. The films demonstrated reasonably low leakage current considering the thickness of the titania layer (30 nm); from figure 2-8a, the leakage current at an applied voltage of 1 V (which corresponds to total field strength of 0.3 MV/cm) is below 1 μA. I-V measurements indicated that the measured leakage current decreased with decreasing electrode size. However, these curves are nearly identical when the measured current data

is normalized by the electrode area (figure 2-8b), demonstrating that the leakage current density is essentially constant across different electrode sizes. The dielectric constant for these films as obtained from the C-V measurements ranged from 102-116.

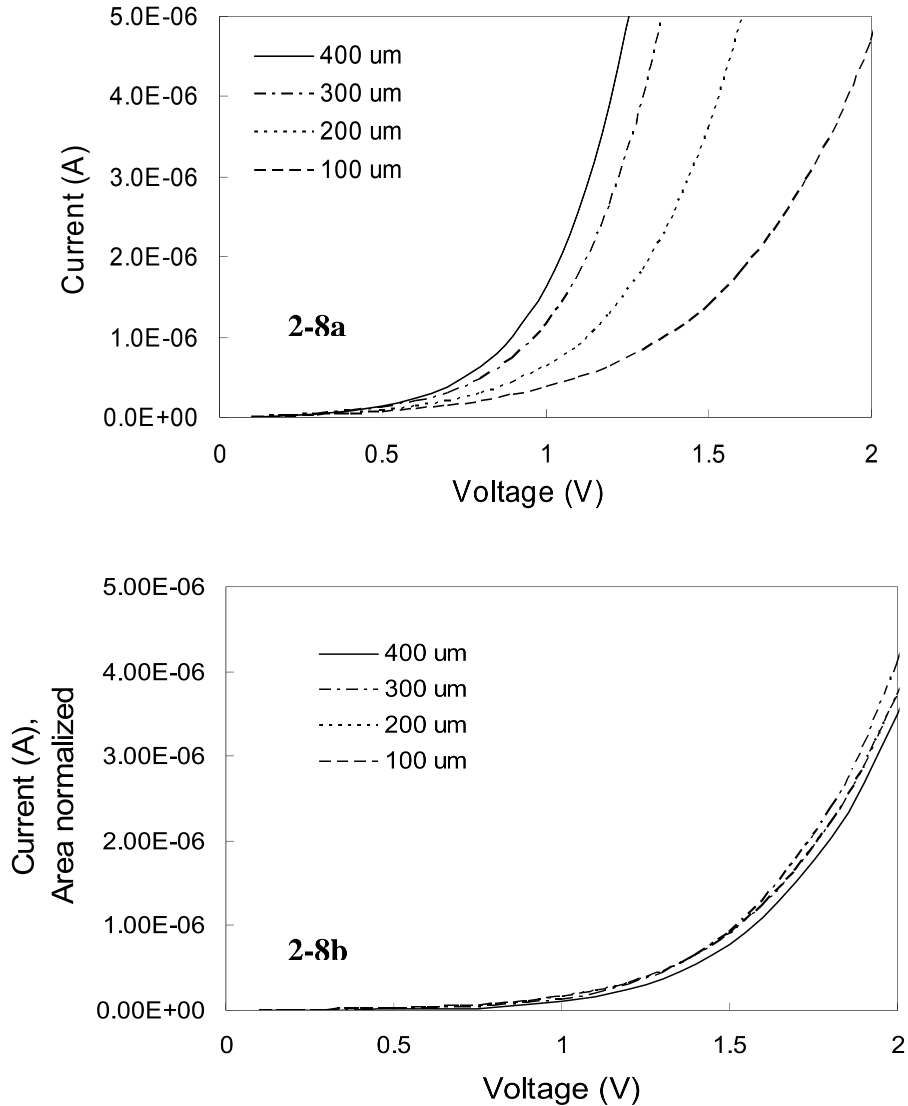

Figure 2-8: (a) I-V characteristic of the parallel plate capacitors (with different electrode size) with ALD titania as the dielectric layer (b) Current (area normalized) versus voltage characteristic

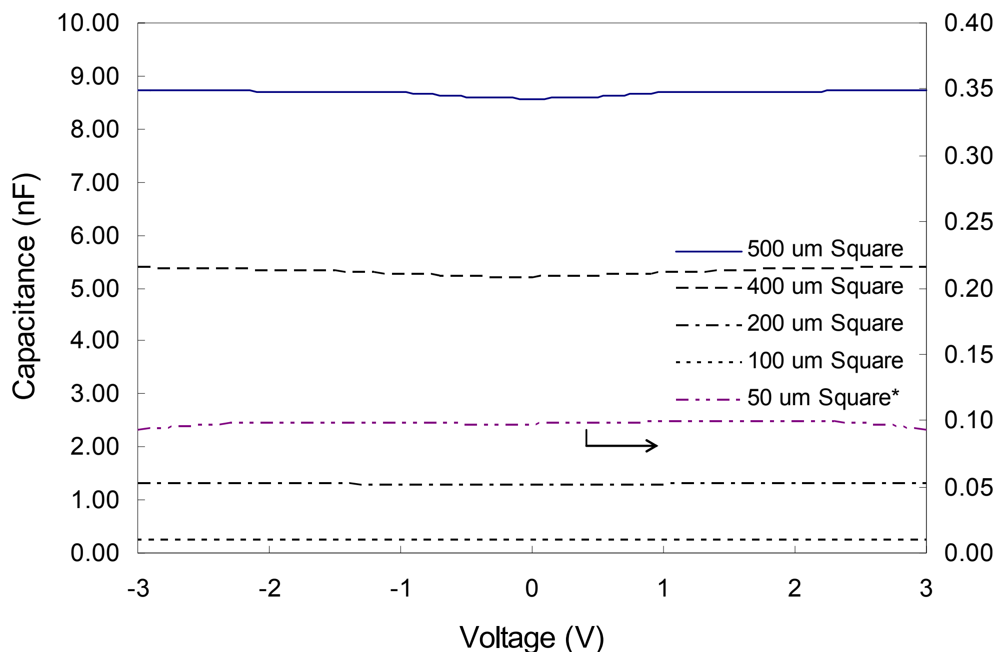

Figure 2-9: C-V plots of the parallel plate capacitors (with different electrode size) made with ALD titania as dielectric layer. Measured capacitance of 50 μm square electrode is plotted on secondary Y-axis for clearer presentation of data.

2.2.3 VERIFICATION OF ALD GROWTH MODE

From previous discussions on the growth mechanism during ALD, we noted that material growth during ALD relies on self saturated surface reactions and thus the thickness of deposited film (at a fixed temperature) varies linearly with the number of ALD cycles. A series of depositions were conducted at varying precursor exposure doses to establish the precursor dose required to achieve saturation of active sites on the surface. The precursor dose can be varied by simply varying the duration of precursor exposure. Figure 2-10 shows the growth rate of TiO_2 films as a function of varying

exposure time for one of the precursors while maintaining a constant exposure time for the other precursor. The data suggest self-saturated reaction and growth of TiO_2 films at precursor exposure times for $TiCl_4$ and water of at least 2.5 s and 2.0 s, respectively at 160°C. Under these conditions, the growth rate of TiO_2 saturates at ~ 0.07 nm per cycle, consistent with results reported previously [8, 9]. Exposure times for $TiCl_4$ and water vapor were thus fixed at 2.5 s and 2.0 s respectively and TiO_2 growth was performed at various numbers of cycles to verify the expected linear dependence of material growth with number of cycles for a true ALD process. Figure 2-11 demonstrates that the TiO_2 film thickness is a linear function of the number of ALD cycles performed. Thus, self-saturated growth and a linear relationship with the number of growth cycles indicate that the above operating conditions provide deposition of TiO_2 in an ALD mode. These results, besides providing a verification of ALD growth mode, also determine the precursor dose required to achieve self saturated growth. Such information assists process design and control, since it is preferable to perform ALD at self saturated conditions because under these conditions, the growth rate is less sensitive to system modification/variation and thereby improves process reproducibility. However there is recent interest in performing ALD processes in a sub-saturation mode so that the duration of the purge step can be reduced.[10] The overall cycle sequence is then optimized to achieve a maximum growth rate on basis of per unit time.

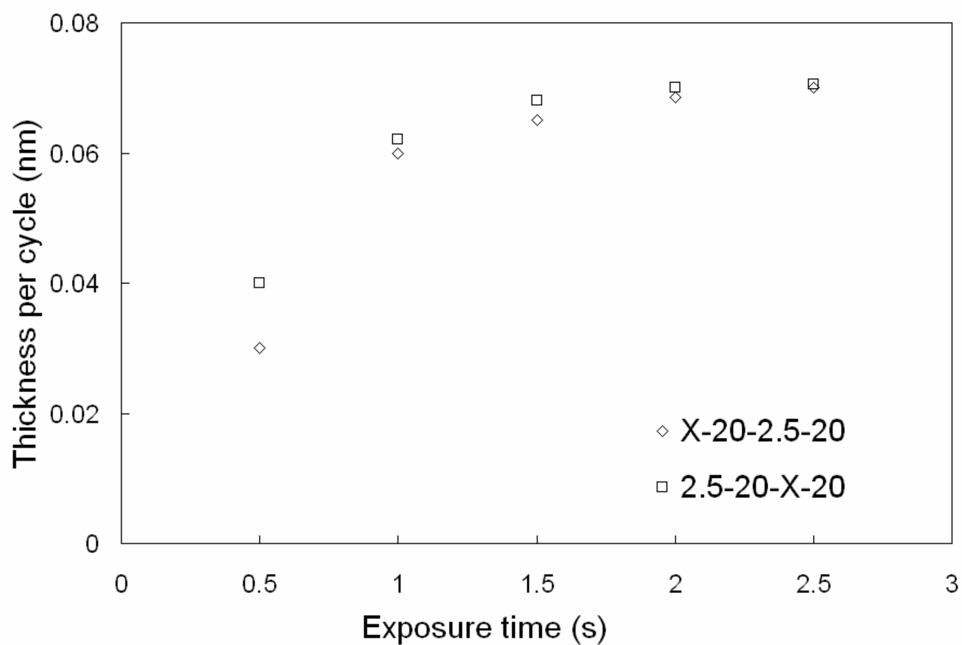

Figure 2-10: Thickness grown per ALD cycle versus exposure time for one of the precursors. The legend format refers to the time duration of each step in the ALD cycle. For example, "X-20-2.5-20" refers to an ALD sequence of (1) X seconds exposure of $TiCl_4$, (2) 20 seconds N_2 purge, (3) 2.5 seconds exposure to water, and (4) 20 seconds N_2 purge. The two different data sets are for varying the (□) water exposure time and the (◊) $TiCl_4$ exposure time.

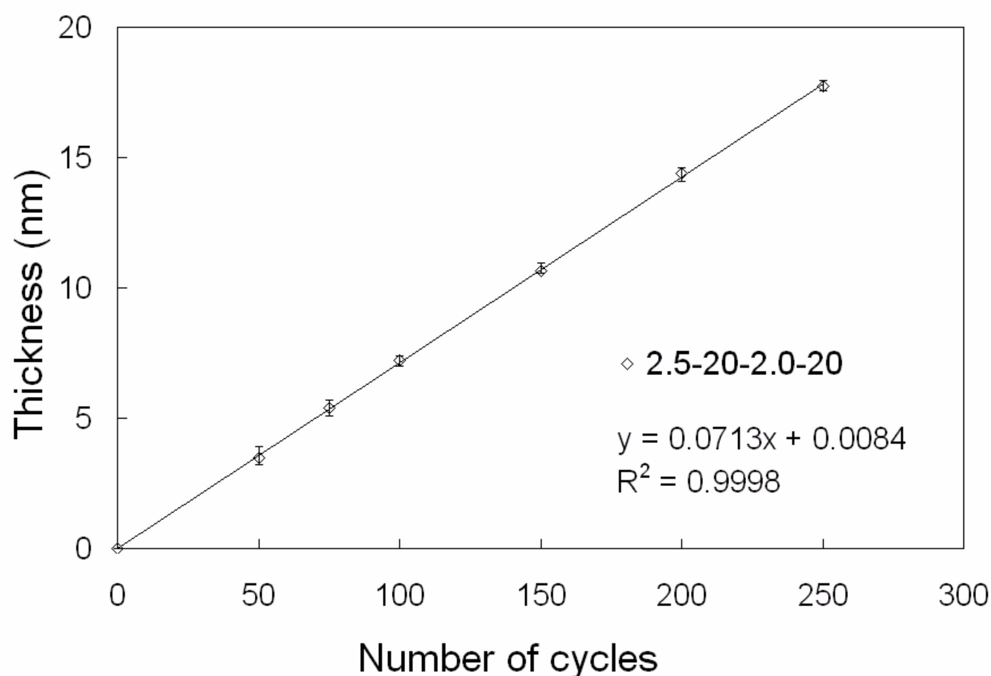

Figure 2-11: Thickness of the TiO_2 film as a function of number of ALD cycles. The linear growth with number of cycles is indicative of an ALD process

2.3 CONCLUSIONS

An ALD reactor system to perform TiO_2 deposition using $TiCl_4$ and H_2O as precursors was designed and fabricated. A clear result of preliminary experiments was that establishing a reactor configuration that offers proper provisions for purging the reactants after each precursor exposure is the key to successful design of ALD reactors. Optimized process parameters and operating conditions to achieve TiO_2 deposition in an ALD mode were determined. At a deposition temperature of 160 ^oC and 1 torr chamber pressure, TiO_2 was deposited at a fixed rate of 0.07 nm per cycle. The resulting films were smooth and free of contaminants. The films demonstrated good electrical properties with high dielectric constant and low leakage current at reasonable field strength.

2.4 REFERENCES

1. Haukka, S.; Lakomaa, E. L.; Root, A., An IR and NMR study of the chemisorption of titanium tetrachloride on silica. *Journal of Physical Chemistry* **1993,** 97, (19), 5085-94.

2. Puurunen, R. L., Formation of metal oxide particles in atomic layer deposition during the chemisorption of metal chlorides. A review. *Chemical Vapor Deposition* **2005,** 11, (2), 79-90.

3. Haukka, S.; Lakomaa, E. L.; Jylha, O.; Vilhunen, J.; Hornytzkyj, S., Dispersion and Distribution of Titanium Species Bound to Silica from Ticl4. *Langmuir* **1993,** 9, (12), 3497-3506.

4. Calistri-Yeh, M.; Kramer, E. J.; Sharma, R.; Zhao, W.; Rafailovich, M. H.; Sokolov, J.; Brock, J. D., Thermal Stability of Self-Assembled Monolayers from Alkylchlorosilanes. *Langmuir* **1996,** 12, (11), 2747-2755.

5. Prabhakaran, K.; Kobayashi, Y.; Ogino, T., Chemically prepared oxides on silicon(001): an XPS study. *Surface Science* **1993,** 290, (3), 239-44.

6. Aarik, J.; Aidla, A.; Uustare, T.; Sammelselg, V., Morphology and structure of TiO2 thin films grown by atomic layer deposition. *Journal of Crystal Growth* **1995,** 148, (3), 268-75.

7. Jill Chastain and Roger C. King, J., *Handbook of X-ray Photoelectron Spectroscopy*. PHI Electronics: 1995.

8. Matero, R.; Rahtu, A.; Ritala, M., In Situ Quadrupole Mass Spectrometry and Quartz Crystal Microbalance Studies on the Atomic Layer Deposition of Titanium Dioxide from Titanium Tetrachloride and Water. *Chemistry of Materials* **2001,** 13, (12), 4506-4511.

9. Aarik, J.; Aidla, A.; Mandar, H.; Uustare, T., Atomic layer deposition of titanium dioxide from TiCl4 and H2O. Investigation of growth mechanism. *Applied Surface Science* **2001,** 172, (1-2), 148-158.

10. Schumacher, M.; Baumann, P. K.; Seidel, T., AVD and ALD as two complementary technology solutions for next generation dielectric and conductive thin-film processing. *Chemical Vapor Deposition* **2006,** 12, (2-3), 99-108.

CHAPTER 3

SELECTIVE ALD USING SELF ASSEMBLED MONOLAYER AS MASKING LAYER

3.1 INTRODUCTION

The concept of using long chain alkyl silanes with a reactive end group as a masking layer for ALD has already been presented in chapter 1. All SAM-based approaches rely on the chemical conversion of sites on the substrate surface which would otherwise be reactive toward ALD precursors into non-reactive form, thus preventing ALD nucleation and growth, and thereby achieving selective ALD on unprotected regions only.

SAM of octadecyltrichlorosilane (OTS) has been previously used to perform selective ALD of ZnO[1]. The authors employed x-ray energy dispersive spectroscopy (XEDS) to evaluate the effectiveness of this SAM in blocking ALD nucleation. Since the sampling depth of XEDS is ~1 μm, the sensitivity of this technique in detecting trace amounts of nucleation on the SAM surface is low. Subsequent studies by Bent and coworkers investigated SAM-based approaches for the selective ALD of HfO_2.[2-4] The authors reported that a SAM of OTS can successfully block ALD nucleation. However, in their studies, only a small number of ALD cycles (50) were investigated. That is, it is possible that during the low number of ALD cycles, the extent of nucleation is not detectable and thus does not represent an accurate assessment of the suitability of SAM-based masking approaches. Studies conducted by Sung and coworker[5, 6] used AFM to probe the patterns obtained using an ASALD process. Because surface analyses were not performed, these

studies do not provide sufficient information to assess the suitability of SAM-based approaches for selective ALD.

Since SAM-based approaches offer some advantages for ASALD, one segment of our initial research focused on the investigation of SAM-based masking approaches for selective ALD. This chapter summarizes the results obtained from those investigations. A variety of SAMs were tested to evaluate the effectiveness of SAM-based masking. Although we could not solve the challenges encountered in this approach, the results offer some insight into the suitability of SAM based ASALD approach.

3.2 SELF ASSEMBLED MONOLAYERS

SAMs of organic molecules have evolved as a new class of thin film materials with exciting prospects for a variety of applications in surface science. SAMs of thiols on gold have been the most widely studied system; however, monolayers of organosilicon compounds such as alkylchlorosilane, alkylalkoxysilane, phenylsilane etc. have also gained significant interest due to their ability to form on a variety of surfaces. Among these organosilicon compounds, SAMs of OTS have received the most attention. This section will review the literature reports on SAMs of OTS.

Solution deposition is a common technique for synthesis of SAMs. This approach involves immersing a cleaned substrate (e.g. Si wafer) in a dilute solution (0.5 mM – 100 mM) of silane compounds for a specified length of time. The trichlorosilane reacts with surface OH groups to produce immobile Si-O-Si linkages with the substrate[7, 8]. Trichlorosilanes are believed to undergo crosslinking among themselves to produce a

network structure. Although the technique appears simple, producing high quality SAMs of alkyltrichlorosilanes is very challenging. There have been conflicting conclusions regarding an optimal recipe for silanizing a surface using OTS. For example, Silberzan et al.[7] reported that 3 min is sufficient for the formation of a monolayer, while Wesserman [9,10] suggested over 24 h and Banga et al.[11] 90 min. Similarly, the content of water in solution and the surrounding atmosphere seem to significantly affect the process. McGovern et al.[12] concluded that 0.15 mg of moisture per 100 mL of solvent is optimum for the formation of closely packed monolayers while Brzoska et al.[13,14] and Parikh et al.[15] reported that performing the synthesis below a transition temperature (32 ^{o}C for OTS) is the most important parameter for producing good quality SAMs. Several other groups have claimed a completely dry environment is required to suppress self-polymerization of silane monomers which leads to poor quality films. However Grunze [16] emphasized that a class 100 clean-room environment is required in order to obtain reproducible, closely packed films.

In addition, there are differing accounts on the mechanism of formation/structure of these surfaces. As shown in figure 3-1, according to Sagiv and Maoz [8], all trichlorosilane chains are attached to each surface OH group, while Angst and Simmons [17]suggested the presence of unreacted OH groups. In contrast, Silberzan et al.[7] proposed that the monolayers are formed on a very thin film of water adsorbed on the substrate surface.

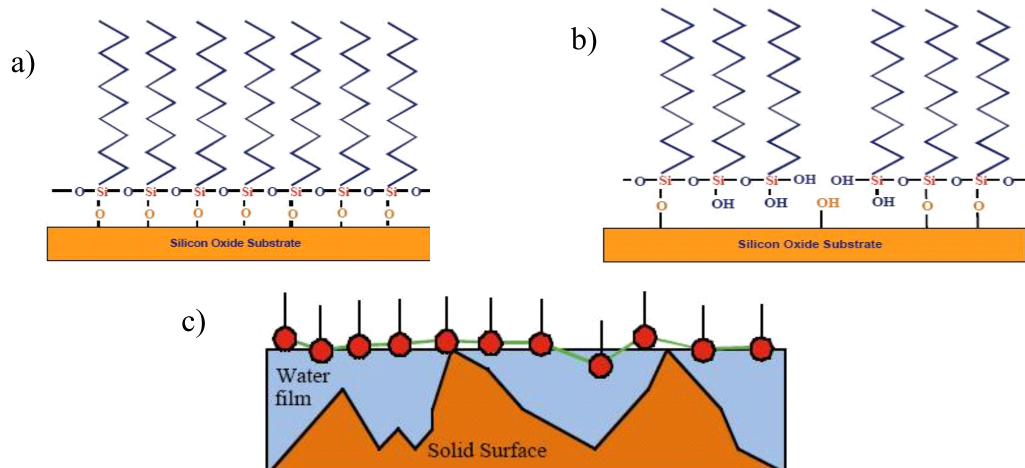

Figure 3-1: Different formation mechanism and structure of OTS SAMs on SiO_2 substrate. a) Sagiv and Maoz; b) Ansgt and Simmons; c) Silberzan et al.

Therefore despite a significant amount of research on SAMs of OTS, little understanding of the exact formation mechanism of these layers is available. SAMs with different anchoring (head) groups such as monochloro, dichloro or alkoxy-silanes have received little attention [18]. Clearly, a standard recipe for the reproducible preparation of SAMs of organosilicon compounds is not yet available.

3.3 MATERIAL SELECTION

A variety of silanes with different anchoring groups and different tail functionalities were tested for their ability to block ALD nucleation. The silanes studied in this work can be divided into two categories.

(a) Nature of anchoring group: The functional group linked to Si in a silane molecule that undergoes reaction with surface moieties on the substrate is termed an anchoring

group. The kinetics of deposition and the surface properties (packing density) of SAMs depend strongly on the nature of the anchoring group [18]. Differences in surface properties can influence the performance of different SAMs as masking layers for ASALD. Thus, silanes having different anchoring groups were investigated to establish the effect of different anchoring groups on the masking performance of specific SAMs. SAMs investigated include: Octadecyltrichlorosilane (OTS) (Gelest), Octadecyldichlorosilane (ODS) (Gelest) and Octadecylmonochlorosilane (OMS) (Gelest). The high reactivity of chlorosilanes can pose problems in controlling the formation of SAMs. Chlorosilane monomers may react with traces of water in the solution and form oligomers which condense on the surface and interfere with formation of well packed monolayers. Thus, failure to control the amount of moisture in solution can lead to the formation of poor quality monolayers. It is expected that less reactive anchoring groups such as alkoxysilanes may not exhibit such problems. Due to the lower reactivity, hydrolysis of alkoxysilane monomers in solution is suppressed, thus enhancing the importance of monomer reactions with the surface. As a result, we also investigated Octadecyltrimethoxysilane (OTMS) (Gelest) as a potential candidate anchoring group.

(b) Nature of tail group: The chemical nature of the tail group directly determines the functional group that will be present on the resulting modified surface. Thus, these groups play a major role in controlling the surface energy or hydrophobicity of the modified surface. The different silane selected have a similar tail group of 18 carbon long alkyl chain; therefore, all modified surfaces have $-CH_3$ groups exposed to ALD precursors. Use of a fluorine terminated tail group will place $-CF_3$ groups on the surface. Presence of fluorinated terminal group makes the resulting surface more hydrophobic,

and thereby reduces the probability of having free hydroxyl groups physisorbed on the surface. Therefore, silanes with fluorinated tail groups may generate better masking layers than will alkyl chain silanes. In order to test this conclusion, Heptadecafluoro-1,1,2,2-tetra-hydrododecyl-trichlorosilane (Gelest) (F-silane) was investigated.

3.4 SILANIZATION PROCEDURE

Si (100) substrates were silanized using a solution deposition method. Sample preparation for silanization included the following steps in sequential order: (1) Rinse substrates in acetone, methanol, IPA, DI water and dry under N_2 (2) Dip substrates in 2M HNO_3 solution for ~ 2h (3) Rinse substrates in DI water and dry under N_2. The samples were then immersed into 5mM solutions of different silanes in anhydrous toluene (Aldrich). The container was then back-filled with N_2, sealed and held at ambient conditions for 40 hrs. After SAM formation, the samples were thoroughly rinsed in toluene and acetone to remove any unreacted silane molecules, and dried under N_2. Samples were stored in ambient environment post SAM formation and they were loaded into ALD reactor after a wait of at least 2h. Since acetone leaves a residue on Si surfaces, samples were rinsed in methanol, IPA, DI water and dried under N_2 before loading them into the reactor.

3.5 CHARACTERIZATION OF SAMS

Contact angle: Water contact angle (WCA) measurements were performed using an AST Products model VCA 2500XE video contact angle system. To measure the contact angle, a 4 μL drop of double distilled water was placed on the sample using a computer-controlled microsyringe. A video capture device recorded the picture of the drop on the surface. Using the outline of the drop, the contact angle was calculated based on the captured image. At least three different points on each sample were measured to determine the average value for WCA. The WCA obtained on different samples is reported in figure 3-2.

Thickness measurement: A V-VASE variable angle spectroscopic ellipsometer (J.A. Woollam Inc.) was used to measure the thickness of the SAM layers. Initially, there was concern that during such long silanization times, the silanes could react with each other in solution and deposit onto the Si substrate as oligomers, thus giving a poor quality SAM. Hence, the primary motivation behind this exercise was to ensure that the sample obtained after silanization is indeed a monolayer. The SAM layers are usually ~2-3 nm in thickness, making ellipsometry measurements challenging. As a result, the ellipsometry measurement for these studies involved more steps than that for the measurements discussed in chapter 2. Four steps were performed to obtain the thickness and refractive index of the SAMs. (1) The ellipsometry parameters, Ψ and Δ, were collected over the wavelength range from 500 nm to 1000 nm at angles of 65º, 70º, and 75º on the bare Si substrate. The Ψ and Δ data were analyzed using the WVASE-32 analysis software (J.A.

Woollam Inc.) by fitting the ellipsometry data using a film stack model composed of a SiO_2 layer for the native oxide and a semi-infinite Si film for the substrate. (2) Thickness is removed from the fit parameter and an n and k data fit was performed. (3) The resulting optical constants (from n&k fit) were then saved as a film stack model. (4) Ellipsometry data were collected on SAM coated substrate in similar wavelength and angle ranges as step 1 and the saved film stack model from step 3 was used as the base substrate while fitting Ψ and Δ obtained in this step (No. 4). A Cauchy model was used as model layer for the SAM.

SAMs of OTS, ODS, OMS displayed a film thickness in the range of 2.4-2.8 nm, which is consistent with the expected monolayer for these silanes[3, 19, 20] suggesting that the silanization procedure produced close to well-packed monolayers. The samples obtained after silanization using fluorinated-silane were rough, causing inconsistent results.

X-ray photoelectron spectroscopy: Chemical analysis of the films and surfaces was performed using x-ray photoelectron spectroscopy (XPS). XPS spectra were collected using a Physical Electronics (PHI) Model 1600 XPS system equipped with a monochromator. The system used an Al Kα source (hν = 1486.8 eV) operating at 350 W beam power. Ejected photoelectrons were detected by a hemispherical analyzer that provided both high sensitivity and resolution. The operating pressure in the sampling chamber was below 5×10^{-9} Torr. Samples were aligned in the beam by maximizing the photoelectron counts corresponding to the primary C1s peak in C—C bonds located at a binding energy of 284.8 eV. A neutralizer beam was used during XPS measurements to

compensate for the shifting of peak locations which occurs due to charging of samples during x-ray exposure. All high resolution spectra were collected with a pass energy of 46.95 eV. The step size and time per step were chosen to be 0.025 eV and 100 ms, respectively. Atomic concentrations of different elements were calculated based on the photoelectron intensities of each element and the elemental sensitivity factors provided by the manufacturer. Samples were scanned at different locations and the peak intensity and composition at different locations were compared to assure uniformity of the film composition over the sample surface. The amount of titanium on the surface is of particular importance in this work; thus, the titanium concentrations were analyzed using the Ti2p3 peak at 458.8 eV (see Figure 4-5) which is characteristic of titanium in TiO_2[21].

Atomic force microscopy: Atomic force microscopy (AFM) using a Digital Instruments Dimension 3100 system with a Nanoscope III controller was used to investigate the morphology and quality of SAMs. All scans were performed in tapping mode using a Si tip (Veeco Nanoprobe) vibrating at a resonance frequency of 100-200 kHz.

3.6 ALD STUDIES ON SAM SURFACES

3.6.1 EFFECT OF ANCHORING GROUP

Depositions were performed on Si substrates silanized using a variety of silanes including OTS, ODS, OMS and OTMS to investigate the masking performance as a

function of anchoring group. After deposition, XPS was performed on each sample and masking performance assessed by the extent of TiO_2 nucleation on the surface (quantified by Ti atomic %). Figure 3-2 shows Ti atomic percent obtained from XPS on different samples after 100 ALD cycles (2s ($TiCl_4$) – 25s (N_2) – 1s (H_2O) – 60s (N_2)).

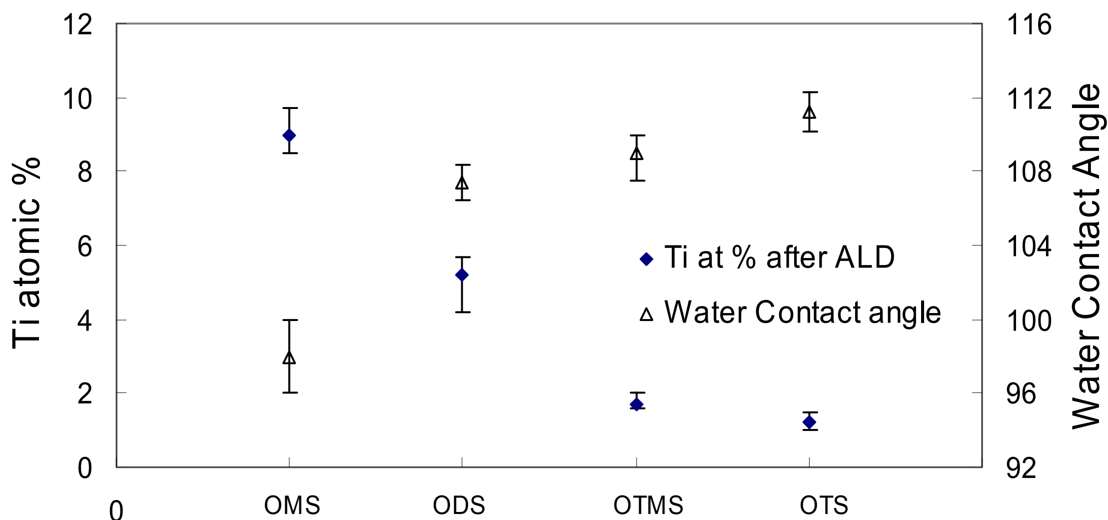

Figure 3-2: Ti atomic% on various SAM surfaces after 100 ALD cycles

In addition, depositions on OTS-SAM coated substrates were also performed for different numbers of ALD cycles. Figure 3-3 compares the Ti2p peak obtained from scans on SAM surfaces after different numbers of cycles and on an unmodified Si substrate.

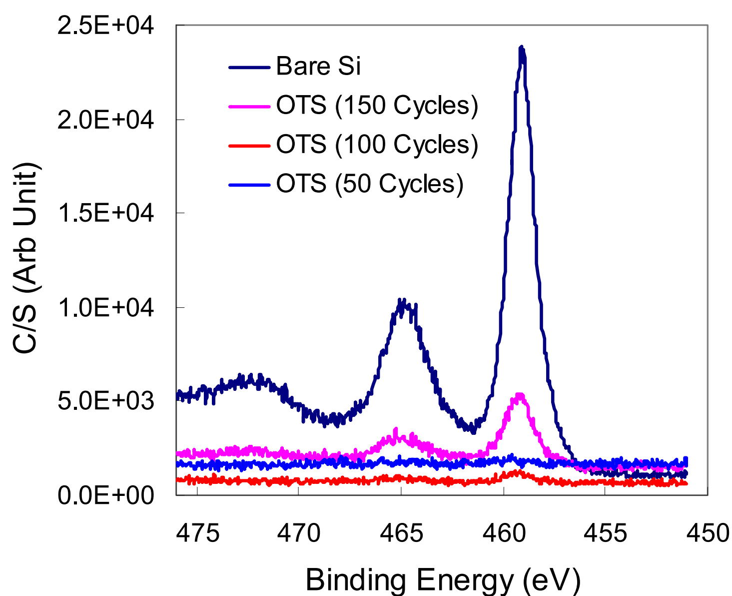

Figure 3-3: Ti2p peak intensity from scans on a bare Si substrate and an OTS-SAM coated substrate after different numbers of ALD cycles.

From figure 3-2 it is evident that although all the SAMs were able to block the ALD nucleation to some extent, none of them could function as a perfect masking material. Interestingly, in the case of OTS-SAM, it was observed that until 50 ALD cycles, the amount of titania nucleation on the SAM-coated surface was negligible (figure 3-3). However, a further increase in the number of deposition cycles resulted in detectable amounts of TiO_2 on the SAM surface, which increased with an increase in number of ALD cycles (~1.0-1.5 atomic% after 100 cycles and 3-4 atomic % after 150 cycles). Further analysis of the data in figure 3-2 indicates the development of an inverse correlation between hydrophobicity of the SAM surface and the extent of nucleation after ALD, i.e. the extent of ALD nucleation decreases with an increase in WCA of the modified surface. However, this trend should not be misinterpreted to conclude that

perhaps extreme hydrophobicity (WCA beyond some threshold) is required to successfully block ALD nucleation on SAM surfaces and consequently ALD nucleation can occur on surfaces with lower WCA even if all the active sites are chemically blocked. We believe that differences in the extent of ALD nucleation on different SAMs is directly linked to differences in their packing density and/or defects in the monolayer. For well-packed SAMs, most of the active –OH sites are blocked whereas the number of unprotected active sites increases with the loss of packing density which also results in lower WCA. Thus, because a higher number of active sites exist on samples with lower WCA, those samples also exhibit poorer masking performance. The significance of packing density on masking ability performance is further strengthened by experiments performed with fluorinated SAMs (discussed later).

At this point, it was still not clear if nucleation occurred on the top of the monolayer or in pinholes/defects present in the monolayer. In order to gain additional insight into this issue, the C1s/Si2p peak area ratio was estimated from XPS data on samples coated with OTS-SAM and different numbers of ALD cycles performed on them. The C1s/Si2p peak area ratio follows the number of ALD cycles: 2.70 (50 cycles), 2.90 (100 cycles) and 3.71 (150 cycles). This trend indicates that TiO_2 nucleates on open Si-OH or Si-O-Si sites and as a result the Si2p photoelectron is attenuated because of the presence of a titania layer which grows during ALD cycles. The thickness of the titania layer increases with the number of ALD cycles causing higher attenuation and a further reduction in Si2p peak intensity. However, no similar layer is formed on the SAM which could lead to attenuation or a drop in intensity for C1s photoelectrons; thus an increase in C1s/Si2p peak area ratio with number of ALD cycles is observed. These results clearly suggest that

titania nucleation occurred on defects/pinholes present in the monolayer and not on monolayer surface.

Calistri-Yeh et al[22]. reported on the thermal instability of OTS-SAM surfaces above 175°C. The authors observed an increase in surface roughness as the OTS-SAM coated substrates were annealed for different times. They concluded that at high temperatures, the silane molecules can rearrange, creating isolated islands of well-packed monolayers which eventually result in increased surface roughness. It is possible that the SAM surfaces in our study also undergo similar changes in morphology and thereby make open up active Si-OH sites during the course of the ALD process. In order to investigate this issue, samples covered with OTS SAMs were annealed for 4h at 160°C (deposition temperature) and AFM scans on samples before and after annealing were compared. Figure 3-4 compares representative AFM scans obtained on both samples. We observed no significant increase in surface roughness on annealed samples, suggesting that the surface does not undergo rearrangement during the course of ALD. In fact, Chen et al[4] have used SAMs of OTS to block ALD of HfO_2 and did not observe any spurious nucleation at temperatures as high as 300 ^{o}C; recently, Kulkarni and co workers[23] also tested the stability of OTS-SAM monolayers on silica surfaces and found them to be stable to 350 ^{o}C. These results suggest that these SAM surfaces are thermally stable and the undesired nucleation observed on SAM surfaces during our experiments arises due to defects present on the original surface.

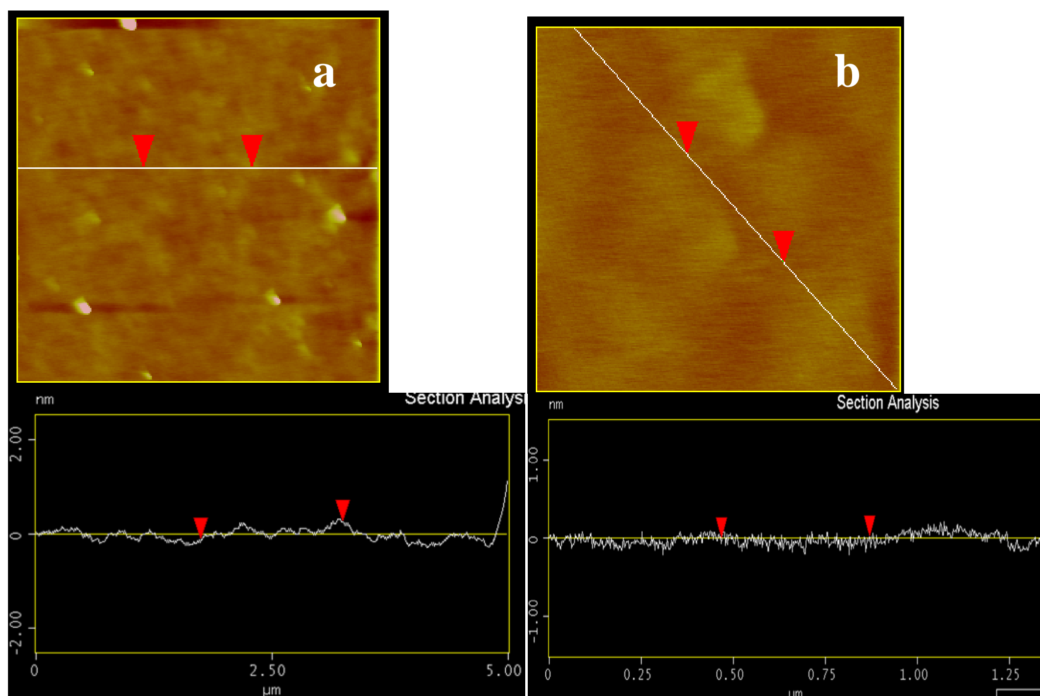

Figure 3-4: AFM images of OTS-SAM surfaces (a) before annealing (b) after annealing.

One interesting observation from results obtained from ALD experiments on OTS SAMs is that although these layers did not completely block the ALD nucleation, they delayed the growth as suggested by an undetectable amount of titania deposited until first 50 cycles. Thus, the SAM-based masking approach can still be implemented for applications where a very thin layer of deposited film is required. After the ALD reactions initiates (at defects), the deposited material continues to grow during subsequent ALD cycles and slowly these islands will merge to completely cover the SAM surface. Beyond this stage, titania will grow on both regions (originally protected or unprotected) at similar rates. Thus even with such a scenario, a relief image of an ALD film can be fabricated.

3.6.2 EFFECT OF TAIL GROUP

Depositions on Si substrates modified with F-silane were performed to assess their masking ability and investigate the effect of more hydrophobic tail groups on masking performance. Samples were prepared using the procedure described in section 3.4. Unlike silane solutions of alkyl chain silanes, the solution of F-silane turned cloudy during the course of the silanization process suggesting self reaction of silane molecules to form particles. Indeed, particles were also found attached to the substrate after removal from the silane solution. The particles could not be removed during the rinse step; however, they could be easily removed by wiping the samples with Kim-wipes soaked in toluene. Although Si substrates coated with F-silane showed a high WCA of 118°-120°, they demonstrated poor masking performance with 9-12 atomic % Ti after 100 ALD cycles. The high level of ALD nucleation on F-silane SAMs can easily be explained by an inferior packing density of the resulting monolayer. Figure 3-5 shows an AFM image of F-silane SAM surface. The surface has high roughness (RMS roughness ~3 nm) and is certainly not an ordered monolayer. These results clearly indicate that the packing density of a SAM is a more important criterion than the WCA in determining the masking performance of SAM surfaces.

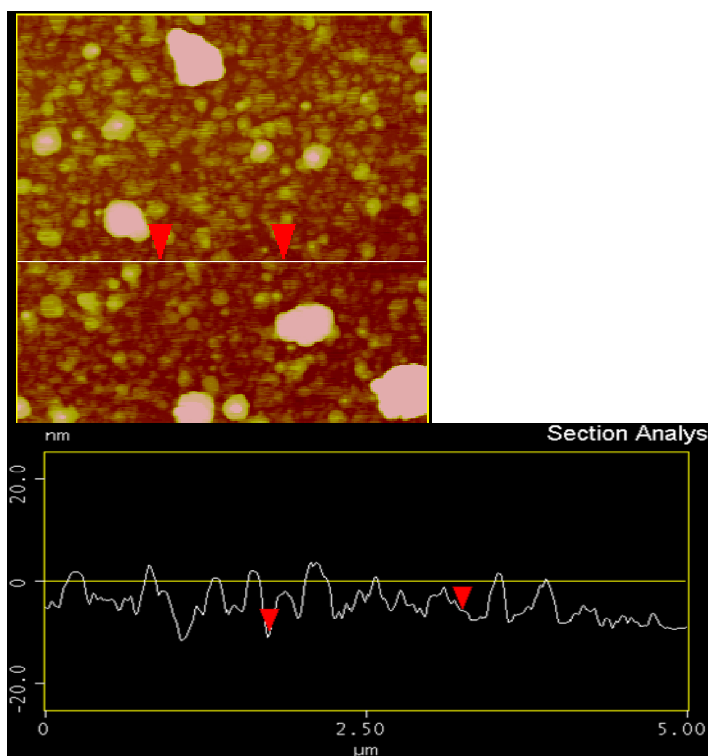

Figure 3-5: AFM image of a F-silane SAM surface

3.7 CONCLUSIONS

SAMs of different silanes were prepared on Si surfaces and tested for their ability to prevent ALD nucleation. OTS-SAM demonstrated the best performance but the silanization scheme was still not successful in blocking all the active sites on the substrate and produced monolayers containing defects/pinholes on the surface. As a result, the reactive titanium precursor eventually found an unprotected reactive silanol site on the silicon surface and reacted to initiate the ALD reaction sequence in that area. The results suggested that the packing density of SAMs plays a critical role in determining the

masking performance of any SAM-based masking approach. However, achieving a well packed monolayer free of defects/pinholes is extremely challenging and may not be possible, at least for high volume manufacturing.

3.8 REFERENCES

1. Yan, M.; Koide, Y.; Babcock, J. R.; Markworth, P. R.; Belot, J. A.; Marks, T. J.; Chang, R. P. H., Selective-area atomic layer epitaxy growth of ZnO features on soft lithography-patterned substrates. *Applied Physics Letters* **2001,** 79, (11), 1709-1711.

2. Chen, R.; Kim, H.; McIntyre, P. C.; Bent, S. F., Self-assembled monolayer resist for atomic layer deposition of HfO2 and ZrO2 high-k gate dielectrics. *Applied Physics Letters* **2004,** 84, (20), 4017-4019.

3. Chen, R.; Kim, H.; McIntyre, P. C.; Bent, S. F., Investigation of self-assembled monolayer resists for hafnium dioxide atomic layer deposition. *Chemistry of Materials* **2005,** 17, (3), 536-544.

4. Chen, R.; Kim, H.; McIntyre, P. C.; Porter, D. W.; Bent, S. F., Achieving area-selective atomic layer deposition on patterned substrates by selective surface modification. *Applied Physics Letters* **2005,** 86, (19), 191910/1-191910/3.

5. Park, M. H.; Jang, Y. J.; Sung-Suh, H. M.; Sung, M. M., Selective Atomic Layer Deposition of Titanium Oxide on Patterned Self-Assembled Monolayers Formed by Microcontact Printing. *Langmuir* **2004,** 20, (6), 2257-2260.

6. Lee, J. P.; Sung, M. M., A New Patterning Method Using Photocatalytic Lithography and Selective Atomic Layer Deposition. *Journal of the American Chemical Society* **2004,** 126, (1), 28-29.

7. Silberzan, P.; Leger, L.; Ausserre, D.; Benattar, J. J., Silanation of silica surfaces. A new method of constructing pure or mixed monolayers. *Langmuir* **1991,** 7, (8), 1647-51.

8. Maoz, R.; Sagiv, J., On the formation and structure of self-assembling monolayers. I. A comparative ATR-wettability study of Langmuir-Blodgett and adsorbed films on flat substrates and glass microbeads. *Journal of Colloid and Interface Science* **1984,** 100, (2), 465-96.

9. Wasserman, S. R.; Tao, Y. T.; Whitesides, G. M. *Structure and reactivity of alkylsiloxane monolayers formed by reaction of alkyltrichlorosilanes on silicon substrates*; Dep. Chem.,Harvard Univ.,Cambridge,MA,USA.: 1989; p 120 pp.

10. Wasserman, S. R.; Tao, Y. T.; Whitesides, G. M., Structure and reactivity of alkylsiloxane monolayers formed by reaction of alkyltrichlorosilanes on silicon substrates. *Langmuir* **1989,** 5, (4), 1074-87.

11. Banga, R.; Yarwood, J.; Morgan, A. M.; Evans, B.; Kells, J., FTIR and AFM Studies of the Kinetics and Self-Assembly of Alkyltrichlorosilanes and (Perfluoroalkyl)trichlorosilanes onto Glass and Silicon. *Langmuir* **1995,** 11, (11), 4393-9.

12. McGovern, M. E.; Kallury, K. M. R.; Thompson, M., Role of Solvent on the Silanization of Glass with Octadecyltrichlorosilane. *Langmuir* **1994,** 10, (10), 3607-14.

13. Brzoska, J. B.; Azouz, I. B.; Rondelez, F., Silanization of Solid Substrates: A Step Toward Reproducibility. *Langmuir* **1994,** 10, (11), 4367-73.

14. Brzoska, J. B.; Shahidzadeh, N.; Rondelez, F., Evidence of a Transition-Temperature for the Optimum Deposition of Grafted Monolayer Coatings. *Nature* **1992,** 360, (6406), 719-721.

15. Parikh, A. N.; Allara, D. L.; Azouz, I. B.; Rondelez, F., An Intrinsic Relationship between Molecular-Structure in Self-Assembled N-Alkylsiloxane Monolayers and Deposition Temperature. *Journal of Physical Chemistry* **1994,** 98, (31), 7577-7590.

16. Bierbaum, K.; Grunze, M., Preparation and characterization of thin organosilane films on oxidized substrates - A surface analysis approach. *Adhesion Society, Proceedings of the Seventeenth Annual Meeting and the Symposium on Particle Adhesion -- Orlando, Fla., Feb. 20-23, 1993* **1994**, 213-21.

17. Angst, D. L.; Simmons, G. W., Moisture absorption characteristics of organosiloxane self-assembled monolayers. *Langmuir* **1991,** 7, (10), 2236-42.

18. McCoY, K. M., *PhD Dissertation,* Georgia Institute of Technology **2004**.

19. Balgar, T.; Bautista, R.; Hartmann, N.; Hasselbrink, E., An AFM study of the growth kinetics of the self-assembled octadecylsiloxane monolayer on oxidized silicon. *Surface Science* **2003,** 532, 963-969.

20. Ulman, A., Formation and Structure of Self-Assembled Monolayers. *Chemical Reviews (Washington, D. C.)* **1996,** 96, (4), 1533-1554.

21. Jill Chastain and Roger C. King, J., *Handbook of X-ray Photoelectron Spectroscopy*. PHI Electronics: 1995.

22. Calistri-Yeh, M.; Kramer, E. J.; Sharma, R.; Zhao, W.; Rafailovich, M. H.; Sokolov, J.; Brock, J. D., Thermal Stability of Self-Assembled Monolayers from Alkylchlorosilanes. *Langmuir* **1996,** 12, (11), 2747-2755.

23. Kulkarni, S. A.; Mirji, S. A.; Mandale, A. B.; Vijayamohanan, K. P., Thermal stability of self-assembled octadecyltrichlorosilane monolayers on planar and curved silica surfaces. *Thin Solid Films* **2006,** 496, (2), 420-425.

CHAPTER 4

AREA SELECTIVE ATOMIC LAYER DEPOSITION: USE OF POLYMER FILM BASED MASKING LAYERS

4.1 INTRODUCTION

In chapter 3 we investigated the use of OTS and other SAMs as surface modifying agents for the area selective ALD of titania onto silicon surfaces. In those studies, titania was deposited using alternating cycles of water and titanium tetrachloride. The results indicated that during the first 50 cycles of titania deposition, nucleation of TiO_2 on the SAM surface was undetectable as measured using x-ray photoelectron spectroscopy (XPS). However, a further increase in the number of deposition cycles resulted in detectable amounts of TiO_2 (~1.0-1.5 atomic% after 100 cycles and 3-4 atomic % after 150 cycles) on the SAM surface. This led to the conclusion that the silanization scheme was not successful in blocking all the active sites on the substrate and produced monolayers that contained defects/pinholes on the surface. The reactive titanium precursor eventually finds an unprotected reactive silanol site on the silicon surface and reacts to initiate the ALD reaction sequence in that location. Previous studies [1-3] that have investigated the mechanism of SAM formation have also reported extraordinary difficulties and challenges associated with obtaining a "defect free" monolayer. This difficulty with defectivity and undesired nucleation, coupled with the facts that SAM deposition is time consuming and the high resolution patterning of SAMs is not a well

established practice, pose serious limitations on the successful use of SAMs as masking layers for area selective ALD.

A masking approach where the surface modification step is simple, rapid, and produces a defect free layer would address the various limitations encountered with a SAM-based masking approach. One method to achieve these requirements involves the use of polymer thin films as making layers, since unlike SAMs, polymers can be quickly and easily spin coated to obtain defect free thin films. This fact is of course exploited extensively in almost all modern microlithography processes. Furthermore, a significant amount of research has been invested in developing a variety of different polymeric materials and processes for the high resolution patterning of polymer films. Materials and processes exist for patterning a range of polymers including materials based on novolac, poly(hydroxystrene), poly(norbornene), poly(methylmethacrylate), polyimides, and polycarbonates. Thus, if a polymer or class of polymers can be identified that can prevent the nucleation and growth of a material on its surface during ALD and which can be patterned lithographically, such a process might offer a better alternative as a masking scheme for area selective ALD compared to SAM-based approaches. After the ALD is completed, the polymer masking layer could be removed using methods currently invoked to strip resist films after plasma etching, and thereby obtain a direct patterned structure of the desired ALD film. A sequence illustrating ASALDT based on polymer films as making layer is presented in figure 4-1.

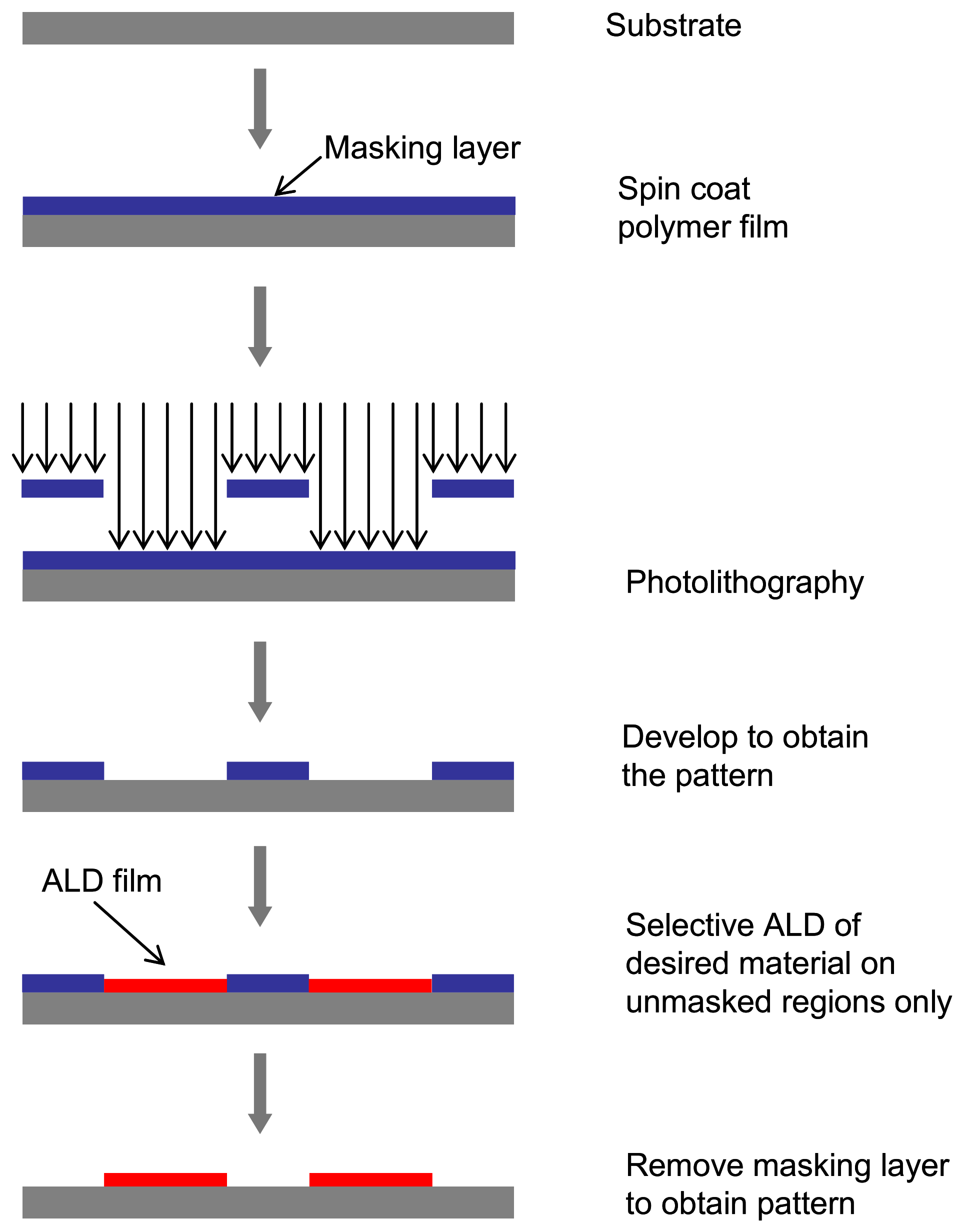

Figure 4-1: Schematic illustration of polymer masking based ASALDT

Davazoglou and co-workers [4, 5] have previously reported the use of polymeric masks (PMMA and AZ 5214 photoresist) to achieve selective deposition of Cu lines on a tungsten-coated Si substrate using 1.5-cyclooctadiene-Cu(I)-hexafluoroacetylacetonate as

a single precursor for copper CVD. Deposition of metal oxide films by ALD often includes water as an oxygen source and may involve highly reactive halides as metal precursors. Thus, finding a polymer system which can successfully serve as a masking layer for area selective deposition of metal oxides could be challenging. A variety of issues such as the chemical functionality and reactivity of the polymer, uptake of water and metal precursor by the polymer, the presence of remnant precursor in the polymer masking film after the purge cycle, and the diffusion of ALD precursors though the polymer masking film can all affect the selective ALD deposition process. In this chapter we describe the successful use of a conventional resist material (PMMA) to obtain the direct patterned deposition of TiO_2 films using $TiCl_4$ and water as ALD precursors. Furthermore, we discuss how the phenomena mentioned above will affect the prospects for the development of a polymer masking-based area selective ALD process.

4.2 MATERIALS AND METHODS

4.2.1 PREPARATION OF POLYMER FILM

A variety of polymer films were tested in this study for their performance as masking layers for selective ALD deposition. The different polymers included: Teflon AF (*Dupont*), polymethylmethacrylate (PMMA) (*Mw: 54,000, Scientific Polymer*), polystyrene (PS) (*Mw: 1.57 Million, Scientific Polymer*), polyhydroxystyrene (PHOST) (*Mw: 11,800, TriQuest*) and bis-trifluoromethyl carbinol substituted polynorbornene (i.e. hexafluoroalcohol-substituted polynorbornene or HFA-PNB) (*Mw: 13,400, Promerus*).

The polymers have been chosen on the basis of their different chemical and physical properties. Toluene was used as a casting solvent for PMMA and PS, PGMEA was used as casting solvent for PHOST and HFA-PNB whereas Teflon-AF was received from the vendor is solution form. All films were spin coated onto Si wafers using a CEE model 100CB spin coater and soft baked (except Teflon AF and HFA-PNB) for 4 minutes at a temperature 5°C greater than their glass transition temperature (T_g). HFA-PNB was soft-baked for 4 minutes at 105 ^{o}C. Following this treatment, samples were placed in a vacuum oven overnight at 90-100 ^{o}C to ensure that there was little residual solvent left in the films. Teflon AF films were cured under a N_2 environment at 100 ^{o}C for 5 minutes, 150 ^{o}C for 5 minutes and 225 ^{o}C for 25 minutes.

4.2.2 FILM THICKNESS MEASUREMENT

Film thicknesses of polymer films were measured using spectroscopic ellipsometry. Spectroscopic ellipsometry measurements were performed with an M-2000 ellipsometer (J.A. Woollam Co. Inc.). Ellipsometry data were collected over a wavelength range from 400 to 1000 nm at angles 65°, 70° and 75° (with respect to normal to the plane of substrate). Data were analyzed and fit to determine the film thickness and refractive index using the WVASE-32 software (J.A. Woollam Co.) by employing a Cauchy model for the films and using a standard silicon substrate library data file.

4.2.3 X-RAY PHOTOELECTRON SPECTROSCOPY (XPS) FOR FILM COMPOSITION

Chemical analysis of the films and surfaces was performed using x-ray photoelectron spectroscopy (XPS). XPS spectra were collected using a Physical Electronics (PHI) Model 1600 XPS system equipped with a monochromator. The system used an Al Kα source (hν = 1486.8 eV) operating at 350 W beam power. Ejected photoelectrons were detected by a hemispherical analyzer that provided both high sensitivity and resolution. The operating pressure in the sampling chamber was below 5×10^{-9} Torr. Samples were aligned in the beam by maximizing the photoelectron counts corresponding to the primary C1s peak in C—C bonds located at a binding energy of 284.8 eV. A neutralizer beam was used during XPS measurements to compensate for the shifting of peak locations which occurs due to charging of samples during x-ray exposure. All high resolution spectra were collected with a pass energy of 46.95 eV. The step size and time per step were chosen to be 0.025 eV and 100 ms, respectively. Atomic concentrations of different elements were calculated based on the photoelectron intensities of each element and the elemental sensitivity factors provided by the manufacturer. Samples were scanned at different locations and the peak intensity and composition at different locations compared to assure uniformity of the film composition over the sample surface. The amount of titanium on the surface is of particular importance in this work; thus, the titanium concentrations were analyzed using the Ti2p3 peak at 458.8 eV (see Figure 4-5) which is characteristic of titanium in TiO_2[6].

4.3 ALD GROWTH STUDIES ON POLYMER FILMS

Various polymer films were prepared as described previously and ALD deposition sequences were conducted at the same temperature and chamber pressure described for the initial ALD growth tests. During the experiments involving SAMs, it was necessary to increase the purge time after each water pulse to 1 minute. Therefore, this same 1 minute purge after each water pulse was initially used in the polymer masking experiments in order to directly compare the polymer masking results with the results from the SAM coated surfaces. Following these initial experiments, the growth selectivity or "growth contrast" on these polymer films as a function of purge time was also studied in detail.

In order to design the best polymeric masking layers for area selective ALD, it is important to develop a fundamental understanding of the parameters that affect the process of selective ALD. Some issues which could be critical include: (1) chemical functionality and reactivity of the polymer with the precursors, (2) reagent sorption and retention in the polymer film, and (3) thickness of the polymer masking layer and diffusion rate of reagents into and through the film. The following sections describe results of experiments performed to investigate each of these issues.

4.3.1 CHEMICAL FUNCTIONALITY AND REACTIVITY OF THE POLYMER

The intrinsic reactivity of a polymer towards the metal precursor and oxidizer is very important. In the case of processes involving water, many polymers that may be

considered as platforms for the development of photodefinable ALD masking layers should show little reactivity with respect to water. However, if the polymer has reactive sites that can react with the metal precursor, then after the metal precursor begins to deposit on the polymer it is expected that this would nucleate growth of a conformal metal oxide layer on the polymer in addition to the exposed regions of the substrate. Such a conformal metal oxide coating over the polymer masking layer would make it difficult for the stripping solvent to penetrate into the polymer mask and remove it from the substrate without leaving residue or causing defects in the deposited oxide patterns. Many conventional resist polymers contain either oxygen or hydroxyl groups. Both of these species could be problematic in terms of their reactivity with highly reactive metal precursors such as $TiCl_4$. Therefore, our initial experiments were designed to screen for the general impact of the inclusion of oxygen and hydroxyl sites in a polymer on the polymer's ability to inhibit ALD on the polymer surface

Figure 4-2 presents the Ti atomic % on different polymer sample surfaces after 100 deposition cycles for TiO_2. PS contains only carbon and hydrogen and as expected does not show nucleation or growth of TiO_2 on its surface. It is encouraging that in the case of PS, it does not appear that absorption and subsequent reaction of remnant precursors in the polymer lead to spurious growth on the polymer. Teflon-AF and PMMA, both contain oxygen and thus it might be anticipated that reactions could occur between $TiCl_4$ and the polymer. Fortunately, both PMMA and Teflon-AF show very low levels, 1.1 atomic % and 0.4 atomic % respectively, of titania growth on their surface. In addition to differences in the manner in which oxygen is bonded into these polymers, PMMA is significantly more hydrophilic than Teflon-AF and thus the ability of PMMA to absorb

and retain water is expected to be much higher than Teflon-AF. This hydrophilicity difference may also contribute to the greater deposition on the PMMA surface as compared to Teflon-AF. The final two polymers, HFA-PNB and PHOST, are both model materials for chemically amplified photoresist materials which contain hydroxyl functional groups. It might be expected that the presence of hydroxyl groups on the polymer would cause substantial reactions with the $TiCl_4$ precursor that would lead to ALD on the polymer surface. Although both of these polymers contain hydroxyl groups and exhibit higher levels of titania deposition on their surface as compared to the non-hydroxyl functionalized polymers, it is interesting to observe that HFA-PNB performs significantly better than PHOST as a masking layer for preventing TiO_2 nucleation. In the case of HFA-PNB only 3-4% Ti is observed after 100 cycles, whereas TiO_2 nucleates easily on PHOST films and quickly grows a conformal film.

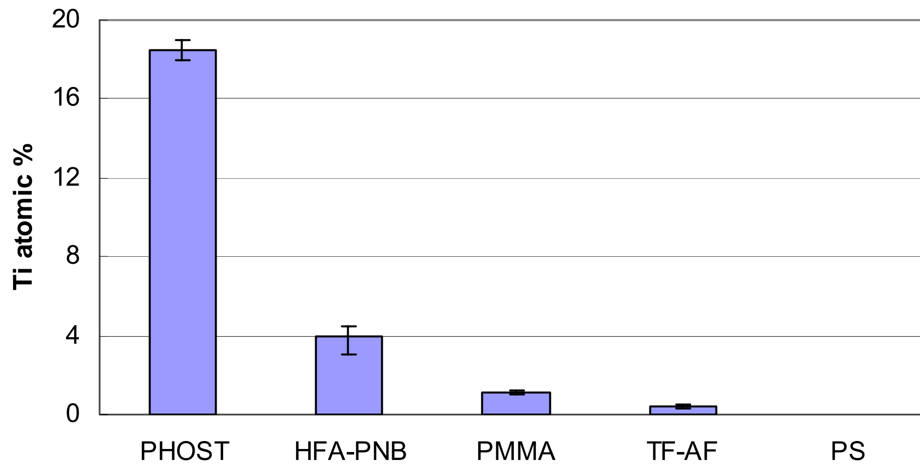

Figure 4-2: Ti atomic % on different polymers after 100 cycles, the pulse sequence is 2s-25s-1s-60s

The results for the model photoresist polymers can be attributed to their specific chemical and physical structures. First, PHOST showed higher Ti content on its surface as compared to HFA-PNB samples when both polymers were exposed to 100 pulses of $TiCl_4$ only (i.e. no water exposure, please refer to Figure 4-3). This suggests that the OH group in PHOST has a higher reactivity towards $TiCl_4$ than the OH group in HFA-PNB. The lower reactivity can be due to at least two factors. The CF_3 groups in HFA-PNB polymer backbone are highly electronegative, thus rendering the attached OH group in HFA electron deficient. The lower electron density in the OH oxygen reduces its ability to share an electron with the electrophilic $TiCl_3$ to favor the formation of O—$TiCl_3$ bond which is a Lewis acid-Lewis base reaction. The bulky CF_3 groups surrounding the OH group in HFA can also sterically hinder access to the OH group in HFA-PNB and may add to its reduced reactivity. Second, PHOST has a higher equilibrium water uptake than HFA-PNB. Thus, it is possible that the additional water absorption in PHOST may lead to higher levels of remnant water in the PHOST films after each water pulse and purge cycle. This remnant water can serve as a potential reactive site in the polymer film and lead to increased nucleation of TiO_2 on PHOST films.

4.3.2 Effect of Remnant Water in the Polymer Film

As suggested in the previous section, all polymers absorb some finite amount of water. Depending upon the values of the diffusivity of water and the equilibrium water uptake in each polymer, different polymers will possess different concentrations of remnant water inside the film after a given purge time. The water present inside the film

or on the surface can allow nucleation of TiO_2 by reacting with the $TiCl_4$ precursor during $TiCl_4$ pulses. Thus, it is important to determine if remnant water appears to play any role in the observed ALD masking performance of the polymers tested in this study. This factor can be very important in deciding the importance of selecting polymers with appropriate diffusivities and equilibrium precursor solubilities as well as the appropriate purge time required during the selective ALD process for a given polymer. In order to investigate this effect, ALD was performed on different polymer substrates while the length of the purge time after a water pulse was varied.

Figure 4-3 shows the Ti atomic % for different polymers at two different purge times. It is observed that increasing the purge time from one minute to two minutes significantly affects the amount of Ti deposited on HFA-PNB, but the effect is marginal in the case of PMMA. PMMA has lower equilibrium water uptake than does HFA-PNB and thus it appears that the required purge time to achieve the best selectivity for any given polymer could relate in part to the equilibrium water uptake of the polymer films. It is also observed that the Ti content on the PMMA sample for the 2 minutes purge case is very similar to what is observed when the PMMA sample was exposed to 150 cycles of $TiCl_4$ only (i.e -2 s ($TiCl_4$) -25 s (Purge)-). Thus it can be concluded that while using PMMA as a mask for selective ALD processes, a purge time of ~ 1-2 minutes is sufficient to eliminate the effect of remnant water in the sample. It is important to revisit the results from the PS case, where almost no Ti was detected. It can be inferred that the purge time of 1 minute was sufficient to remove the absorbed water in the film, which could have caused the TiO_2 to nucleate despite the absence of reactive sites in the polymer backbone. These results indicate that the presence of remnant water does appear to play an

important role in determining the performance of a masking layer, but by choosing polymers with low water absorption or by choosing sufficiently large purge times, the impact of remnant water can be minimized.

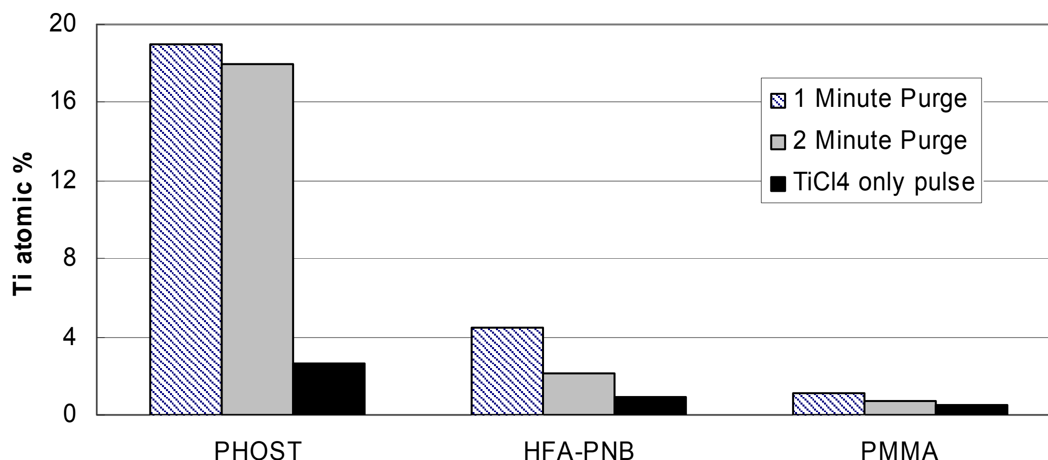

Figure 4-3: Ti atomic % on different polymers at different purge time after water pulse and for $TiCl_4$ only case; pulse sequence is, diagonal stripes: -2s-25s-1s-60s-, grey: -2s-25s-1s-120s-, black: -2s-25s-

4.3.3 THICKNESS OF THE MASKING LAYER

In addition to either reacting directly with the polymer or with remnant precursor absorbed into the polymer masking layer, the possibility that the ALD precursors can also diffuse through the entire polymer masking layer and react directly with the substrate surface must be considered. Unlike previous efforts in which SAMs were used to passivate reactive surface functional groups by chemically reacting them with the SAM, the polymer coatings in this work do not directly react with the substrate surface but instead simply physically coat the surface. While this permits the polymer films to

be easily removed from the surface after deposition, it also means that reactive surface functional groups still exist at the bottom of the protective polymer masking layer. Therefore, in the case of the titania deposition described in this work, if the $TiCl_4$ precursor has sufficient time to diffuse through the polymer film and reach the silicon substrate, it will react with surface hydroxyl species and nucleate growth of titania below the polymer film. Then, if water also has sufficient time to diffuse through the polymer film during its cycle, titania growth will occur at the substrate surface below the polymer coating. Two factors are extremely important in preventing this behavior. First, the distance over which a penetrant molecule can diffuse in the polymer film in a given time period depends on its diffusion coefficient in the polymer. Therefore, combinations of polymers and precursors which have low diffusivities for the precursor in the polymer are advantageous in reducing the impact of this problem. Second, the amount of time that the precursor is exposed to the substrate during each deposition cycle is also important since it controls the time scale for diffusion of the precursor to the substrate surface. Therefore, it is best to utilize precursor exposure cycle times which are as short as possible while still maintaining well-controlled ALD growth. All of this translates into the fact that for a given precursor-polymer combination and a specific ALD cycle time sequence, the thickness of the masking layer becomes the controlling parameter which determines if the polymer film can prevent unwanted growth of ALD material on the substrate beneath the polymer.

In order to investigate this issue, a series of depositions were conducted on PMMA samples of different thicknesses and possible titania growth under the polymer film was assessed. After 100 ALD cycles (2s($TiCl_4$)-25s(N_2)-1s(H_2O)-60s(N_2)), the polymer film

was removed using acetone and the underlying substrate surfaces analyzed by XPS. First, it was observed in the case of thicker PMMA films (180 and 420 nm) that the films were removed easily by dipping the samples in acetone and then thoroughly rinsing them with acetone, methanol and de-ionized (DI) water. However, with thinner films (32, 56, and 103 nm) it was necessary to assist the removal process by physically wiping the film off the substrate in the presence of the solvent. It has been previously reported that PMMA can strongly interact with silica surfaces, and that this interaction can lead to physical property changes in ultra-thin PMMA films[7, 8]. However, the difficulty in removal of the polymer film is not simply the result of thin film effects on the dissolution behavior of the PMMA film. Solvent removal of PMMA films at all thicknesses was possible using acetone prior to sample exposure to $TiCl_4$. Instead it is believed that two phenomena are responsible for this observed difficulty in removing the thinner PMMA films: (1) titania deposition at the substrate-polymer interface and (2) deposition of titania in the polymer near the free surface. It is believed that a lift-off mechanism is responsible for polymer removal by solvent in cases where the PMMA was exposed to a large number of ALD cycles. The polymer near the free surface also has titania incorporated into it which forms a PMMA-titania layer whose dissolution by solvent is difficult. In cases where there is a region of relatively pure PMMA under this PMMA-titania layer (i.e. the 180 nm and 420 nm thick PMMA films) solvent dissolution of the pure PMMA layer can result in undercutting and lift-off of the polymer film. In cases where the PMMA film is sufficiently thin (i.e. the 32, 56, and 103 nm thick PMMA films), it is believed that little if any pure PMMA layer exists, and therefore dissolution and lift-off the polymer are inhibited. Figure 4-4 presents data showing that titania is

clearly deposited on the silica surface in the case of the thinner PMMA films. It is even possible that the PMMA chains near the silicon surface can be covalently attached to the surface if the same $TiCl_4$ molecule reacts with both the PMMA and the silicon surface. These observations would be consistent with the idea that no pure PMMA polymer region exists in the thinner films which can aid in dissolution and removal of the polymer, and thus the thinner films are difficult to remove without mechanical assistance. XPS scans were performed on the cleaned samples to measure the total Ti content on the surface. Figure 4-4 presents the Ti2p peak on the surface of samples after polymer removal for different initial thicknesses of the PMMA layer. As evident from the figure, noticeable amounts of Ti deposition are observed in the case of the thinner polymer samples while no Ti deposition is detectable on the 420 nm thick samples. Furthermore, the amount of Ti detected on the surface scales with the polymer film thickness. This would be expected if the precursor must diffuse through the polymer since higher concentrations of the titanium precursor would have been present at the substrate surface in the case of thinner polymer film thicknesses. It is also observed that the Ti2p3 peak position (in TiO_2) obtained for a 180 nm sample (spectra d) appears at a binding energy of 459.0 eV, which is 0.2 eV higher than the peak location obtained on thinner samples. This shift in peak location can be attributed to a difference in the chemical environment of Ti-O bonds. As discussed above, in the case of 180 nm thick films, fewer $TiCl_4$ molecules reach the polymer substrate interface than in the case of thinner films. Thus the titania layer formed in this case can have a greater fraction of Ti-O-Si bonds formed at the interface. As the masking layer thickness is reduced, a greater amount of titania forms underneath the polymer film and as a result the fraction of Ti-O-Ti bonds in the

deposited titania layer increases. Thus, the observed XPS peak position is closer to that of the characteristic Ti2p3 location for pure TiO_2 films. XPS scans on a Si surface exposed to 1 and 2 pulses of only $TiCl_4$ also exhibited Ti2p3 peaks appearing at 459.0 eV. This further supports the observed shift in the Ti2p peak presented in figure 4-4. These results confirm that selection of a proper film thickness for the polymer masking layer is required for a given polymer-precursor-cycle time process combination.

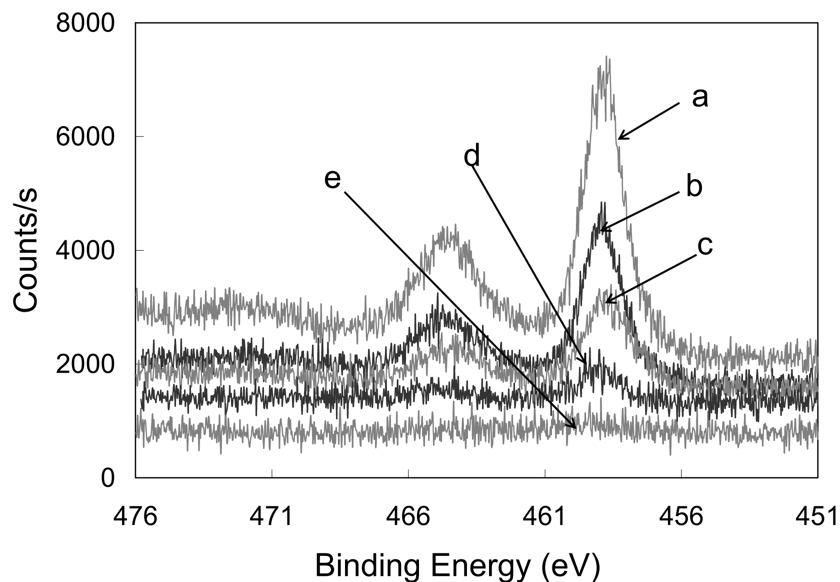

Figure 4-4: XPS spectra showing Ti2p peak on the substrate for different initial thickness of PMMA film. The scans are taken after the PMMA film is removed from the Si wafer. a: 32 nm, b: 56 nm, c: 103 nm, d: 180 nm, e: 420 nm. The spectra have been relatively shifted along the Y axis for clearer representation.

4.4 DEPOSITION OF PATTERNED FILM

The previous data suggest that PMMA films show low reactivity towards $TiCl_4$ and can be successfully used as a masking layer for area selective ALD processes. One reason that PMMA was selected as a candidate material is that it has been successfully patterned

directly using both optical and electron beam methods. Therefore, in this work PMMA has been used a proof-of-concept photodefinable masking layer for area selective ALD. PMMA films were coated onto clean silicon substrates and patterned by exposing them under 55.35 J/cm^2 dose of deep-UV light source followed by developing in 1:1 IPA: MIBK solution for 60 seconds. The samples were thoroughly rinsed with IPA and DI water after removal from the developer solution and then dried under N_2. The samples were further dried in a vacuum oven at 100 ^oC for 1 hour to remove residual moisture or solvent. TiO_2 films were grown on the patterned substrates by depositing for 150 cycles (2s($TiCl_4$)-25s(N_2)-1s(H_2O)-60s(N_2)) at 160 ^oC . Following deposition, the polymer masking film was removed by first dipping the sample in warm acetone for 20 minutes and then sonicating in acetone for an additional 30 minutes. Figure 4-6 shows optical micrographs of the different size square patterns obtained using this masked area selective ALD technique. Figure 4-5 shows the Ti2p peak region of the XPS spectra of both the open and masked regions of the silicon substrate after deposition and removal of the polymer mask. The XPS data clearly show that the patterned PMMA mask was successful in achieving area selective ALD.

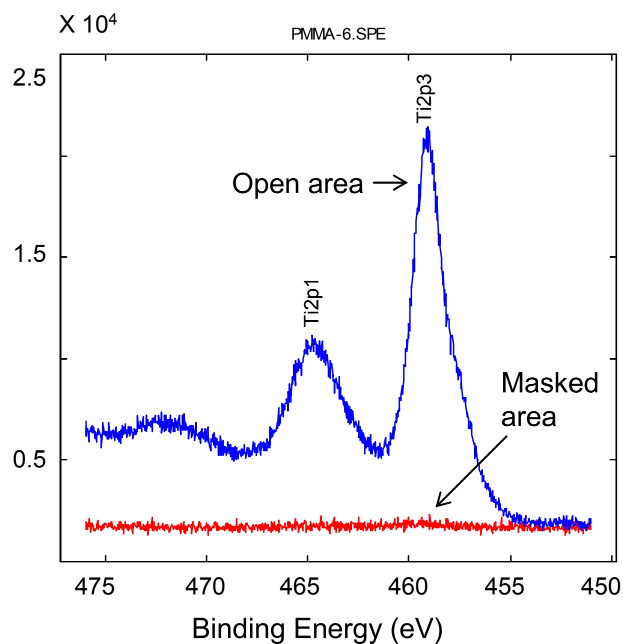

Figure 4-5: XPS scan showing Ti2p peak in different region after stripping the PMMA film. Open area: regions which were not covered with polymer film. Masked area: regions which were initially covered with the polymer film

Figure 4-6: Optical micrographs of different size TiO_2 patterns fabricated via area selective ALD.

4.5 CONCLUSIONS

ALD relies on the use of self-limited surface reactions to perform well controlled, conformal deposition of materials. This surface reaction limited approach offers the possibility to selectively modify a surface in order to deposit the ALD material only in desired regions of the surface. Self assembled monolayers have been previously investigated as a surface modifying agent for area selective ALD deposition. Thus far, challenges in achieving defect free monolayers have posed serious limitations on the successful use of this SAM masking technique. Polymer thin films offer a potentially more facile route to achieving successful masking for area selective ALD. The results presented in this chapter suggest that: (1) the presence of oxygen or free OH groups in the polymer is not necessarily a problem or constraint for masking material design, (2) the presence of remnant precursors in the film after purging can be an important parameter in choosing both a masking polymer and appropriate purge cycle times for the ALD process, and (3) the thickness of the polymer masking layer and diffusion rates of precursors in the polymer film are important considerations to prevent reactive precursors from diffusing to the substrate and reacting with the substrate surface. Area selective deposition of TiO_2 has been successfully demonstrated using PMMA masking layer lithographically patterned directly using deep-UV exposure. $TiCl_4$-H_2O-PMMA based ASALDT still pose certain challenges which will be addressed in the next chapter.

4.6 REFERENCES

1. Calistri-Yeh, M.; Kramer, E. J.; Sharma, R.; Zhao, W.; Rafailovich, M. H.; Sokolov, J.; Brock, J. D., Thermal Stability of Self-Assembled Monolayers from Alkylchlorosilanes. *Langmuir* **1996,** 12, (11), 2747-2755.

2. Ulman, A., Formation and Structure of Self-Assembled Monolayers. *Chemical Reviews (Washington, D. C.)* **1996,** 96, (4), 1533-1554.

3. Silberzan, P.; Leger, L.; Ausserre, D.; Benattar, J. J., Silanation of silica surfaces. A new method of constructing pure or mixed monolayers. *Langmuir* **1991,** 7, (8), 1647-51.

4. Davazoglou, D.; Raptis, I.; Gleizes, A.; Vasilopoulou, M., Fabrication of very fine copper lines on silicon substrates patterned with poly(methylmethacrylate) via selective chemical vapor deposition. *Journal of Vacuum Science & Technology, B: Microelectronics and Nanometer Structures--Processing, Measurement, and Phenomena* **2004,** 22, (2), 859-860.

5. Davazoglou, D.; Vidal, S.; Gleizes, A., Fabrication of fine copper lines on silicon substrates patterned with AZ 5214 photoresist via selective chemical vapor deposition. *Microelectronics, Microsystems and Nanotechnology, Papers presented at MMN 2000, Athens, Greece, Nov. 20-22, 2000* **2001**, 131-134.

6. XPS Handbook, PHI Electronics.

7. Singh, L.; Ludovice, P. J.; Henderson, C. L., Influence of film thickness, molecular weight, and substrate on the physical properties of photoresist polymer thin films. *Proceedings of SPIE-The International Society for Optical Engineering* **2003,** 5039, (Pt. 2, Advances in Resist Technology and Processing XX), 1008-1018.

8. Kawaguchi, M.; Yamagiwa, S.; Takahashi, A.; Kato, T., Adsorption of polystyrene and poly(methyl methacrylate) onto a silica surface studied by the infrared technique. Comparison with theory. *Journal of the Chemical Society, Faraday Transactions* **1990,** 86, (9), 1383-7.

CHAPTER 5

AREA SELECTIVE ATOMIC LAYER DEPOSITION OF TITANIUM DIOXIDE: EFFECT OF PRECURSOR CHEMISTRY

5.1 INTRODUCTION

Results discussed in the previous chapter established that polymer film based masking approaches can be successfully implemented to perform ASALD. In particular, we developed a methodology to perform direct patterned deposition of TiO_2 on a Si substrate using $TiCl_4$ and H_2O as ALD precursors and PMMA as a photodefinable mask. However, several limitations of this ASALDT process were identified which arose from a combination of the intrinsic reactivity of PMMA with $TiCl_4$ and the diffusion of $TiCl_4$ through the PMMA film. For example, it was discovered that a minimum masking layer thickness of approximately 200 nm was required to prevent undesired titania formation beneath the PMMA polymer mask. It was also discovered that although a PMMA film thicker than 200nm could block nucleation on underlying Si surfaces, some TiO_2 nucleation on the PMMA top surface was still observed. This incorporation of titania into the PMMA film made it difficult to remove the film using simple solvent washes after ALD. Such limitations are of course undesirable, and thus further investigations of the influence of process conditions, precursor chemistry, and masking layer chemistry on the resulting ASALDT process performance were undertaken. In this chapter, we introduce the use of titanium isopropoxide (TiIP) as an alternate titanium precursor to overcome

limitations of $TiCl_4$-H_2O based ASALDT. First, process parameters to perform ALD using TiIP and H_2O are developed and results are compared with the $TiCl_4$-H2O system. Similar to studies discussed in chapter 4, selectivity contrast of TiIP-H_2O on different polymer masks was investigated. The results of using the TiIP-H_2O system with PMMA masking layers are compared to those of the $TiCl_4$-H_2O-PMMA system. Results demonstrate that a PM-ASALDT process based on TiIP-H_2O-PMMA overcomes the limitations of the $TiCl_4$-based process and greatly enhances the PM-ASALDT process window for deposition of TiO_2 ultra-thin films.

5.2 EXPERIMENTAL APPARATUS & PROCEDURE

Blanket film depositions were initially conducted in order to identify the required precursor dose to achieve film growth in a self saturation mode and the saturation growth rate for TiIP-H_2O system. The growth rate data are important in order to compare the selectivity contrast for TiIP-H_2O with the $TiCl_4$-H_2O case. For simplicity, during TiIP case, the cycle sequence and the number of cycles have been chosen such that in both cases, equal thicknesses of TiO_2 layers deposit on the Si substrate. Titanium-isopropoxide (TiIP, 98%) was received from Dupont and was degassed using a series of freeze-pump-thaw cycles before use. Deionized (DI) water was used as the oxygen precursor source. Water was maintained at approximately 25 ºC while the titanium-isopropoxide precursor was heated to 82 ^oC – 85^oC to increase its vapor pressure (3.8 torr). During deposition, all flow lines containing the precursor were also heated in order to avoid condensation of the precursor. All depositions were conducted using the procedure outlined in chapter 2.

The ALD deposition cycle consisted of: (1) TiIP pulse, (2) N_2 purge, (3) H_2O pulse, and (4) N_2 purge.

All other experimental procedures including: (1) preparation of polymer films (2) film thickness measurements and (3) chemical analyses employed similar procedures described in chapters 2 and 4.

5.3 DEPOSITION ON SILICON SUSBTRATE

Growth rate data for ALD of TiO_2 films using $TiCl_4$ and H_2O as precursors has been presented in chapter 2. Figure 5-1 shows the growth rate of TiO_2 films using the titanium-isopropoxide precursor as a function of varying precursor pulse duration for one of the precursors while maintaining a constant pulse time for the other precursor. The data suggest self-saturated reaction and growth of TiO_2 films at precursor exposure times for Ti-isopropoxide and water of at least 1.5 s and 2.0 s, respectively at 160°C. Under these conditions, the growth rate of TiO_2 saturates at ~ 0.068 nm per cycle. The growth also exhibits the characteristic ALD behavior that the deposited film thickness is linearly proportional to the number of ALD cycles (see Figure 5-2). The data presented in Figures 5-1 and 5-2 clearly demonstrate self saturated ALD growth of TiO_2. Previous studies[1] investigating the reaction mechanism of the titanium isopropoxide-water ALD process also reported that similar precursor exposure pulse durations were required for saturated growth at 150 °C. However, previous literature reports for the TiO_2 growth rate using the TiIP-H_2O precursor system exhibit some contradictory results. Doring and coworkers[2] measured a growth rate of 0.15 nm/cycle at 150 °C, while Ritala and coworkers reported a growth rate of only 0.015 nm/cycle at the same substrate

temperature[3]. Recent studies have reported more consistent growth rates in the range of 0.05-0.06 nm/cycle at temperatures of 200-250 °C [4] and 0.068 nm/cycle at 150 °C [5]. The growth rate obtained in this work appears to be in good agreement with these more recent studies.

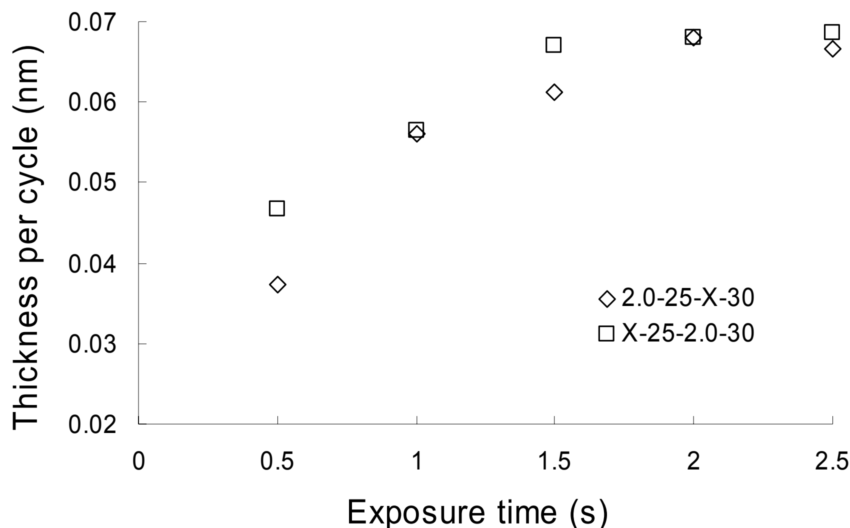

Figure 5-1: Thickness grown per ALD cycle versus exposure time for one of the ALD precursors. The legend format refers to the time duration of each step in the ALD cycle. For example, "X-25-2.0-30" refers to an ALD sequence of (1) X seconds exposure of $Ti(OCH(CH_3)_2)_4$, (2) 25 seconds N_2 purge, (3) 2.0 seconds exposure to water, and (4) 30 seconds N_2 purge. The two different data sets are represent variations in the (□)$Ti(OCH(CH_3)_2)_4$ exposure time and the (◊) water exposure time.

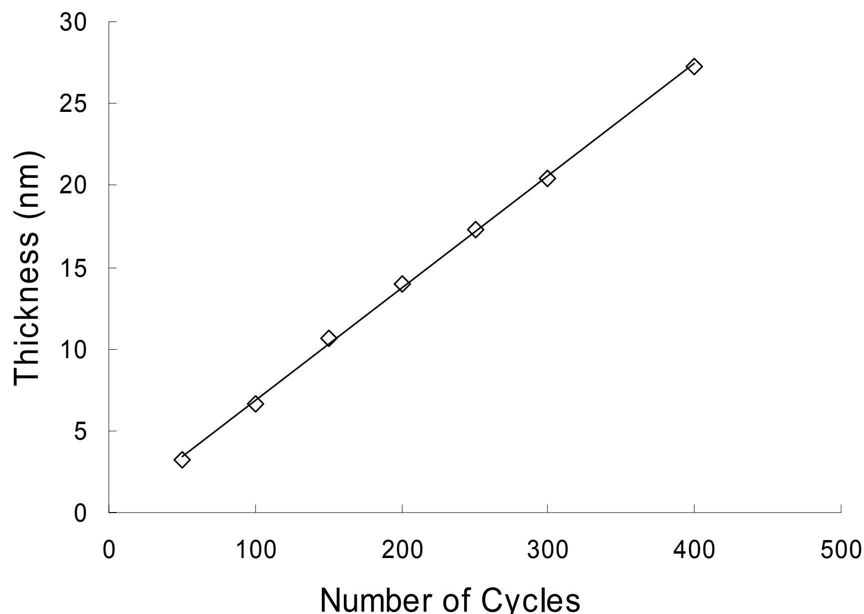

Figure 5-2: Thickness of the TiO_2 film as a function of number of ALD cycles for TiIP-H_2O process. The linear growth with number of cycles is indicative of an ALD process

Comparison of the TiIP-H_2O data with the previous $TiCl_4$ process indicates that a slightly shorter titanium precursor pulse time is required for self-saturated growth in the case of the TiIP process (~1.5s) as compared to the $TiCl_4$ (~2.0s - 2.5s) process. In both cases, a similar water pulse time of approximately 2 seconds is sufficient to achieve self-saturated growth. However, titania growth rates for both the TiIP (0.068 nm/cycle) and $TiCl_4$ (0.07 nm/cycle) processes are essentially the same. One marked difference between the isopropoxide and chloride precursors is the ligand size of the leaving group. Titanium isopropoxide is a significantly larger molecule than $TiCl_4$. Also, reaction mechanism studies on the TiIP-H_2O ALD process indicate that at 150-200 ^oC, two ligands per titanium isopropoxide molecule are released during the exchange reaction

with a hydroxylated surface, whereas $TiCl_4$ reacts with either 1 or 2 hydroxyl groups under the same conditions[1, 4, 6-8]. Therefore, on average, one TiIP molecule reacts with a larger number of hydroxyl groups on the surface than does one $TiCl_4$ molecule. This larger consumption of hydroxyl sites, combined with the larger steric hindrance of the remaining ligands on the TiIP molecule, leads to a lower number of TiIP molecules saturating the substrate surface compared to that for $TiCl_4$. Such considerations may partially explain the faster saturation of the surface by titanium isopropoxide during the titanium precursor pulse. If indeed a lower number of titanium molecules are deposited per layer, then a density difference between titania deposited using TiIP versus $TiCl_4$ might be expected. Spectroscopic ellipsometry measurements showed that the refractive indices of titania films deposited from the $TiCl_4$ precursor were in the range of 2.15-2.30 while the refractive indices for films made using the TiIP precursor were in the range of 2.10-2.20 (refractive indices reported at a wavelength of 580 nm). Since refractive index is an indicator of film density for a specific material composition, it can be inferred that the TiO_2 films obtained using the isopropoxide precursor process are indeed slightly less dense than those obtained using the chloride precursor process.

5.4 ALD GROWTH STUDIES ON POLYMER FILMS

Our previous experiments showed that $TiCl_4$ does not nucleate and grow on a PMMA surface as readily as on a Si surface. Therefore, patterned PMMA films served as effective masking layers for area selective ALD. After 100 ALD cycles (2s ($TiCl_4$) – 25s (purge) – 1s (H_2O) – 60s (purge)), a titanium concentration of 1.1 atomic% was measured on a PMMA surface exposed to the ALD atmosphere. However, 0.7 atomic% of Ti was

detected on PMMA film surfaces after exposure to 150 pulses of only the $TiCl_4$ precursor (i.e. -2s ($TiCl_4$) – 25s (purge)-). This indicates that $TiCl_4$ can directly react with the PMMA resin. Chlorine is a highly electronegative atom that significantly reduces electron density on the titanium atom in $TiCl_4$. Thus, the titanium center in $TiCl_4$ behaves as an electron acceptor and functions as a strong Lewis acid. The carbonyl oxygen in PMMA possesses a lone pair of electrons with which $TiCl_4$ can complex or react. In fact, it has been reported that strong Lewis acids (e.g., $AlCl_3$, $TiCl_4$, $SnCl_4$) can easily complex with carbonyl groups present in acrylates [9]. This reactivity of $TiCl_4$ imparts a limitation on its use as a successful precursor for area selective ALD since it severely limits the types of materials which can serve as non-reactive masking layers. After TiO_2 nucleates on a PMMA surface, it will serve as an active site for further growth during subsequent ALD cycles. Eventually this will result in deposition of a conformal TiO_2 layer on top of the PMMA film. The presence of such a titania film on the masking layer, which would eventually merge with the titania grown in unmasked areas given a sufficient number of ALD cycles, makes it difficult to remove the PMMA mask after ALD deposition and results in complete loss of pattern definition after a fully conformal film is produced. This means that in order to perform a successful ASALDT process using $TiCl_4$ and PMMA, only a limited number of ALD cycles can be conducted while preventing TiO_2 buildup on the PMMA, which would prevent PMMA removal. For the $TiCl_4$-H_2O-PMMA system, a maximum of ~250 ALD cycles could be run at 160 ^oC, thus limiting the film thickness attainable. These difficulties with $TiCl_4$ led us to investigate alternative ALD precursors that possess less reactivity toward masking layers such as PMMA.

Metalorganic precursors with alkyl or alkoxy groups have been widely investigated as precursors for the deposition of a variety of inorganic oxides including Al_2O_3, HfO_2, ZrO_2, TiO_2, and ZnO. Such ligand groups are not as electronegative as chlorine atoms and thus should not easily cause coordination or reaction with the carbonyl groups found in PMMA. For TiO_2 deposition, titanium isopropoxide is probably the most extensively used precursor among different Ti-alkoxy precursors because of its reasonably high vapor pressure[3]. The isopropoxide ligand is also significantly larger than the Cl substituents in $TiCl_4$, and thus access of TiIP to any C=O group in PMMA should be more sterically hindered. As expected, no Ti was detected on PMMA samples exposed only to Ti-isopropoxide pulses. Depositions were conducted on different PMMA samples with successive increases in the number of ALD cycles on different samples. XPS scans of the PMMA samples showed no detectable Ti on the polymer surface after 500 ALD cycles (2s – 25s – 2s – 30s). For comparison, during the same 500 cycles, a 35nm thick TiO_2 film was deposited on a bare Si substrate.

Figures 5-3 and 5-4 show the C1s and Ti2p XPS spectra of the PMMA surface after 400 ALD cycles using $TiCl_4$-H_2O and 500 ALD cycles using $Ti(OCH(CH_3)_2)_4$-H_2O, respectively. As mentioned previously, no Ti is detected when the titanium isopropoxide precursor was used. In contrast, for the $TiCl_4$ process, a large Ti2p peak is observed due to a TiO_2 layer which has formed on the PMMA film during ALD. Figure 5-4 presents XPS peak deconvolution results for C1s spectra following ALD using the isopropoxide precursor, where four different peaks corresponding to different C species present in the PMMA film are evident. The peak locations and relative percentage match closely with those reported in standard XPS database spectra from a PMMA polymer.

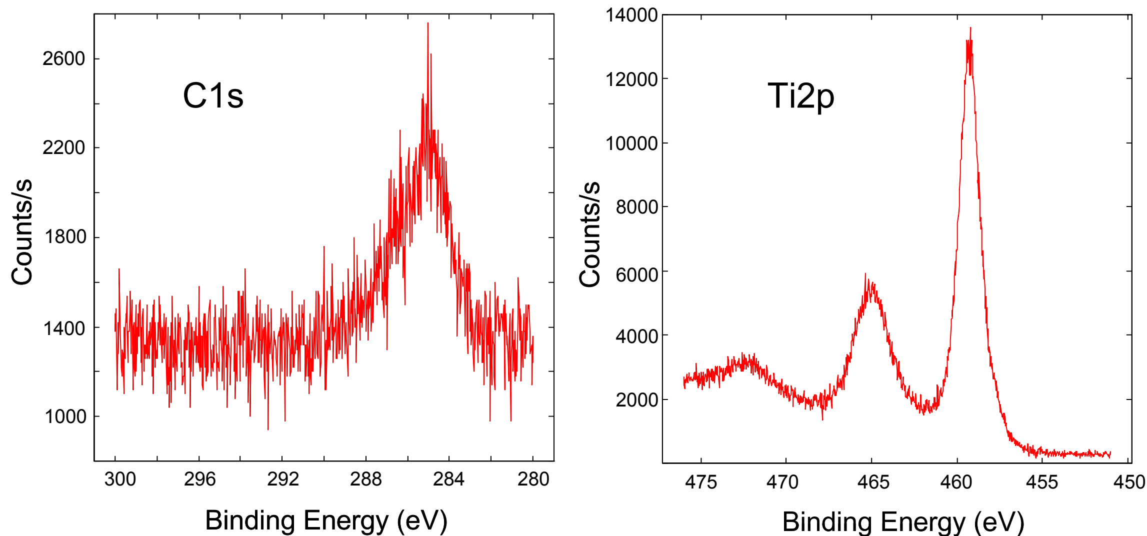

Figure 5-3: C1s and Ti2p spectra as obtained from XPS scans on PMMA film post 400 ALD cycles for $TiCl_4$ process

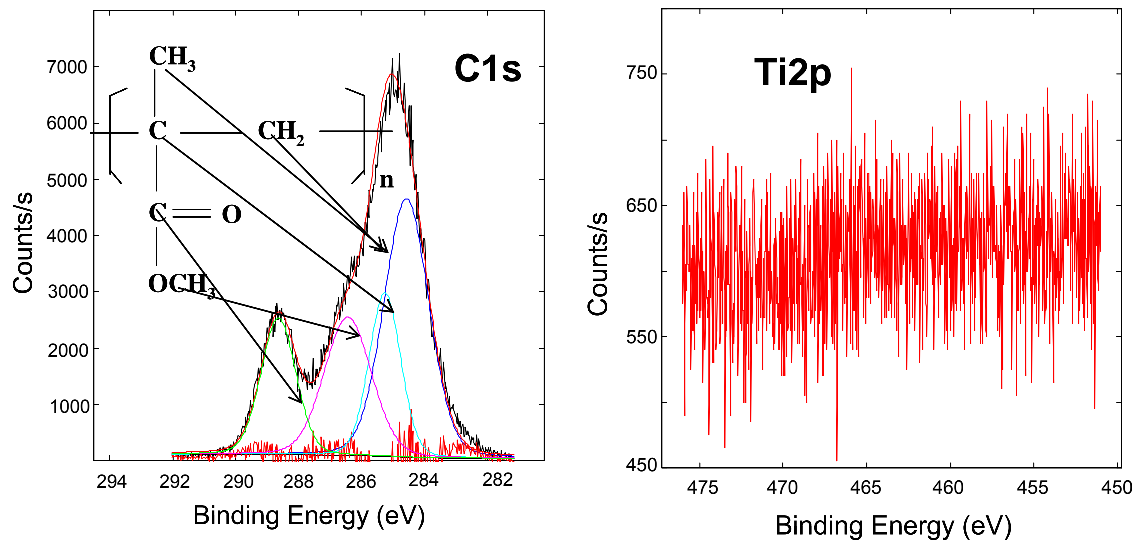

Figure 5-4: C1s and Ti2p spectra as obtained from XPS scans on a PMMA film after 500 ALD cycles for the $Ti(OCH(CH_3)_2)_4$ process

These results further indicate that titanium isopropoxide does not interact with PMMA and that the ALD process does not induce chemical changes in the polymer layer. However, for the $TiCl_4$ process (Fig. 5-3), a conformal layer of TiO_2 (~ 25 nm) is deposited on the PMMA surface, and thus only one C1s peak at 284.5 eV is observed which is due to adventitious carbon present on the TiO_2 film. The attenuation length of ejected photoelectrons in XPS is usually 8-10 nm and thus photoelectrons ejected from the underlying PMMA film (which lies beneath ~ 25nm of TiO_2 film) are not detected by XPS.

As previously mentioned, it is desirable that the polymer masking layers be easily removed after the ALD process is complete. The PMMA films after TiIP-H_2O ALD were easily removed by rinsing them in acetone (or other solvents for PMMA such as methanol) and DI water. Apparently, the PMMA films simply dissolved in the rinse solvents. In stark contrast, after the $TiCl_4$-H_2O process, the PMMA films were extremely difficult to remove and it was necessary to aid the removal by scratching the film surface at a few locations before washing with warm (T = 45 ^{o}C) solvent. In this case, PMMA film removal appeared to occur by a lift-off process in which the relatively pure PMMA material at the bottom of the film was dissolved allowing the titanium contaminated PMMA surface layer to lift-off and partially dissolve. This clearly suggests that it is desirable to use precursors which do not react with the polymer masking film; otherwise, there is a limit on the number of ALD cycles which can be performed and the ease and cleanliness of masking film removal process suffers. Optical micrographs showing direct pattern deposition of TiO_2 using TiIP-H_2O-PMMA-based ASALDT are presented in figure 5-5. Thirty-five nm thick titania patterns were deposited using 500 ALD cycles

(2s – 25s – 2s – 30s) on lithographically defined patterns of PMMA on a Si substrate. As discussed previously, post ALD, the PMMA film was removed easily by rinses in acetone and DI water. In addition, XPS scans on the TiO_2 pattern and the surrounding substrate region are also included. Complete removal of the polymer masking layer from regions adjacent to the deposited titania is evident from the micrographs. In addition, the relative difference in Ti2p photoelectron intensity observed in scans on open and masked regions on the substrate demonstrate an improved and simpler ASALDT than the previously reported $TiCl_4$-H_2O-PMMA-based approach.

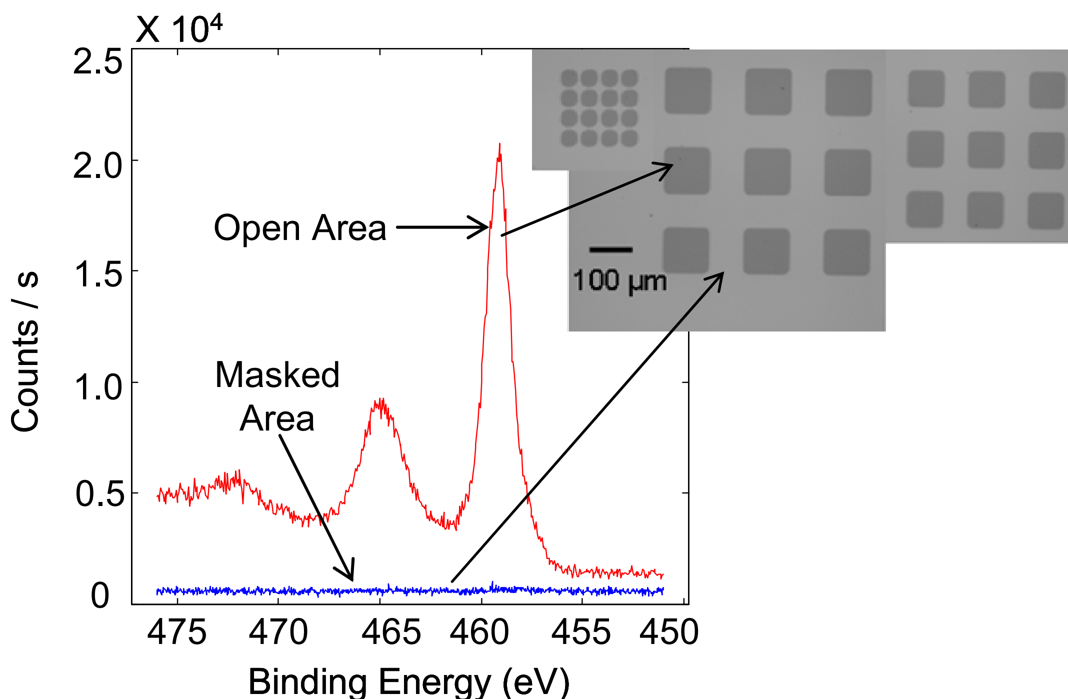

Figure 5-5: Comparison of XPS spectra showing the Ti2p peak on a silicon substrate surface after 500 ALD cycles using the TiIP-H2O precursor system for surface areas that were covered by a 100 nm PMMA film, and for surface areas that were open directly to the ALD atmosphere. Deposition of titania occurred on the open surface while no visible deposition of Ti or titania occurred under the PMMA masked areas. Optical micrographs displaying different size titania patterns deposited using TiIP-H_2O/PMMA ASALDT are also shown.

It is important to note that the results of previous studies which attempted to block ALD nucleation using SAM modified surfaces indicated a direct correlation between surface energy or water contact angle (WCA) of the modified surface with the amount of nucleation observed [10, 11]. In studies by Chen et al.[10], it was observed that only octadecyltrichlorosilane and fluorinated-octlytrichlorosilane resulted in sufficiently high water contact angles (109° and 112° respectively) to successfully block nucleation. Other shorter or branched chain alkyl silanes resulted in lower water contact angles on the masked area surface, and correspondingly the detected concentration of Hf on these SAM modified regions consistently increased with decreasing SAM surface water contact angle. Similarly, Lee et al.[11] observed that the extent of Ti nucleation on mixed SAM surfaces with different surface free energies consistently increased with an increase in surface energy and only the low free energy surface with WCA of 108° showed no nucleation. In general, results in both these studies suggested that a highly hydrophobic masking layer surface (WCA $\geq 108^o$) was essential to successfully block nucleation on the SAM modified regions. Chen et al. [10] also indicated that a high contact angle is only achieved in a well packed monolayer, and that this high degree of packing order is the important feature which prevents ALD precursor access to available reactive sites on the surface. It has also been stated that highly hydrophobic surfaces or low free energy surfaces also reduce the concentration of physisorbed water on the masking layer surface after each water pulse, and thus can provide lower nucleation as compared to more hydrophilic surfaces. However, these previous studies did not clearly identify if one of these two phenomena plays a more dominant role in establishing the performance of a SAM surface for selective ALD. The PMMA used in this work has a water contact angle

of ~74°, which is significantly lower than that of the SAM surfaces previously reported to show successful ALD masking. The XPS data demonstrate that no Ti is detected on the PMMA surface for 500 ALD cycles when titanium isopropoxide is used as the metal species precursor. Furthermore, only 30s of purge after the water pulse was sufficient for successful selective ALD. These results strongly indicate that attainment of selective growth is controlled predominantly by two criteria: (1) ability of the masking layer to provide a sufficient barrier to the metal ALD precursor species to prevent it from reaching reactive sites on the substrate surface and (2) absence of undesired reactions between the masking layer material and the ALD precursors. Blocking of reactive sites on the surface may take the form of a simple diffusional resistance, as is the case with the PMMA films used in this work, or may be due to chemical conversion of reactive sites to a more inert form as is the case with reactive consumption of surface sites by the reactive SAM coatings. Physisorption of water on the masking layer surface appears to play a much less important role and does not appear to pose a serious limitation on the use of less hydrophobic masking layers such as PMMA.

TiIP-H_2O ALD was also performed on other polymer films including PHOST and HFA-PNB to examine the selectivity contrast for this precursor system for polymers having –OH bonds chemically linked to their backbone. In addition, polymer films were also exposed to only TiIP pulses in order to gather information about their intrinsic reactivity with those polymeric materials. Figure 5-6 presents the data obtained from these experiments.

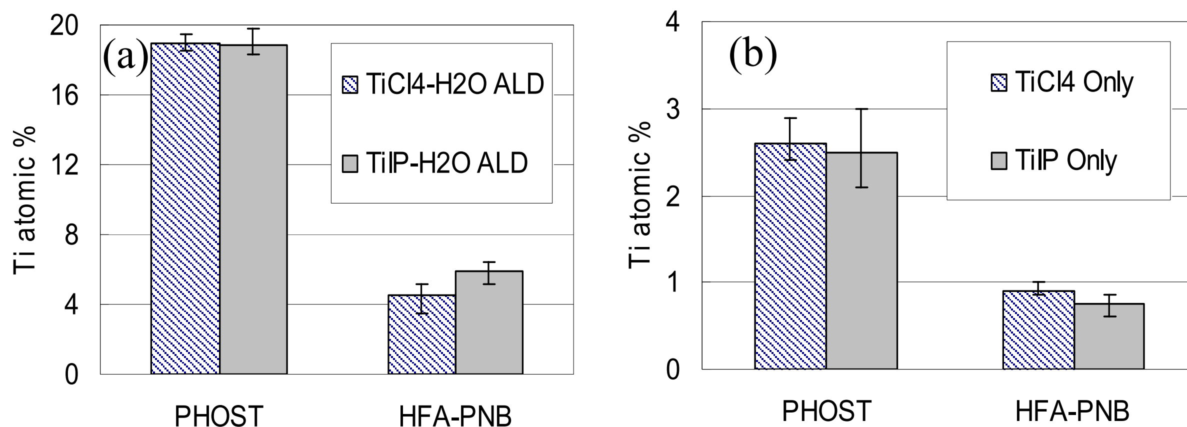

Figure 5-6: Comparison of Ti at. % on PHOST and HFA-PNB; (a) After 100 ALD cycles, cycle sequence is $TiCl_4$-H_2O: 2s-25s-1s-60s, TiIP-H_2O: 2s-25s-1.5s-60s; (b) After 150 cycles of $TiCl_4$ (-2s-25s-) and TiIP (-2s-25s-)

The above data indicate that TiIP does not offer any advantage over $TiCl_4$ for the polymers with direct –OH groups available. In fact, the levels of Ti detected were very similar to those obtained with $TiCl_4$. These results are also consistent with the fact that $TiCl_4$ and TiIP exhibit similar growth rates on Si substrates, suggesting that on a surface with a particular –OH site concentration, $TiCl_4$ and TiIP shows equivalent material deposition.

For both SAM coatings and polymer masking layers, an important issue identified in our previous work was the potential ability of ALD precursors to diffuse through the masking layer and reach reactive sites on the substrate surface. Although SAMs in principle reactively passivate the substrate surface, complete elimination of reactive sites on the substrate is essentially impossible. Thus, even the SAM film must serve as an effective diffusion barrier in order to successfully prevent nucleation and growth from the

substrate on the small number of surface sites which do not react with the silane SAM compounds. In the case of physically coated polymer films, although the presence of polymeric chains in the vicinity of surface sites may physically or sterically block their accessibility, the masking layer does not in principle reactively passivate surface sites. Hence, they serve purely as a diffusion barrier preventing precursor access to active sites on the substrate.

The distance over which a precursor penetrant molecule can diffuse in the masking layer during an ALD precursor exposure cycle is dependent on two factors: (1) the specific time period of the precursor exposure and (2) the diffusion coefficient of the precursor in the masking layer. Although the time scale for precursor diffusion can be reduced by reducing the precursor exposure cycle time, this can result in sub-saturation coverage of the desired areas. This in turn leads to lower ALD growth rates and overall longer ALD deposition times due to the added ALD cycles needed to obtain the same deposition thickness. Therefore, in order to produce successful masking layers and area selective deposition processes, it is prudent to adjust the masking layer film thickness with a knowledge of the diffusivity of the ALD precursors in the masking films to optimize the process. This issue reveals one more advantage of polymer-based ASALDT over SAM-based approaches since the thickness of polymer films can be controlled easily by tuning the concentration of casting solvent and the spin speed. On the other hand, SAM-based approaches do not offer such flexibility. The ability to adjust the polymer masking layer film thickness for a given polymer-precursor system to produce successful passivation of the substrate surface has been demonstrated in our previous study on titania deposition using the $TiCl_4$-H_2O precursor system. In the case of the TiIP-

H_2O system discussed in this chapter, the TiIP precursor is significantly larger than the $TiCl_4$ precursor used previously. Both Ti precursors are larger than the water molecules used as an oxidizing agent in both processes; thus, diffusion of the Ti precursor is expected to be the limiting step in titania growth under the polymer film. Therefore, it is expected that the minimum PMMA masking layer thickness for TiIP-H_2O should be significantly smaller than in the $TiCl_4$-H_2O case. A series of depositions on silicon substrates were conducted with different PMMA film thicknesses using the TiIP-H_2O precursor system to investigate the effect of precursor size on diffusion through the polymer film. After ALD, the polymer film was removed and XPS of the resultant surface was performed to quantify titania deposition under the polymer film. It was observed that the thickness of PMMA could be reduced to ~10 nm without detection of TiO_2 deposition on the substrate beneath the polymer film. Attempts to form PMMA films thinner than 10 nm were unsuccessful due to dewetting phenomena[12, 13].

Diffusion coefficients of the above precursors through PMMA have been measured as part of the current thesis; details of these experiments are presented in chapter 7. The diffusion coefficient for TiIP through PMMA at 160 ^{o}C is estimated to be 1.35×10^{-16} m^2/s where as that for $TiCl_4$ is 1.53×10^{-14} m^2/s. The measurements suggest that the diffusion coefficient of $TiCl_4$ in PMMA is approximately 2 orders of magnitude higher than that for the isopropoxide precursor. These results indicate that the ratio of diffusion lengths, which scales with square root of D, should be approximately ten. Previously we observed that ~200 nm thick films were required in order to prevent nucleation at the polymer-substrate interface during $TiCl_4$-H_2O ALD. From a simple calculation of the ratio of diffusion lengths, nucleation at the interface should be observed at ~20 nm film

thickness for the isopropoxide precursor system. However, the isopropoxide precursor displays much lower solubility in PMMA than does $TiCl_4$ (details available in chapter 7), which reduces the overall permeability and the concentration that will be observed at the polymer substrate interface. Furthermore, with ultra thin films (25-30 nm), a greater fraction of polymer chains are confined near the substrate than will be the case with a thicker film. This confinement reduces the polymer chain mobility and is manifested into a lower diffusion coefficient in this thickness regime[14, 15]. These two phenomena partially explain why no nucleation was observed for film thickness down to 10 nm in titanium isopropoxide-H_2O ALD. In addition, the absolute value of average diffusion length for both precursors can be estimated by evaluating $(D.t)^{1/2}$. For an exposure time of 2 seconds, this value is 175 nm and 16 nm for $TiCl_4$ and titanium isopropoxide respectively. The estimated values are reasonably consistent with the required masking layer thickness for both systems.

One of the advantages of using polymer films as masking layers is that conventional and commercially established optical lithography techniques can be easily used to pattern these masks. The resolution and depth of focus for a given optical lithography system can be described by the following equations

$$resolution = k\frac{\lambda}{NA} \qquad (1)$$

$$Depth\ of\ focus = \pm\frac{\lambda}{2NA^2} \qquad (2)$$

As the resolution of optical lithography tools continues to increase by decreasing the exposure wavelength and increasing the numerical aperture of the lens systems, the

depth of focus for such tools is reduced. This leads to a reduction in the thickness of the resist films used in the fabrication process. According to the ITRS roadmap[16], the required resist thickness will be in the range of 120-160 nm by the year 2010 (45 nm node) and 50-80 nm by 2016 (22 nm node). The new TiIP-H_2O process presented in this work has demonstrated the ability to be utilized in conjunction with polymer film thicknesses well below these optical lithography thickness requirements. Thus, by choosing combinations of optical polymer resists and precursors which display low precursor diffusivities in the masking layer along with low reactivities toward one another, area selective ALD at essentially the resolution limits of the high throughput optical lithography patterning technologies should be possible. Obviously, PMMA is not an ideal choice for high volume manufacturing using optical lithography due to its relatively low sensitivity to ultraviolet light, and therefore more effort is required to develop high photospeed photodefinable masking layers for use with UV optical lithography tools. However, the PMMA process demonstrated in this work is a good choice for extremely high resolution electron beam lithography-based production of titania nanopatterns.

5.5 CONCLUSIONS

Area selective ALD of titanium dioxide has been investigated and compared using two different precursors, $TiCl_4$ and $Ti(OCH(CH_3)_2)_4$, in conjunction with PMMA as a photodefinable polymer masking layer. Inherent reactivity of the precursors with the masking layer and diffusion of the ALD precursors through the masking layer have

clearly been shown to be two critical characteristics in the design of a successful polymer masked-area selective ALD (PM-ASALDT) process. It is believed that $TiCl_4$ can coordinate with the C==O bond present in PMMA since it is a strong Lewis acid, thus allowing reaction and nucleation of TiO_2 on PMMA. In contrast, titanium isopropoxide was virtually unreactive towards PMMA and thus no Ti was detected on PMMA surfaces even after 500 ALD cycles using the TiIP-H_2O precursor system. This negligible reactivity between TiIP and PMMA allows the PMMA masking film to be easily removed after ALD using simple solvent washes. The experimental results also indicate that extreme hydrophobicity of the masked surface may not be as critical a pre-requisite for successful polymer masking based selective ALD as has been reported previously for SAM-based area selective ALD processes (e.g. a minimum water contact angle on the masking surface greater than 109° was reported previously[10, 11]). The larger size of the titanium isopropoxide precursor molecule slows its diffusion through PMMA films as compared to $TiCl_4$, and thus allows the use of much thinner polymer masking layers for TiIP-H_2O as compared to $TiCl_4$-H_2O. A PMMA masking layer film thickness of approximately 10 nm was effective to mask the TiIP-H_2O system while a PMMA film at least ~200 nm thick was required to avoid titania deposition under the polymer film for the $TiCl_4$-H_2O system. These results suggest that the intrinsic reactivity of the polymer resin with ALD precursors, the presence of remnant precursors in the polymer film after each precursor pulse, and diffusion of precursors through the masking layer are the critical parameters which must be considered in establishing a successful polymer mask-based area selective ALD process. Overall, the use of the TiIP- H_2O-PMMA system has

been shown to be a good first example of a lithographically compatible area selective deposition process for titania.

5.6 REFERENCES

1. Rahtu, A.; Ritala, M., Reaction mechanism studies on titanium isopropoxide-water atomic layer deposition process. *Chemical Vapor Deposition* **2002,** 8, (1), 21-28.

2. Doring, H.; Hashimoto, K.; Fujishima, A., TiO2 thin-films prepared by pulsed-beam chemical vapor-deposition from titanium tetraisopropoxide and water. *Berichte Der Bunsen-Gesellschaft-Physical Chemistry Chemical Physics* **1992,** 96, (4), 620-622.

3. Ritala, M.; Leskela, M.; Niinisto, L.; Haussalo, P., Titanium isopropoxide as a precursor in atomic layer epitaxy of titanium dioxide thin films. *Chemistry of Materials* **1993,** 5, (8), 1174-81.

4. Aarik, J.; Aidla, A.; Uustare, T.; Ritala, M.; Leskela, M., Titanium isopropoxide as a precursor for atomic layer deposition. Characterization of titanium dioxide growth process. *Applied Surface Science* **2000,** 161, (3-4), 385-395.

5. Park, M. H.; Jang, Y. J.; Sung-Suh, H. M.; Sung, M. M., Selective Atomic Layer Deposition of Titanium Oxide on Patterned Self-Assembled Monolayers Formed by Microcontact Printing. *Langmuir* **2004,** 20, (6), 2257-2260.

6. Matero, R.; Rahtu, A.; Ritala, M., In Situ Quadrupole Mass Spectrometry and Quartz Crystal Microbalance Studies on the Atomic Layer Deposition of Titanium Dioxide from Titanium Tetrachloride and Water. *Chemistry of Materials* **2001,** 13, (12), 4506-4511.

7. Aarik, J.; Aidla, A.; Sammelselg, V.; Siimon, H.; Uustare, T., Control of thin film structure by reactant pressure in atomic layer deposition of TiO2. *Journal of Crystal Growth* **1996,** 169, (3), 496-502.

8. Puurunen, R. L., Formation of metal oxide particles in atomic layer deposition during the chemisorption of metal chlorides. A review. *Chemical Vapor Deposition* **2005,** 11, (2), 79-90.

9. Assfeld, X.; Garcia, J.; Garcia, J. I.; Mayoral, J. A.; Proietti, M. G.; Ruiz-Lopez, M. F.; Sanchez, M. C., X-ray absorption spectroscopy investigation on the structure of methyl acrylate-TiCl4 complexes in solution. *Journal of the Chemical Society, Chemical Communications* **1994**, (18), 2165-6.

10. Chen, R.; Kim, H.; McIntyre, P. C.; Bent, S. F., Investigation of self-assembled monolayer resists for hafnium dioxide atomic layer deposition. *Chemistry of Materials* **2005,** 17, (3), 536-544.

11. Lee, J. P.; Jang, Y. J.; Sung, M. M., Atomic layer deposition of TiO2 thin films on mixed self-assembled monolayers studied as a function of surface free energy. *Advanced Functional Materials* **2003,** 13, (11), 873-876.

12. Reiter, G., Dewetting of thin polymer films. *Physical Review Letters* **1992,** 68, (1), 75-8.

13. Ashley, K. M.; Raghavan, D.; Douglas, J. F.; Karim, A., Wetting-Dewetting Transition Line in Thin Polymer Films. *Langmuir* **2005,** 21, (21), 9518-9523.

14. Singh, L.; Ludovice, P. J.; Henderson, C. L., Effect of nanoscale confinement on the diffusion behavior of photoresist polymer thin films. *Proceedings of SPIE-The International Society for Optical Engineering* **2004,** 5376, (Pt. 1, Advances in Resist Technology and Processing XXI), 369-378.

15. Singh, L. Effect of nanoscale confinement on the physical properties of polymer thin films. PhD Dissertation, 2004.

16. *International Technology Roadmap for Semiconductors*; Semiconductor Industry Association: 2003.

CHAPTER 6

A NOVEL TOP SURFACE IMAGING METHOD USING AREA SELECTIVE ATOMIC LAYER DEPOSITION ON CHEMICALLY AMPLIFIED POLYMER PHOTORESIST FILMS

6.1 INTRODUCTION

The continued quest for miniaturization of feature sizes in microelectronic, optoelectronic, and microelectromechanical systems places strong demands on the lithographic and patterning processes used to fabricate such devices. In particular, semiconductor device manufacturing is continuing to push the limits of high volume optical lithography processes and materials used for fabricating device features beyond the 45nm technology node. Developing so-called "single layer" resist (SLR) materials and processes that can enable such high resolution patterning methods in the face of the extremely limited focus latitude available in modern optical projection lithography tools and yet still provide sufficient etch barrier toughness continues to be a significant challenge and potential future roadblock. In SLR approaches, these two issues are coupled because they both depend directly on the resist film thickness. One way to overcome these issues is to decouple the depth of focus limitation from the etch barrier toughness by transitioning to bilayer resist materials and processes. The basic idea in these bilayer methods is to form the initial pattern in an extremely thin imaging film which is coated onto a thicker etch barrier layer and subsequently transfer that pattern through the barrier layer via etching techniques to form the final resist pattern. Such

bilayer methods have been developed but have suffered from a number of problems including material compatibility limitations which inhibit materials design flexibility, process complexity of the multiple coating steps required, and difficulty in controlling deposition of the extremely thin imaging film layers[1-3]. A related but different approach employs so-called "top surface imaging" approaches in which a single layer resist is subsequently chemically modified in its surface or near-surface region after pattern-wise exposure to render selected regions of the resist film surface more resistant to subsequent etching processes[1, 4-7]. Again, the final patterned resist is formed by transferring the pattern formed by exposure and chemical modification of the resist surface throughout the entire resist film thickness by an etching technique.

Such top surface imaging (TSI) techniques using vapor or liquid phase silylation have been investigated extensively as alternatives to conventional resist processing. Indeed, a variety of different process schemes including Si-CARL, DESIRE[5], PRIME[7], SUPER[6], and Digital-Top-Surface-Imaging[4] have been considered over the past 20 years. Ideally, TSI via silylation methods involves the selective silylation of specific regions of a resist while the other regions are not silylated, i.e. the incorporation of silicon into either only the exposed or unexposed regions of the resist film. Patterns are obtained by selectively etching away the unsilylated regions with an oxygen plasma. In these cases, the silicon present in silylated regions forms a glassy SiO_2 layer on the resist surface during the early stages of the oxygen plasma etch which serves as an oxygen plasma etch barrier and prevents further etching of the underlying organic resist layer in these regions[3-5, 8].

TSI imaging schemes have several potential benefits. Since only the top portion of the resist film is imaged, the resist may be relatively opaque at the wavelength of the imaging

tool, thus allowing the use of a wider variety of organic resist materials with a particular exposure wavelength. In addition, since the imaging reaction in principle only needs to occur in the surface layer of the resist film, the required depth of focus for the imaging tool and process can be minimized and the resist film thickness can be arbitrarily large, thereby widening the process window of the imaging and etch processes. A further advantage is that extremely high aspect ratio resist features can be produced since the development of the pattern in the organic film is achieved by pattern transfer from the surface image into the bulk of the organic resist film using a plasma etch which can be tailored to be highly anisotropic. One final advantage is that resist pattern collapse that is encountered in the wet development of conventional SLR materials can be avoided in TSI processes since a wet development step of the resist features is never required. However, a variety of difficulties have limited the successful application of such TSI approaches. One of the main challenges with TSI processes has been finding ways to reduce the line edge roughness (LER) of the TSI-generated patterns to within acceptable values (LER $3\sigma < 6$ nm at 65 nm node and 4.2 nm at 45nm node).[3, 4, 9-11] Earlier imaging schemes such as DESIRE relied on crosslinking of the polymer resist film in the exposed areas to slow the diffusion of the silylating agent into the exposed areas, thus producing different concentrations of Si in the exposed and unexposed regions. Since some Si remained even in exposed regions where it was not desired, a plasma descum process was required to remove the thin layer of silicon incorporated into the crosslinked regions before performing the O_2 plasma pattern transfer etch.[4, 5] Furthermore, differences in the crosslink density and subsequent amount of silicon incorporation across the width of an optical projection printed feature resulted in non-uniform silylation profiles, commonly

referred to as “bird’s beak” profiles, which ultimately led to difficulty with critical dimension (CD) control of the feature and increased the LER of the overall process. So-called “digital silylation” techniques were developed to overcome these problems with the cross-linking based silylation processes. Digital silylation offered the potential to eliminate the need for a descum step because the active sites on the polymer which participate in the silylation are generated during exposure and post exposure baking (PEB) of the resist. In this manner, the unexposed areas are nominally unreactive towards the silylating agents and thus a descum etch is in principle not required.[4] However, due to the non-uniform energy deposition profile across a feature which results from the non-ideal aerial image produced using optical projection tools, the concentration of active sites in the exposed polymer varies across the feature width. The amount of Si incorporated into the near-surface volume of such features using the digital silylation processes thus decreases from the feature center to the feature edges. Therefore, the thickness of the silicon etch barrier formed at the feature edges is still thinner than that in the feature bulk, so that the barrier material does not serve as an effective etch mask in the oxygen plasma, which still results in CD control problems and unacceptable LER. One solution to help reduce such CD control and LER problems in digital silylation processes is to perform a trim or descum etch to remove the very thin silylated regions of the features at the feature edges, but such issues are still a major problem.

Recently, significant efforts have been undertaken to develop area selective atomic layer deposition techniques (ASALDT).[12-15] During atomic layer deposition (ALD), thin film growth is controlled by self limiting surface reactions. Thus, if a surface can be modified to prevent the surface reactions involved in the ALD process, nucleation and

film growth during ALD can also be prevented on those regions of the surface. ASALDT utilizes this approach to block nucleation in certain areas while allowing film deposition only in desired areas. Early studies focused on the use of self assembled monolayers as masks for achieving area selective ALD of metal oxides on Si substrates and reported the use of octadecyltrichlorosilane SAMs to inhibit nucleation of ALD films.[12, 13] More recently, we have shown that patterned polymer films can provide a much more robust and simpler method for achieving selective ALD.[14,15] In these previous studies, micron scale direct patterned deposition of TiO_2 on Si was achieved using titanium tetrachloride or titanium isopropoxide as the metal precursor, water as an oxygen source, and poly (methylmethacrylate) as a photodefinable polymeric masking layer. These investigations have demonstrated that nucleation of titania films produced by ALD can be successfully blocked on polymer materials that do not contain reactive OH groups in their backbone. In addition, it was observed that under surface conditions where ALD films do nucleate on the polymer film, a conformal and defect free film can be formed directly on the polymer surface. These earlier studies ultimately inspired the novel TSI technique presented here.

In this chapter, a novel method for utilizing area selective ALD to perform TSI is presented. The approach involves the selective deposition of an inorganic etch barrier, i.e. a metal oxide in this work, on predefined reactive areas of a polymer film surface which have been delineated by radiation exposure. Subsequent selective etching of the regions of the polymer film not masked by the etch barrier layer is then performed to obtain the desired resist pattern. Figure 6-1 illustrates the process scheme utilized in this new TSI process. This method offers the potential to overcome the problem of thin etch

barrier thickness at the feature edge encountered in other TSI methods which result from low silicon incorporation at the feature edge. In the ALD-based TSI approach presented here, the amount of etch barrier material incorporated into the film structure does not depend on the total concentration of active sites generated in the exposed polymer volume as is the case with previous TSI approaches. Nucleation of the ALD film growth in the method presented here depends only on the presence of active sites on the polymer film surface. Thus, the thickness and amount of ALD etch barrier deposited does not depend on the total hydroxyl concentration in the volume of the polymer film but instead depends on the number of ALD growth cycles performed. Therefore, it should be possible to use ALD to grow thicker more robust etch barrier layers that can withstand the plasma pattern transfer etching processes and thereby reduce LER in such features. Finally, because deposition of the etch barrier material can be extremely selective, a plasma descum etch is not required which offers the potential to simplify the overall imaging process. While there are many questions that must be answered to fully validate the promise of such a technique, the preliminary experimental results demonstrate the feasibility of achieving TSI using an area selective ALD process on polymer films.

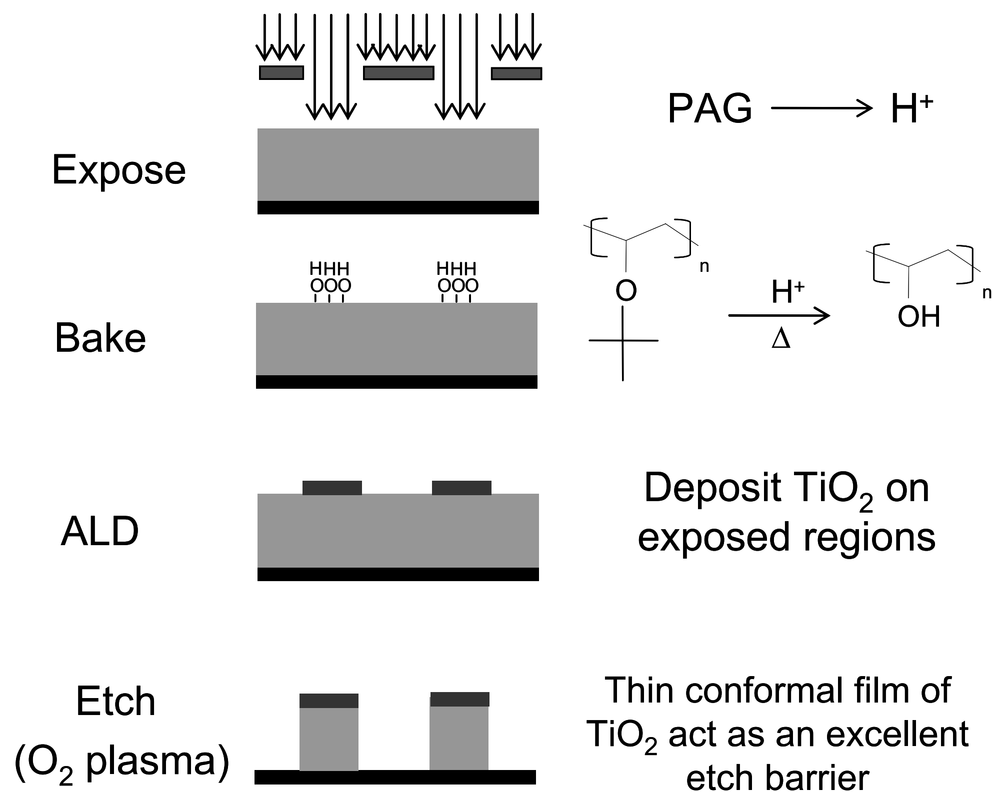

Figure 6-1: Schematic of the new top surface imaging approach which utilizes area selective atomic layer deposition in conjunction with a radiation sensitive reactive polymer film to achieve direct patterned deposition of an etch barrier film.

6.2 EXPERIMENTAL PROCEDURE AND RESULTS

Poly-tertbutylmethacrylate (PtBMA) (Scientific Polymer) was used as a model resist film for the area selective ALD TSI process since it does not contain OH groups and the tert-butyl ester group can undergo acid catalyzed deesterification to produce hydroxyl containing poly-methacrylic acid (PMAA)[16]. A 5 wt% solution of PtBMA in toluene was mixed with 1 wt% (by solids) triphenylsulfonium tris(perfluoromethanesulfonyl) methide (TPS-C1) (3M Corporation), which serves as a photo acid generator (PAG). Resist films

were spin coated onto a Si <100> wafer and then soft baked at 90 ^{o}C for 4 minutes to remove residual casting solvent. Ultraviolet exposure of the resulting films was performed at a total dose of 60mJ/cm^2 using an Oriel 87000 series DUV exposure tool. The exposure tool was equipped with 500 W Hg-Xe lamp and an external bandpass filter (center wavelength of 248 nm and full-width half max of approximately 20 nm) that narrowed the spectral width of the UV radiation. All exposures were conducted in a base-free cleanroom environment and a post exposure bake (PEB) was conducted immediately after exposure at 130 ^{o}C for 15-20 s to promote the acid catalyzed deprotection reaction of the polymer. After PEB, films were exposed to room ambient where airborne base quickly quenched excess acid present in the exposed regions of the film. Acid generated in the exposed regions of the film resulted in cleavage of the tert-butyl ester groups on the polymer to produce PMAA in the presence of moisture after baking. Figure 6-2 shows FTIR spectra of the starting PtBMA and the PMAA obtained after exposure and PEB. Tert-butyl ester group cleavage is clearly evident from: (1) the reduction in peak intensity at 3000 cm^{-1} (CH_3 stretch) and 1365 cm^{-1} ($C(CH_3)_3$ stretch), (2) the appearance of a strongly hydrogen bonded broad OH peak at 3100 – 3400 cm^{-1} and (3) a peak shift from 1725 cm^{-1} (COOR stretch in PtBMA) to 1700 cm^{-1} (dimeric COOH stretch in PMAA). A reduction of the water contact angle from 88-90° on unexposed surfaces to 75-78° on surfaces after UV-exposure and PEB further confirms the generation of hydrophilic -COOH groups on the surface of the polymer film. These surface hydroxyl groups eventually act as active sites for nucleation of TiO_2 during subsequent ALD processing.

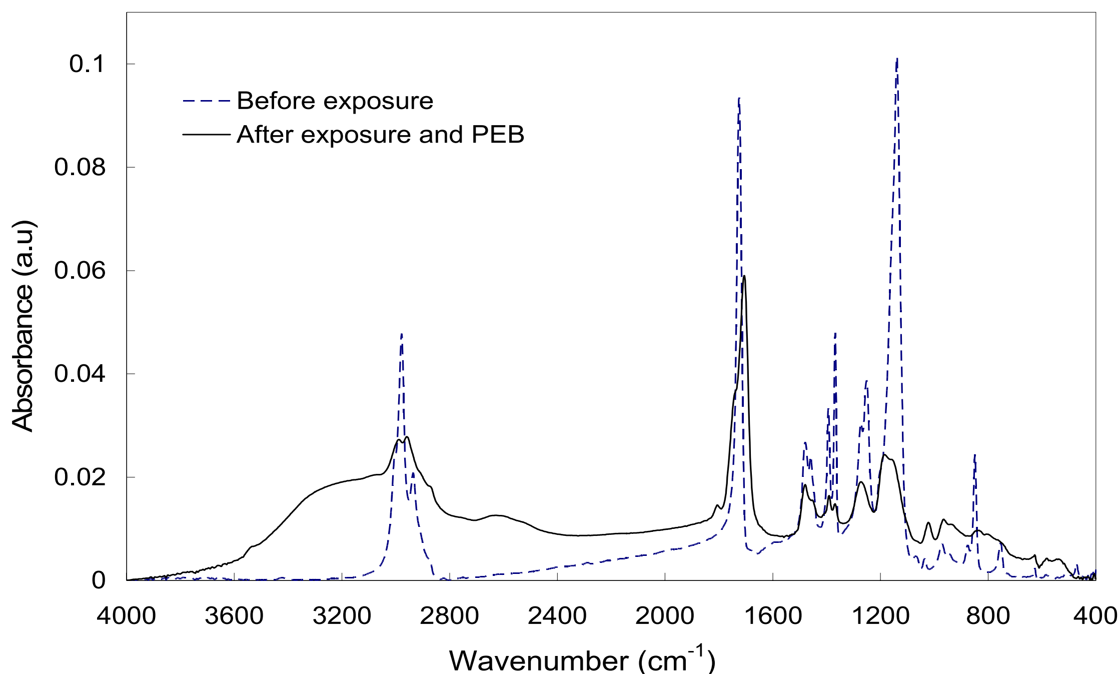

Figure 6-2: Representative FTIR spectra of the PtBMA polymer used as the reactive imaging film in this work both before exposure and after exposure and post-exposure bake (PEB).

Deposition of TiO_2 was conducted in an ALD reactor that has been described previously in chapter 2. Titanium isopropoxide (TiIP), volatilized at 82 ^oC, was used as the metal precursor and deionized water maintained at room temperature (~22-24 ^oC) was used as the oxygen source for titania deposition by ALD. The reactor was evacuated before starting ALD film deposition to a base pressure of 10-20 mTorr after loading the samples and heating the reactor walls to 95-100 ^oC. Nitrogen was used as both the purge gas and carrier gas, and thus a constant nitrogen flow rate of 78 SCCM was maintained throughout the ALD deposition process. All depositions were conducted at a chamber pressure of 1 torr and a substrate temperature of 140 ^oC. The ALD precursor pulse and purge sequence times for all the depositions was fixed at 2s (TiIP) – 25s (N_2) - 2s (H_2O) –

60s (N_2). Under these operating conditions TiO_2 grows at a controlled growth rate of approximately 0.07 nm per cycle. During ALD, the absence of active sites on the unexposed regions of the polymer film prevents TiO_2 from nucleating in these areas. On the other hand, active -COOH sites generated in exposed regions lead to nucleation and growth of a thin, conformal titania film on the polymer surface as demonstrated in the X-ray photoelectron spectra (XPS) presented in Figure 6-3. Selective deposition of TiO_2 only in exposed regions is clearly evident from the difference in intensity of the Ti2p peaks in spectra from the two different regions of a pattern-wise exposed polymer film. The C1s peak observed for the titania regions deposited in exposed areas of the polymer film arises from adventitious carbon and not from carbonaceous material incorporation from the polymer film, and thus appears as a single sharp peak at 284.8 eV (C-C bonds). This is clearly distinct from the more complicated C1s spectra for the polymer as visible in the spectra from the unexposed regions of the sample. These XPS results also indicate the presence of a TiO_2 layer on top of exposed regions of the polymer that has a thickness greater than the attenuation length (~ 10 nm in this case) of the photoelectrons ejected from the underlying polymer layer. The SEM image presented in Figure 6-4 also shows that a conformal layer (~21 nm) of TiO_2 is deposited onto the exposed regions of the PtBMA polymer film. Attempts were made to obtain a similar image for the acrylate polymer and the edge transition between the unexposed and exposed regions of a patterned sample. However, the acrylate polymer backbone decomposes under electron beam irradiation in the SEM and thus causes focus problems which have prevented successful generation of clear images of these other regions at this time.

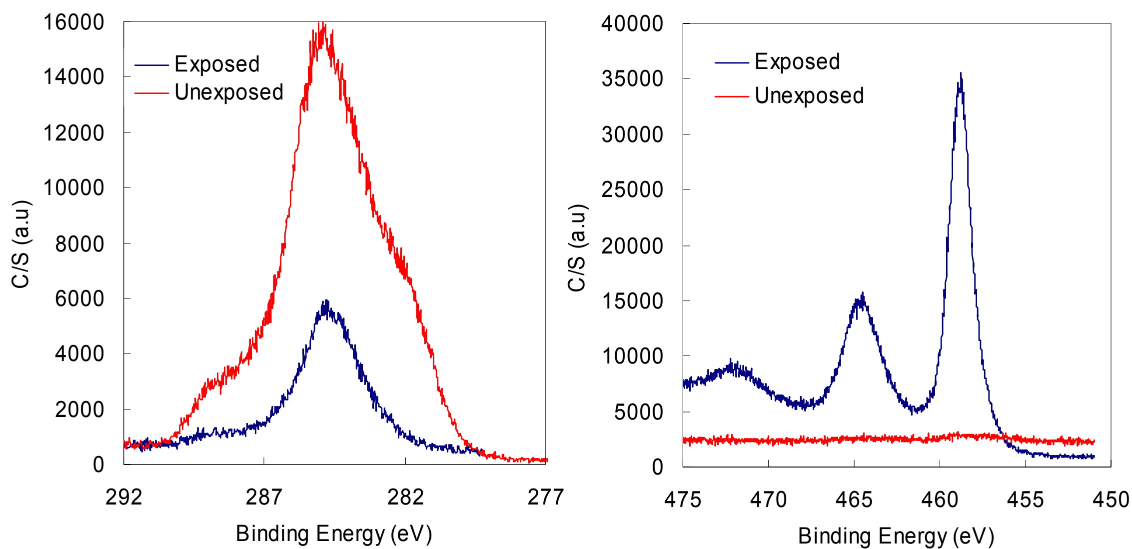

Figure 6-3: XPS spectra comparing the surface composition of the unexposed and exposed regions of the PtBMA polymer after exposure, PEB, and ALD. (A) C1s spectra and (B) Ti2P spectra.

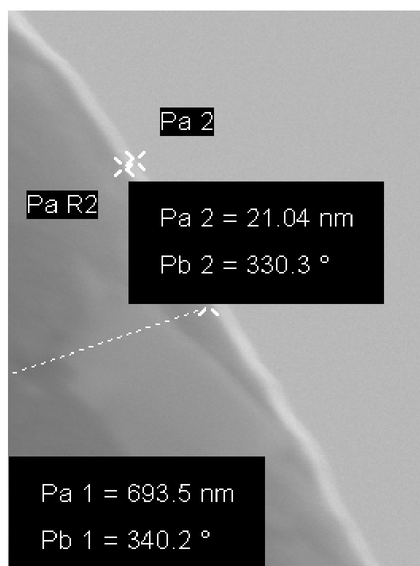

Figure 6-4: Cross-section SEM image showing conformal TiO_2 layer grown on PtBMA film after UV exposure and PEB baking.

After exposure, baking, and ALD, the inorganic etch barrier pattern is transferred into the polymer layer using an oxygen plasma to obtain a final negative tone image in the polymer film. Plasma pattern transfer etching was performed in a parallel plate plasma reactor operating at 13.56 MHz and 1 Torr O_2. Figure 6-5 shows optical micrographs of the resulting patterns produced after etch pattern transfer for features printed using contact lithography at sizes ranging from 25 μm to 100 μm. While these features are not extremely small, they do demonstrate that the overall process scheme described in Figure 1 can be successfully applied to allow TSI using an ALD approach. Furthermore, it is worth mentioning that these patterns were produced without the use of a plasma descum etch, furthering lending support to the idea that the metal oxide deposition is highly selective to only the exposed area. Optical and SEM inspection of the samples after imaging, ALD, an etching have not revealed any significant "grass" formation or other residual etch artifacts that have been common in other TSI approaches.

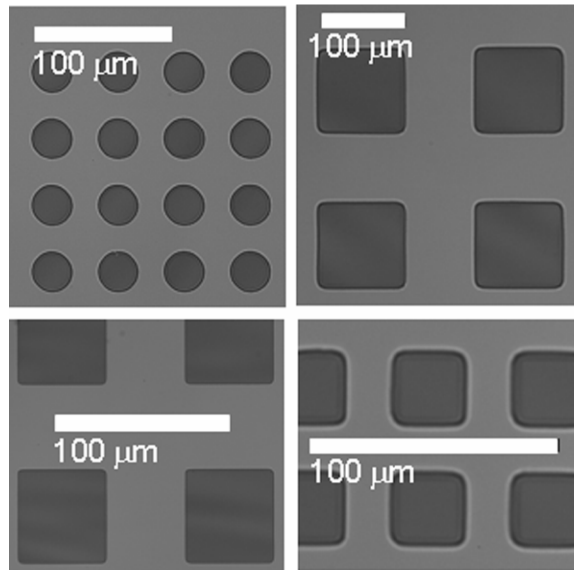

Figure 6-5: Optical micrographs showing different size and shape patterns obtained after completion of the four step process illustrated in Figure 6-1.

6.3 FUNDAMENTAL BEHAVIOR OF ASALD-TSI PROCESS

As described above, a proof of concept for an ASALD-based TSI scheme has been demonstrated. Subsequent experiments focused on understanding the overall behavior of this process. During digital silylation-based TSI process a major contributor to line edge roughness is the silylation contrast of the system. The silylation contrast can be defined as the amount of Si incorporated to the polymer matrix as a function of exposure dose. The silylation response for an ideal system should be as close to a step function as possible. The threshold for silylation can then be tuned to correspond to the feature edge and the undesired exposure that occurs in the "dark" areas of the photoresist can be mitigated. Unfortunately, to date, most of the digital-TSI approaches using a 248 nm exposure tool exhibit linear contrast (as shown in figure 6-6) which makes the edge of silylated feature somewhat indistinct due to a pseudo-gaussian shape of the aerial image, which manifests itself as line edge roughness in the final image. Silylation contrast for 248 nm tBOC-PHOST resist is presented in figure 6-6.

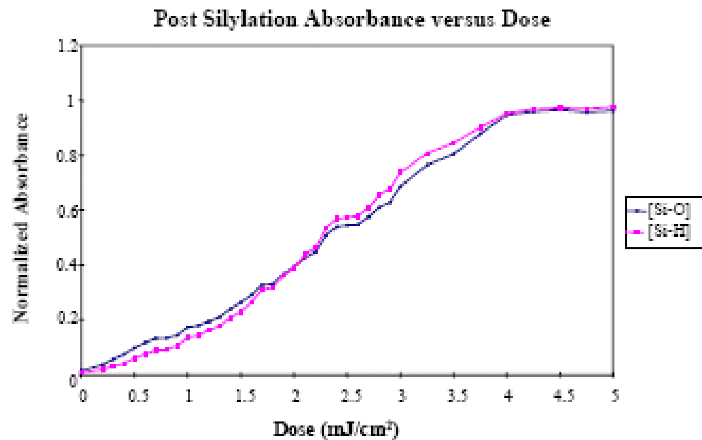

Figure 6-6: Silylation contrast plot for tBOC-PHOST [4]

Thus, in order to establish the feasibility of an ASALD-TSI process it is important to investigate analogous contrast curves for this process as well. Resist films were prepared using the procedure outlined in section 6.2 and exposed to different exposure doses. Different exposure dose leads to different levels of deesterification in the resist matrix, thus creating samples with different concentrations of active surface sites (-COOH). These samples were then subjected to different numbers of ALD cycles and analyzed using XPS. Contrast curves for ASALD-TSI processes were obtained by measuring Ti atomic % on surfaces exposed to different exposure doses and subjected to a varying number of ALD cycles (shown in figure 6-7). XPS analysis was performed with the photoelectron detector positioned at an angle of 45° to the sample plane where the sampling depth is ~8 nm. In this way, the atomic % of Ti saturates after the thickness of TiO_2 layer grown over polymer film reaches ~ 8 nm. In our experiments, a Ti atomic concentration of ~22% corresponds to a TiO_2 layer thicker than 8 nm. The etch resistance of TiO_2 with an oxygen plasma at 1 torr is very high and a conformal titania layer of this thickness is expected to serve as robust etch barrier.

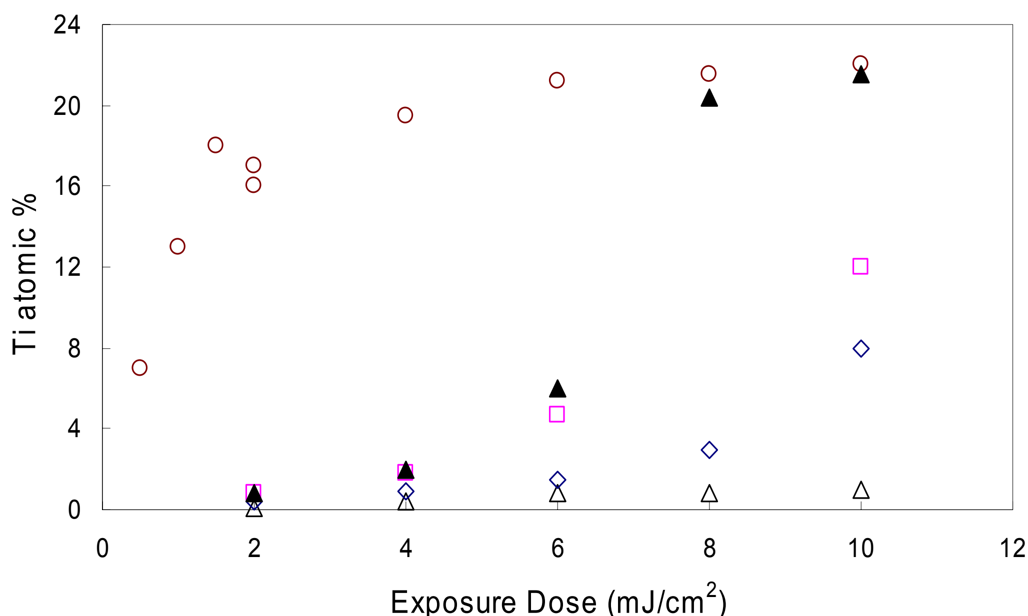

Figure 6-7: ALD deposition contrast for an ASALD-TSI process (Δ – 50 cycles, ◊ - 100 cycles, □ – 150 cycles, ○ – 250 cycles, ▲ – 250 cycles (DBU loaded))

Before we discuss the data presented in figure 6-7 in further detail, it is important to know the concentration of active sites on the surface as a function of exposure dose. Semi-quantitative estimation of the concentration of a functional group on a surface can be performed using XPS since it provides information about elemental composition and the chemical state of atoms within 8-10 nm of the surface. Unfortunately it is difficult to differentiate between carbon or oxygen photoelectron signal from carboxylic acid and ester groups. Thus, in order to quantify the amount of acid functionalities at the surface, it is necessary to carry out chemical derivatization. Chemical derivatization of any functional group includes attaching a unique element to that group via chemical reaction. Derivatization of carboxylic acid groups by reacting them with trifluoroethanol (TFE) has been investigated previously[17-22]. The derivatization protocol outlined by Chilkoti et. al[18]

has been used in our study. The reaction scheme (shown in figure 6-8) uses a carbodiimide reagent to activate the carbonyl carbon of the acid group towards nucleophilic attack. Subsequently, TFE reacts with the intermediate to form an ester.

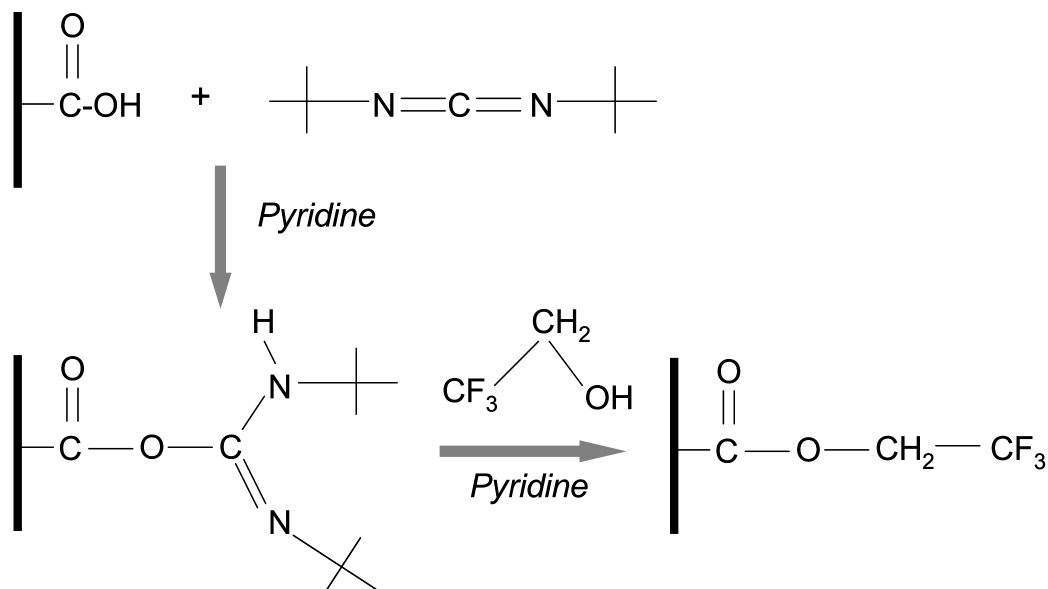

Figure 6-8: Reaction scheme for chemical derivatization of carboxylic group using TFE[20]

It can be observed from the reaction scheme that the derivatization reaction adds 3 F atoms without altering the number of O atoms present in the parent carboxyl molecule. Thus, F/O atomic ratio can be used to obtain a semi-quantitative estimate of the number of acid groups present in the sample.

Derivatization procedure: Tirifluroethanol, 99.5%+ (Alfa Aesar), Pyridine (Burdick & Jackson) and di-tertbutylcarbodiimide (di-tBuC) (Aldrich) were used as reagents for the derivatization reactions. Resist films were prepared on Si substrates by the procedure

described in section 6.2. Samples were then subjected to different exposure doses and PEB was performed at 130 ^{o}C for 20s. Samples were placed on a Teflon stage maintained inside a glass bottle. One hundred µl of TFE, 45 µl of pyridine and 35 µl of di-tBuC were sequentially injected into the glass bottle (avoiding contact of liquids with the samples) at intervals of 15 mins. The glass bottle was sealed with a Teflon-lined cap and the reaction was allowed to proceed at ambient temperature (22-24 ^{o}C) for ~40 hrs. Samples were analyzed using XPS without any further treatment. F/O atomic ratios of samples exposed to different exposure dose are presented in figure 6-9.

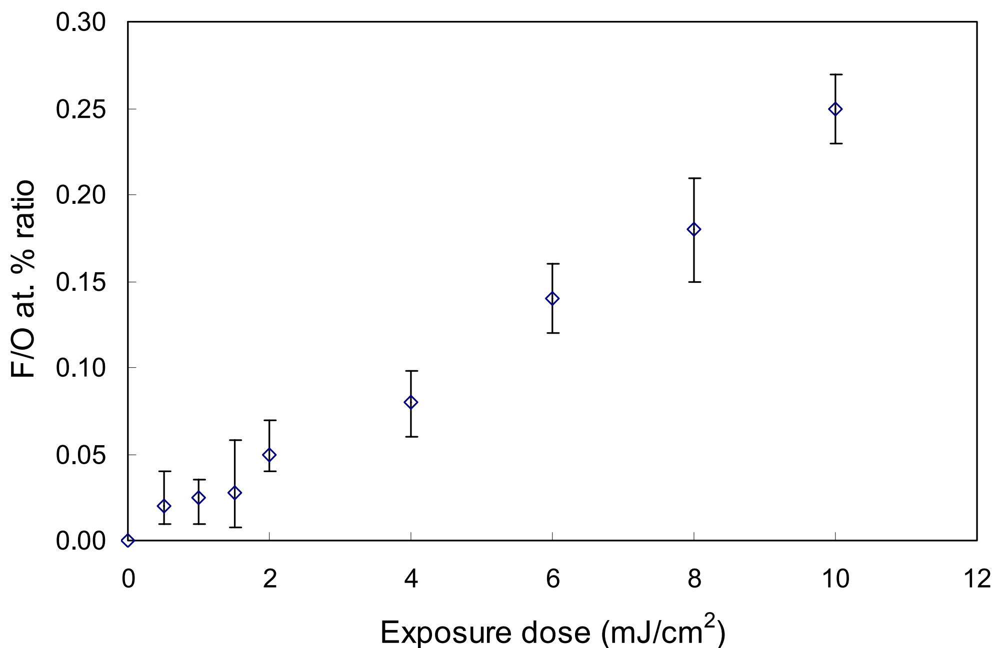

Figure 6-9: Semi-quantitative estimation of active sites: F/O at. % ratio obtained from XPS of samples exposed to different exposure doses and chemically derivatized

The concentration of –COOH groups at the film surface (within ~8nm sample depth) shows an approximate linear response with exposure dose. In addition, relative to the high dose regime, the slope of the line is significantly lower in the low exposure dose region. Such observations could be due to trace base contaminants present in the laboratory atmosphere where exposure was performed. These base contaminants can neutralize the acid generated at the surface causing fewer de-esterification events to occur. As the exposure dose is increased, a smaller fraction of acid will be neutralized by air-borne base contamination, thus leading to the shallower slope in the low exposure dose region. Further, such behavior could also occur due to steric hindrance effects. The reaction scheme (Fig 6-8) indicates that initially, di-tBuC reacts with –COOH groups to produce an intermediate with a particularly stable leaving group. This attack can be sterically more hindered for sites surrounded by a higher number of bulky tert-butyl groups from the parent polymer backbone. As a result, for lower exposure dose samples, fewer fractions of carboxyl groups may be derivatized than for samples subjected to higher doses.

Considering the data presented in figure 6-7 and 6-9, it is clear that for a smaller number of ALD cycles, the extent of surface Ti incorporation follows the concentration of active sites present on the surface. After nucleation initiation, the nucleated site will serve as an active site for subsequent ALD cycles. In fact, the number of active sites should increase with the number of cycles since TiIP attachment to one site will create at least 3 active sites if no Ti-O-Ti bridge is formed. These nucleated islands continue to grow during subsequent ALD cycles and eventually merge to produce a continuous titania layer on the polymer film surface. Therefore, after 250 cycles we observe ~20-22

% Ti on the surface which corresponds to at least 8 nm of TiO_2 layer on the polymer film. In addition, polymer surfaces treated with higher exposure doses have higher concentrations of active sites and require fewer ALD cycles to form a continuous layer. More importantly, it is encouraging to observe that the ALD-TSI process demonstrates high contrast and a non linear response to exposure dose for a higher number of ALD cycles. As a result, even the regions corresponding to low exposure dose can be covered with a conformal etch barrier of sufficient thickness to serve as an effective etch mask provided that a sufficient number of ALD cycles have been used. This supports our initial hypothesis that for ASALD-TSI, the amount of etch barrier material (e.g., Ti) incorporated into the film structure does not depend on the total concentration of active sites generated in the exposed polymer volume as is the case with previous TSI approaches. Unfortunately, since the spread of an aerial image is considerable in low exposure dose regions, it is not preferable to have such high contrast close to low dose regions, since this can cause difficulty in controlling the feature dimensions and reduce the exposure latitude. However, this problem can be solved by adding a certain amount of base to the resist solution. To test this hypothesis, 1, 8 diazabicyclo(5.4.0)undec-7-ene(1,5-5) (DBU, Fluka) (1:3 mole ratio DBU:TPS-C1) was added to the resist solution and similar experiments to those described above, performed with the base loaded samples. Ti atomic % obtained on these samples after 250 ALD cycles is shown in figure 6-6. Clearly, the addition of base neutralized the acid generated within the samples exposed to lower doses and simply shifted the contrast curve to a higher dose region without any apparent reduction in the contrast curve slope. This observation suggests

that the process parameter can be tuned to control the critical dimension of desired feature and also improve the exposure latitude of imaging process.

6.4 CONCLUSIONS

Area selective ALD in conjunction with protected polymer thin films offers a new and promising approach to perform top surface imaging. Direct area selective patterned growth of titania on a chemically amplified protected polymer film and subsequent pattern transfer by oxygen plasma etching has been demonstrated. It has been shown that successful pattern transfer can be achieved without requiring a plasma descum, thus simplifying the TSI process. Furthermore, this ASALD-TSI process has demonstrated sharp contrast and therefore offers the potential to overcome many of the challenges experienced with conventional TSI schemes.

6.5 REFERENCES

1. Dammel, R., *Diazonaphthoquinone-based Resists*. SPIE-The International Society for Optical Engineering: Bellingham, 1993; Vol. TT 11.

2. Willson, C. G.; Thompson, L. F.; Bowden, M. J., *Introduction to Microlithography*. Second ed.; American Chemical Society: Washington, 1994.

3. Seeger, D. E.; La Tulipe, D. C., Jr.; Kunz, R. R.; Garza, C. M.; Hanratty, M. A., Thin-film imaging: past, present, prognosis. *IBM Journal of Research and Development* **1997,** 41, (1/2), 105-118.

4. Somervell, M. H.; Fryer, D. S.; Osborn, B.; Patterson, K.; Byers, J.; Willson, C. G., Study of the fundamental contributions to line edge roughness in a 193 nm, top surface imaging system. *Journal of Vacuum Science & Technology, B: Microelectronics and Nanometer Structures* **2000,** 18, (5), 2551-2559.

5. Coopmans, F.; Roland, B., DESIRE: a new route to submicron optical lithography. *Solid State Technology* **1987,** 30, (6), 93-9.

6. Mutsaers, C. M. J.; Vollenbroek, F. A.; Nijssen, W. P. M.; Visser, R. J., ImRe, BIM and SUPER using patternwise esterification. *Microelectronic Engineering* **1990,** 11, (1-4), 497-502.

7. Pierrat, C.; Tedesco, S.; Vinet, F.; Lerme, M.; Dal'Zotto, B., Positive resist image by dry etching: new dry developed positive working system for electron beam and deep ultraviolet lithography. *Journal of Vacuum Science & Technology, B: Microelectronics and Nanometer Structures* **1989,** 7, (6), 1782-6.

8. Willson, C. G.; Bowden, M. J., Organic resist materials. *Advances in Chemistry Series* **1988,** 218, (Electron. Photonic Appl. Polym.), 75-108.

9. International Technology Roadmap for Semiconductors. **2004 Update**.

10. Sugihara, T.; Van Roey, F.; Goethals, A. M.; Ronse, K.; Van Den Hove, L., Resist surface investigations for reduction of line-edge-roughness in top surface imaging technology. *Microelectronic Engineering* **1999,** 46, (1-4), 339-343.

11. Mori, S.; Morisawa, T.; Matsuzawa, N.; Kaimoto, Y.; Endo, M.; Matsuo, T.; Kuhara, K.; Sasago, M., Reduction of line edge roughness in the top surface imaging process. *Journal of Vacuum Science & Technology, B: Microelectronics and Nanometer Structures* **1998,** 16, (6), 3739-3743.

12. Park, M. H.; Jang, Y. J.; Sung-Suh, H. M.; Sung, M. M., Selective Atomic Layer Deposition of Titanium Oxide on Patterned Self-Assembled Monolayers Formed by Microcontact Printing. *Langmuir* **2004,** 20, (6), 2257-2260.

13. Yan, M.; Koide, Y.; Babcock, J. R.; Markworth, P. R.; Belot, J. A.; Marks, T. J.; Chang, R. P. H., Selective-area atomic layer epitaxy growth of ZnO features on soft lithography-patterned substrates. *Applied Physics Letters* **2001,** 79, (11), 1709-1711.

14. Sinha, A.; Hess, D. W.; Henderson, C. L., Area-Selective ALD of Titanium Dioxide Using Lithographically Defined Poly (Methyl methacrylate) Films. *Journal of the Electrochemical Society* **2006,** 153, (5), G465-G469.

15. Sinha, A.; Hess, D. W.; Henderson, C. L., Area Selective Atomic Layer Deposition of Titanium Dioxide: Effect of Precursor Chemistry. *Journal of Vacuum Science & Technology, B: Microelectronics and Nanometer Structures* **Submitted**.

16. Ito, H.; Ueda, M., Thermolysis and photochemical acidolysis of selected polymethacrylates. *Macromolecules* **1988,** 21, (5), 1475-82.

17. Alexander, M. R.; Wright, P. V.; Ratner, B. D., Trifluoroethanol derivatization of carboxylic acid-containing polymers for quantitative XPS analysis. *Surface and Interface Analysis* **1996,** 24, (3), 217-220.

18. Chilkoti, A.; Ratner, B. D.; Briggs, D., Plasma-Deposited Polymeric Films Prepared from Carbonyl-Containing Volatile Precursors - Xps Chemical Derivatization and Static Sims Surface Characterization. *Chemistry of Materials* **1991,** 3, (1), 51-61.

19. Everhart, D. S.; Reilley, C. N., Chemical Derivatization in Electron-Spectroscopy for Chemical-Analysis of Surface Functional-Groups Introduced on Low-Density Polyethylene Film. *Analytical Chemistry* **1981,** 53, (4), 665-676.

20. Hutt, D. A.; Leggett, G. J., Functionalization of hydroxyl and carboxylic acid terminated self-assembled monolayers. *Langmuir* **1997,** 13, (10), 2740-2748.

21. Markkula, T. K.; Hunt, J. A.; Pu, F. R.; Williams, R. L., Surface chemical derivatization of plasma-treated PET and PTFE. *Surface and Interface Analysis* **2002,** 34, (1), 583-587.

22. Popat, R. P.; Sutherland, I.; Sheng, E. S., Vapor-Phase Chemical Derivatization for the Determination of Surface Functional-Groups by X-Ray Photoelectron-Spectroscopy. *Journal of Materials Chemistry* **1995,** 5, (5), 713-717.

CHAPTER 7

TRANSPORT BEHAVIOR OF ALD-PRECURSORS THROUGH POLYMER MASKING LAYERS

7.1 INTRODUCTION

Our previous work demonstrated the successful implementation of a polymer-based masking approach for ASALD of titanium dioxide on a Si substrate. During the course of that investigation, it was observed that precursor sorption and diffusion through polymer masks play critical roles in establishing a successful ASALD process. In particular, the diffusion coefficient of metal precursors controlled the masking layer thickness required. In addition, equilibrium uptake of the precursors in combination with the diffusion coefficient, directly determine the remnant precursor concentration after each ALD half cycle. If the reactor is not adequately purged, these remnant precursors can act as nucleation sites and cause failure of the ASALD process. In this chapter, we investigate the transport properties of ALD precursors through different polymer films studied in previous experiments,. Specifically, the transport properties of water have been investigated in different polymers including PHOST, HFA-PNB and PMMA at different temperatures. Transport properties of metal precursors have only been investigated for PMMA.

7.2 BACKGROUND

7.2.1 FUNDAMENTALS OF MASS TRANSPORT

In the absence of convective flow and for an ideal gas, the transport of a penetrant A through a medium is described by [1]

$$\frac{\partial C_A}{\partial t} = \nabla . C D_A \nabla x_A \tag{7.1}$$

where C_A = Concentration of penetrant A

t = time

D_A = Diffusion coefficient

x_A = mole fraction of A

When the penetrant concentration (in region surrounding the medium) and diffusion coefficient (through the medium) are constant, equation 7.1 simplifies to

$$\frac{\partial C_A}{\partial t} = D_A \nabla^2 C_A \tag{7.2}$$

Equation 7.2 is the well-known Fick's second law that has found wide application in determining diffusion coefficients. For a planar geometry with x and y dimensions much greater than the z dimension, equation 7.1 further reduces to a simpler 1-D diffusion equation. In the situation where one face in the x-y plane is impermeable (insulated from mass transport) and the other face is exposed to a constant concentration of a single

penetrant A, the system can be described by equation 7.3 with specific boundary conditions as listed below; the geometry of this scenario is illustrated by figure 7-1. In our experiments, the polymer films were spin coated onto a planar substrate and thus represent a geometry appropriate to this analysis.

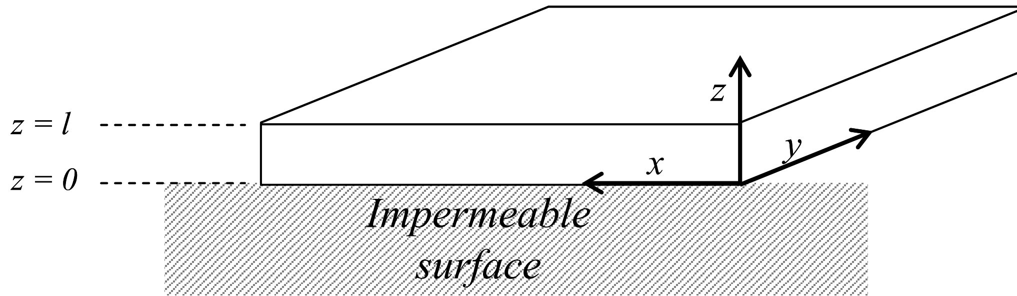

Figure 7-1: Schematic of the 1-D geometry used in this study

$$\frac{\partial C_A}{\partial t} = D_A \frac{\partial^2 C_A}{\partial z^2} \tag{7.3}$$

Boundary conditions:

BC 1: $\frac{\partial C_A}{\partial z} = 0$ at $z=0 \quad \forall \ t$

BC 2: $C_A = C_{A1}$ at $z = l$ for $t > 0$

BC 3: $C_A = C_{A0}$ at $t = 0$ for $0 < z < l$

With these boundary conditions, equation 7.3 can be solved for the penetrant concentration in the polymer film at a given z and t. The concentration profile is then integrated over the thickness of polymer film to obtain the total mass of the penetrant inside the film at any time t as described by expression 7.4.

$$\frac{M_t}{M_\infty} = 1 - \frac{8}{\pi^2}\sum_{n=0}^{\infty}\frac{1}{(2n+1)^2}\exp\left[-\frac{(2n+1)^2\pi^2 Dt}{4l^2}\right] \tag{7.4}$$

where M_t is the mass uptake at time t, M_∞ is the amount absorbed at equilibrium, D is the diffusion coefficient (since this is a single penetrant sorption, subscript A from D_A is dropped for convenience), and l is the film thickness. Thus, by performing sorption experiments for different penetrants in a polymer system, we can estimate the equilibrium uptake and diffusion coefficient of the penetrant through a specific polymer film.

7.2.2 QUARTZ CRYSTAL MICROBALANCE

The quartz crystal microbalance (QCM) technique is widely used to investigate transport properties of molecules through polymer films. Quartz is a piezoelectric material which resonates at a fundamental frequency under the effect of an oscillating electric field (AC voltage). The frequency of oscillation decreases when mass is loaded onto the crystal surface. Sauerbrey, in 1959, demonstrated that the change in resonance frequency of the crystal is linearly proportional to the change in mass loading as described by equation 7.5 [2].

$$\Delta f = -\frac{2 f_o^{\,2} \Delta m}{A\sqrt{\mu\rho}} = -C\Delta m \qquad (7.5)$$

where, Δf = change in frequency
f_o = fundamental resonant frequency of unloaded quartz crystal
Δm = mass change
A = surface area
μ = shear modulus of the AT-cut quartz
ρ = density of quartz

Sauerbrey's discovery revolutionized the application of QCM as an analytical tool for studies involving a mass change on the surface of a QCM crystal or inside a coating on the crystal. In our experiments, the mass of the polymer films coated onto QCM crystals changes as penetrants are absorbed into the film; hence QCM can be conveniently used to monitor the extent of mass increase in the polymer films during sorption experiments. It is important to note that the Sauerbrey equation is only valid for thin films that can be considered rigid masses[3, 4]. If the film is not a rigid mass, the shear wave in the QCM crystal propagates into the coated film and losees a significant amount of energy. This energy loss will in turn affect the frequency measurement and the crystal behavior can deviate strongly from the Sauerbrey relationship. The rigid mass requirement for the Sauerbrey equation is especially important for high mass loadings on QCM crystals. A good indicator of the elastic behavior of the quartz crystal/polymer film system is the ratio of the acoustic impedance (Z) of the respective materials. As the elastic behavior of the polymer film changes, the value of Z changes as well. It has been shown that for high mass loadings on a QCM, significant deviations from the Sauerbrey equation can occur for small changes in Z. This may result in errors in the mass calculated as penetrant is

absorbed into the polymer films, plasticizes them, and changes their elastic behavior (Z value). Fortunately, any changes in the elastic behavior of the polymer films studied in this work should not create a significant deviation from the Sauerbrey equation. This conclusion is supported by the observation that although a change in Z at high mass loadings created significant measurement errors, at low mass loadings or crystal frequency shifts, (i.e. delta frequency due to mass addition divided by crystal resonant frequency less than 0.05) the mass/frequency relationships for all values of Z converge on the Sauerbrey relationship[3]. The frequency shift ratios observed in the experiments reported here were very small (0.001–0.002), and thus the use of the Sauerbrey relationship to determine the mass added to the crystal from the resonance frequency shift should introduce insignificant error. In addition, dissipation factors of polymer coated crystals at all temperatures investigated were also monitored by QCM-D (Q-sense, QCM with dissipation monitor) measurements. Dissipation factor is defined as the ratio of the loss modulus to the storage modulus and thus is an indicator of the softness or damping ability of the film coated on the crystal. The difference in dissipation factor of uncoated and polymer coated crystals at all temperatures studied were <6 %, which further supports the validity of the Sauerbrey relationship for our calculations.

7.3 EXPERIMENTAL

7.3.1 EXPERIMENTAL APPARATUS

A schematic of the experimental apparatus used for sorption studies is presented in figure 7-2. The apparatus consisted of two different size chambers placed inside a mechanical convection oven (Yamato Scientific, DKN 600 series). The smaller chamber housed two QCM crystals while the other chamber served as a reservoir. Pressure in both chambers was monitored using Barocel 622 series pressure transducers with bakeable sensor heads. The sensor heads can be heated to 200 ^{o}C and offer reliable measurements independent of vapor phase composition when operated within this temperature limit. However, the zero reading for the pressure transducer connected to the larger chamber shifted by 0.13-0.14 Torr when heated above 60 ^{o}C, thus causing a fixed offset of 0.13-0.14 Torr in the pressure readings. The transducer connected to the smaller chamber delivered stable pressure measurements at all temperatures. Temperature measurement was performed using a K-type thermocouple (TC) (Omega Inc.) with SS sheath and grounded junction. The SS sheath protected the TC junction from corrosive environments ($TiCl_4$) and the grounded junction type was chosen for its rapid response relative to that of an ungrounded junction type. The penetrants were stored in a round bottom flask and were subjected to at least three freeze-pump-thaw cycles before use in order to remove any non-condensable gases absorbed in the penetrant liquid.

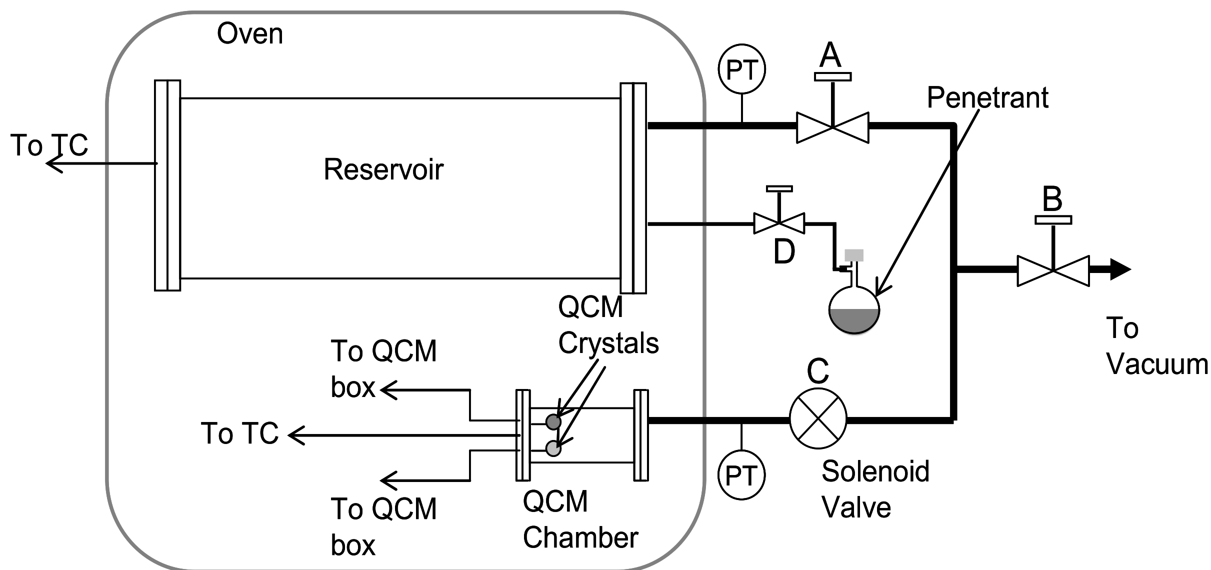

Figure 7-2: Schematic of the QCM apparatus

Gold plated AT-cut quartz crystals (Anderson Electronics Inc., electrode size: 0.435" diameter (top) and 0.250" diameter (bottom)) with a nominal resonance frequency of 5 MHz in the fundamental mode were used for QCM measurements. A crystal holder (HC-51) also obtained from Anderson Electronics Inc. was converted into a vacuum seal crystal holder for our experiments by passing the lead wire through holes drilled in a 2.75" Conflat blank and then sealing the holes with an epoxy sealant (Duralco 4700 series, Cotronics Corp.), which is stable for continuous operation up to 350°C. This custom-made crystal holder allowed the use of a small QCM chamber (Volume: ~55 cm^3). The crystal frequency was measured using a commercial Maxtek RQCM system and the data was logged at a frequency of 20 Hz. The entire system was maintained under vacuum using an Alcatel 2033 C2 series vacuum pump. A liquid nitrogen trap was

installed upstream of the vacuum pump to prevent penetrant vapors from entering the pump.

7.3.2 MATERIALS AND SAMPLE PREPARATION

Polymethylmethacrylate (PMMA) (*Mw: 54,000)* was obtained from Scientific Polymer; polyhydroxystyrene (PHOST) (*Mw: 11,800)* was obtained from TriQuest Chemical Company and bis-trifluoromethyl carbinol substituted polynorbornene (i.e. hexafluoroalcohol-substituted polynorbornene or HFA-PNB) (*Mw: 13,400)* was obtained from Promerus Inc. Toluene (99%, Aldrich) was used as a casting solvent for PMMA and PGMEA (99%, Aldrich) was used as casting solvent for PHOST and HFA-PNB. Polymer resins were dissolved in the respective casting solvents to prepare a solution containing 5 – 15 wt% of solids. Solutions were filtered through a 0.45 μm Teflon filter and spin-coated onto QCM crystals using a CEE Model 100 CB spin coat and bake system to create films 400 – 1000 nm in thickness. A soft bake of 94 ^{o}C for 4 minutes was performed for PMMA and PHOST films, whereas HFA-PNB films were soft-baked for 4 minutes at 105 ^{o}C to remove residual casting solvent left in the film. The films were exposed to vacuum for at least 1 hr after being loaded into the QCM chamber which further ensured that little residual solvent remained in the films.

7.3.3 FILM THICKNESS MEASUREMENTS

Polymer film thicknesses were measured using spectroscopic ellipsometry (M-2000 ellipsometer, J.A. Woollam Co. Inc.). Ellipsometry data were collected over a wavelength range of 400 to 1000 nm at angles 65°, 70° and 75° (with respect to the normal to the substrate plane). Data were analyzed to determine the film thickness and refractive index using WVASE-32 software (J.A. Woollam Co.) by fitting the ellipsometry data using a film stack model composed of a Cauchy layer model for the polymer film and a semi-infinite gold film for the substrate.

7.3.4 SORPTION/DESORPTION MEASUREMENTS

Two crystals, one polymer coated and other blank, were loaded into the QCM chamber during each experiment. The blank crystal served as a reference and was used to record changes in frequency due to pressure fluctuations which result from pressure increase/decrease inside the QCM chamber during sorption/desorption experiments. After loading the samples, both reservoir and QCM chambers were evacuated to a base pressure of 10 mTorr and heated to the desired temperature for sorption experiments. All flow lines were also heated to the desired temperature to eliminate the possibility of vapor condensation/cooling. After the crystal frequency stabilized, valves B and C were closed and the reservoir was filled to a desired pressure with penetrant vapor. Vapors were allowed to equilibrate to the chamber temperature for at least 10 minutes and then valve C was opened. The reservoir volume is approximately 24 times the volume of

QCM chamber and thus the pressure in the smaller chamber stabilized quickly to 96% of the initial reservoir pressure due to pressure differential driven flow. Also, valve C is a solenoid operated valve with response time less than 100 ms. This configuration and operation allowed a change in the vapor concentration inside the QCM chamber that approximated a step function. The sequence during penetrant desorption was: (1) close valve C, (2) evacuate reservoir and all the flow lines to base pressure, and (3) open valve C. This operation quickly dropped the pressure inside the QCM chamber to initiate desorption of penetrant from the polymer film. The M_t/M_∞ value for a given penetrant polymer system was obtained by following expression,

$$\frac{M_t}{M_\infty} = \frac{f_t - f_{t=0}}{f_\infty - f_{t=0}} \tag{7.6}$$

where f_t = frequency at time t

f_∞ = stabilized frequency after sorption/desorption

$f_{t=0}$ = frequency at the start of sorption/desorption

and equilibrium mass uptake was determined from the following expression

$$\frac{M_\infty}{M_{Polymer}} = \frac{f_\infty - f_{t=0}}{f_{uncoated} - f_{coated}} \tag{7.7}$$

where $f_{uncoated}$ = frequency of crystal without polymer coating

f_{coated} = frequency of crystal after polymer film coating

7.4 WATER SORPTION STUDIES

Water sorption studies were conducted on three different polymers: PMMA, PHOST and HFA-PNB. DI water was used as the penetrant and was maintained at room temperature (22-23 ^{o}C). Transport properties of water through PMMA[5-9] have been studied extensively; however; limited literature is available for PHOST and HFA-PNB[4, 10, 11]. One of the objectives of our study was to estimate equilibrium water uptake by these polymers at elevated temperatures. Figure 7-3 presents Van't Hoff plots for PMMA, PHOST and HFA-PNB in the temperature range of 295-398 K, where ϕ is percent equilibrium mass uptake of water by polymer. The data presented are for sorption when the polymer films were exposed to a water vapor pressure of 20 Torr.

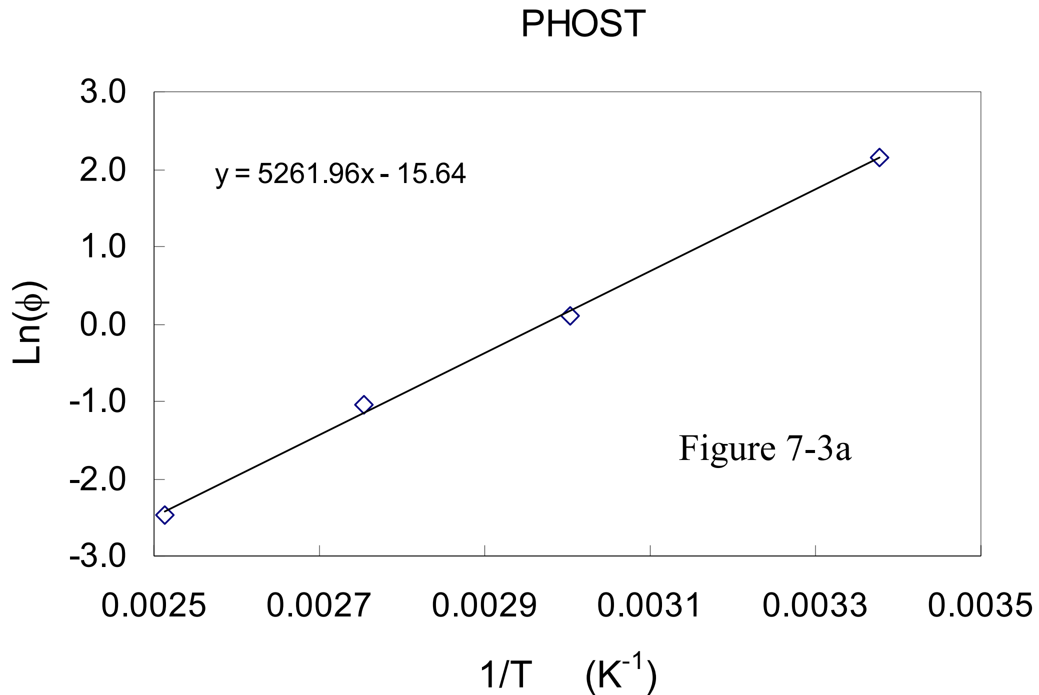

Figure 7-3a

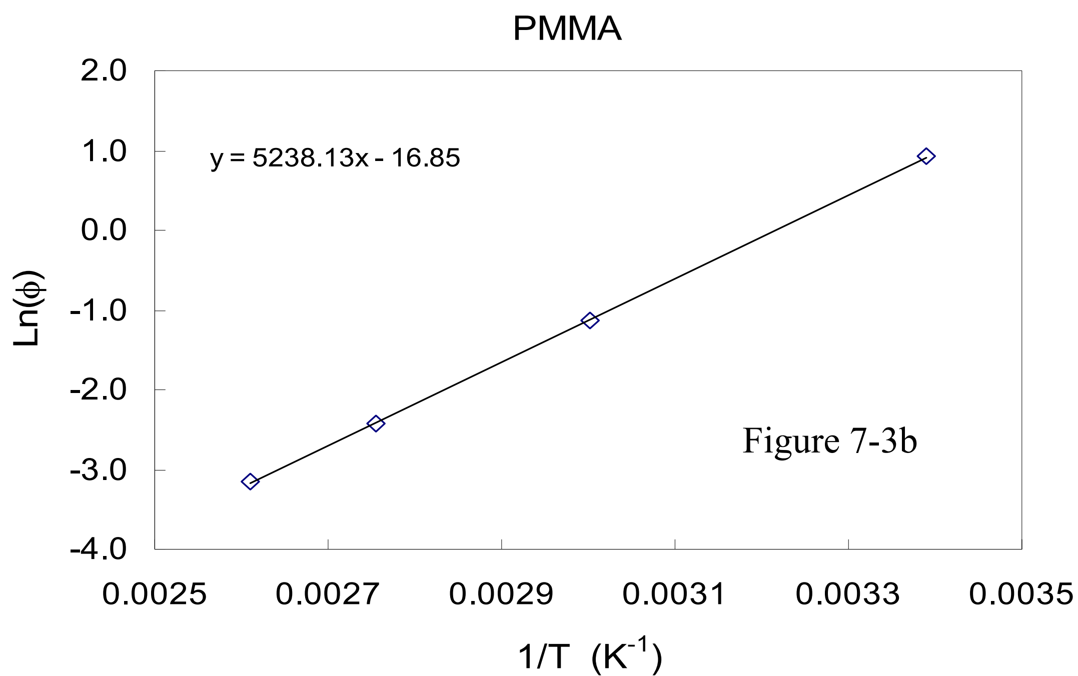

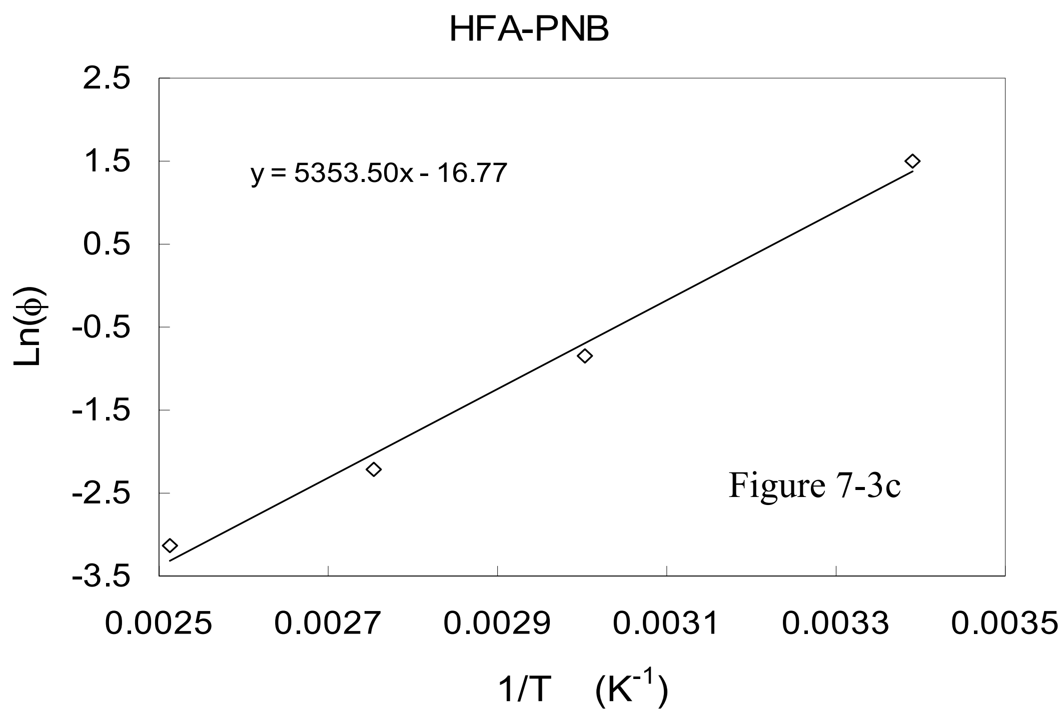

Figure 7-3: Van't Hoff plots for water sorption in PHOST (7-3a), PMMA (7-3b) and HFA-PNB(7-3c) films

Figure 7-3 indicates that at a fixed pressure, the equilibrium sorption uptake decreased monotonically with an increase in temperature; all polymers displayed an Arrhenius type behavior for water sorption. The slopes of lines in Figure 7 can be used to estimate the heat of sorption of water in these polymers and the calculated values are listed in table 7-1.

Table 7-1: Estimated heat of sorption of water in PHOST, HFA-PNB and PMMA

Polymer	***Heat of sorption (-ΔHs), kJ/mol***
PHOST	43.75
HFA-PNB	44.47
PMMA	43.55

Interestingly, despite very different molecular structures and equilibrium uptake, the three polymers showed very similar heats of sorption which are essentially the same as the heat of condensation of water (-43.5 kJ/mol), suggesting a negligible heat of mixing of water in these polymers. The equilibrium solubilities at different temperatures were also compared after normalizing the activity (pressure) by saturation vapor pressure (P_{sat}) at the corresponding temperatures. Values of water solubility at different temperatures collapsed on a single curve, which also confirmed a negligible heat of mixing of water in these polymers[12].

Unfortunately, direct measurement of equilibrium moisture uptake at 433 K (160 ^oC) could not be performed because of very low mass uptake at that temperature which resulted in <1 Hz frequency change upon exposure to 20 Torr of water vapor. The observed change in frequency of the blank crystal due to a change in pressure was also of the same order, making it difficult to acquire reliable data. However, the mass uptake at 160 ^oC can be estimated by extrapolating the Van't Hoff plots presented in figure 7-2. It should be noted that the glass transition temperature of PMMA and PHOST is ~115-120 ^oC and ~105-110 ^oC respectively; as a result, they are in a rubbery phase at 160 ^oC. Heat of sorption is generally reduced when a polymer is heated beyond its Tg; thus, the estimated value of equilibrium uptake could differ from the actual value[13]. Nevertheless, estimations can be obtained from the data collected; these are shown in table 7-2.

Table 7-2: Estimated solubility of water in PHOST, HFA-PNB and PMMA under different conditions

Polymer	**ϕ T= 295 K, P = 20 Torr**	**ϕ T= 433 K, P = 20 Torr**	**ϕ T= 433 K, P = 0.22 Torr**	**Mol H_2O/mol monomer unit T =433 K, P = 0.22 Torr**
PHOST	8.52	0.029	0.00032	2.13×10^{-5}
HFA-PNB	4.52	0.011	0.00012	1.84×10^{-5}
PMMA	2.51	0.008	0.000086	4.76×10^{-6}

In addition, the actual pressure increase during the water exposure step in our ALD experiments was measured to be only 0.21-0.22 Torr. Thus, assuming that Henry's law is applicable under these conditions, the values of mass uptake have been linearly scaled to

an exposure pressure of 0.22 Torr. The last column in table 7-2 provides the estimated mol of water uptake at saturation per mol of monomer unit in the polymer chain. It is evident that all the polymers investigated in this study demonstrated very low water uptake under actual ALD conditions. Furthermore, the reported data represent the equilibrium absorbed amount; and hence the remnant water after the purge is expected to be much lower. All the polymers investigated in this study have one active site per monomer unit (although of varying reactivity and accessibility). Hence, the data presented in Table 7-2 clearly indicate that the increase in the number of active sites upon water sorption is minimal, thus most of the observed nucleation on these polymer films during ALD results primarily from active sites present in the polymer backbone. These results demonstrate that water sorption in masking layers is not critical and does not pose a significant limitation in the successful application of polymer-based masking approaches for ASALD processes. However, it is important to point out that this observation not consistent with our observations discussed in chapter 4 where a reduction in nucleation on HFA-PNB was observed when the purge time after a water pulse was increased from 1 minute to 2 minutes.

7.5 TITANIUM ISOPROPOXIDE AND TITANIUM TETRACHLORIDE SORPTION STUDIES

The next set of experiments involved the estimation of diffusion coefficients of titanium isopropoxide and $TiCl_4$ through PMMA. Titanium isopropoxide sorption studies were conducted at an exposure pressure of 3.7-3.8 Torr whereas $TiCl_4$ sorption was conducted at 9.8-10 Torr. Titanium isopropoxide was heated to ~85 ^{o}C to generate

sufficient vapor pressure, while $TiCl_4$ was maintained at room temperature (~ 22-23 ^oC). Figure 7-4 is a representative sorption curve (fractional mass uptake versus square root of time) obtained at 433 K (160 ^oC). The diffusion coefficient has been estimated from the slope of the first half of the sorption curve using equation 7.8 and the fickian curve is then plotted using equations 7.4.

$$\frac{\left(\frac{M_t}{M_\infty}\right)_{t_1} - \left(\frac{M_t}{M_\infty}\right)_{t_2}}{\sqrt{t_1} - \sqrt{t_2}} = \frac{2}{l}\left(\frac{D}{\pi}\right)^{\frac{1}{2}} \tag{7.8}$$

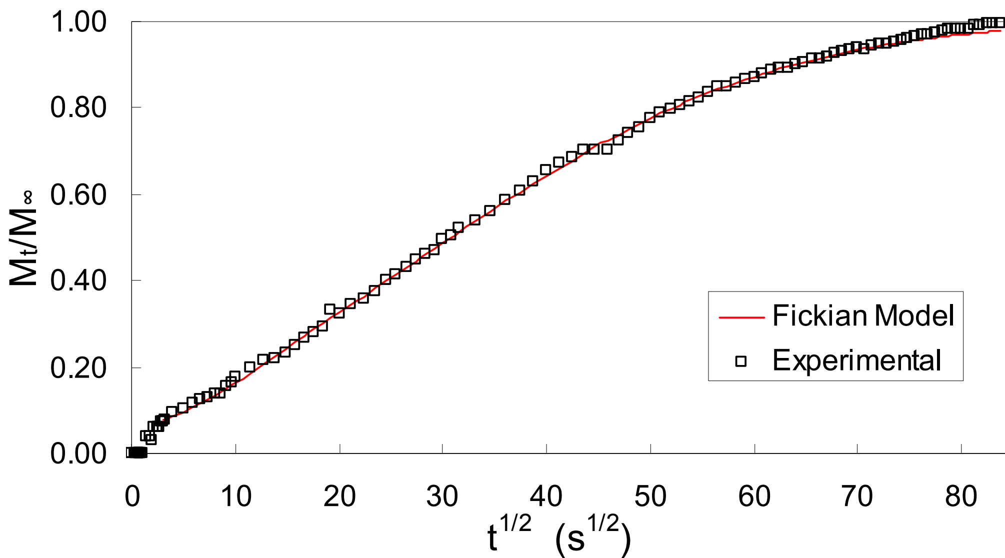

Figure 7-4: Sorption kinetics for titanium isopropoxide in PMMA at 160 ^oC. P = 3.8 Torr, film thickness = 805 nm

Sorption experiments were also conducted at temperatures of 125 ^oC, 135 ^oC and 145 ^oC in order to estimate mass uptake and the diffusion coefficient of titanium isopropoxide as a function of temperature; such information is valuable for further experimental

design. The diffusion coefficient and percent equilibrium mass uptake at these temperatures are presented in figures 7-5 and 7-6 respectively.

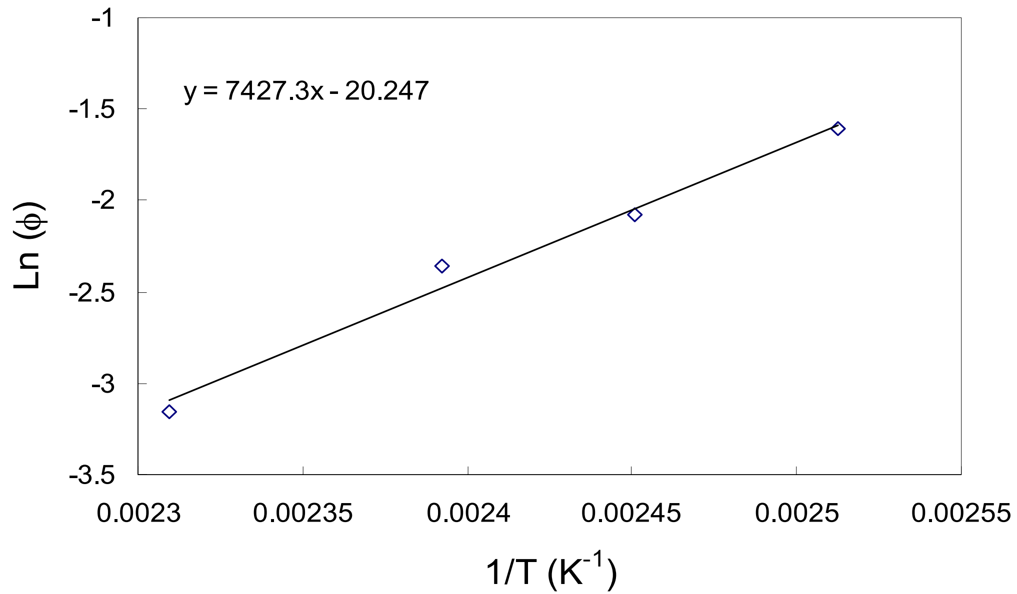

Figure 7-5: Van't Hoff plot for titanium isopropoxide sorption in PMMA

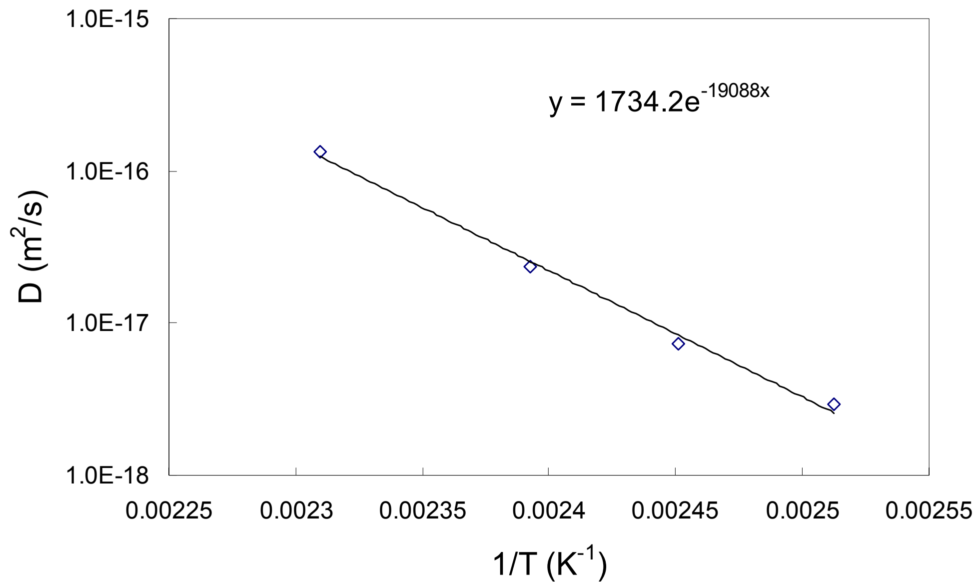

Figure 7-6: Diffusion coefficient of titanium isopropoxide in PMMA at different temperatures

Titanium isopropoxide follows Fickian kinetics of sorption into PMMA in the temperature range 125 ^{o}C – 160 ^{o}C. The equilibrium mass uptake at 160 ^{o}C was 0.043 wt % of the polymer and the diffusion coefficient was estimated to be 1.35×10^{-16} m^2/s. However an uptake of 0.043 wt % is observed when the polymer films were exposed to a vapor pressure of 3.8 Torr. In our experiment the pressure pulse observed during isopropoxide exposure for 2 s was ~ 0.03 Torr. Thus, very similar to water sorption case, actual uptake (at saturation) of isopropoxide during our ALD experiment is estimated to be 0.00034 weight % of the polymer.

Sorption experiments were also performed for $TiCl_4$. $TiCl_4$ exhibited significantly higher uptake in PMMA than did titanium isopropoxide at all the temperatures. In addition, the equilibrium uptake of $TiCl_4$ in PMMA increases with temperature. The mass uptake value (obtained from sorption experiment at 9.5 Torr) increased from ~1.1 wt% to ~7.4 wt% as the temperature increased from 125 ^{o}C to 160 ^{o}C, suggesting that the overall uptake process is endothermic. As expected, $TiCl_4$ reacted with PMMA as indicated by a partial desorption of mass originally absorbed during the sorption step. Complexation of $TiCl_4$ with carbonyl groups in PMMA added a bulky pendant group to the polymer chain. Furthermore, Ti is a six coordination site and thus cross-linking of the polymer chains could occur if the same $TiCl_4$ molecule reacts with C=O sites from two different chains. This complexation of $TiCl_4$ with PMMA reduces the mobility of polymer chains resulting in a reduction in diffusion coefficient as $TiCl_4$ is absorbed into the polymer film. This effect is evident from significant deviation of sorption curve (at 1.4 Torr) from Fickian kinetics as shown in figure 7-7.

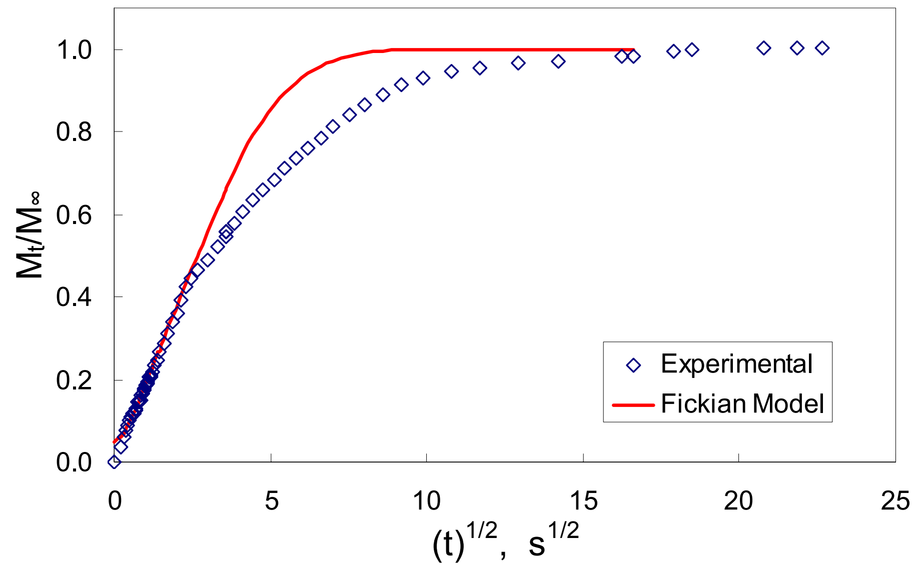

Figure 7-7: Sorption kinetics of $TiCl_4$ in PMMA at 160 °C. P = 1.4 Torr, Film thickness: 748 nm

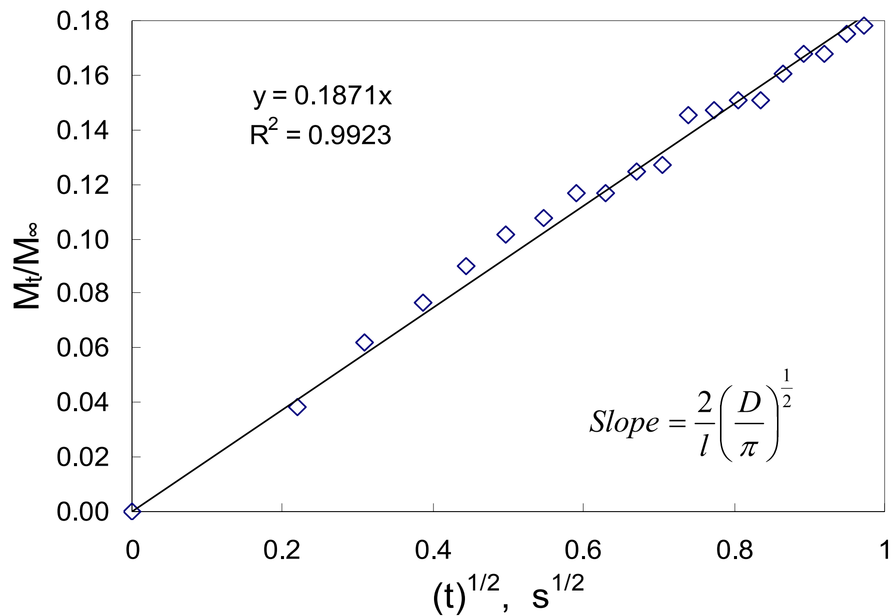

Figure 7-8: Estimation of diffusion coefficient of $TiCl_4$ in PMMA at 160 °C using the initial portion of the sorption curve

During ALD experiments, PMMA is exposed to very low concentrations of $TiCl_4$ (pressure pulse of ~0.09-0.1 Torr) and hence sorption kinetics was also acquired at exposure pressure of 1.40 Torr (sorption kinetics present in figure 7-7 and 7-8) in order to estimate the diffusion coefficient at condition which would represent actual ALD conditions more closely. Moreover since $TiCl_4$ reacts PMMA and changes its transport properties, the diffusion coefficient of $TiCl_4$ in unmodified PMMA is estimated by the slope of the curve where $M_t/M_\infty \rightarrow 0$ as shown in figure 7-8. The estimated diffusion coefficient is 1.53×10^{-14} m^2/s. It should be noted that since the diffusion coefficient of $TiCl_4$ is strongly concentration dependent (decreases with an increase in concentration) the estimated diffusion coefficient based on initial time data from sorption at 1.4 Torr could still be lower than the actual diffusivity of $TiCl_4$ molecules exposed to the lower activity (i.e. lower vapor pressure) experienced during ALD experiments. The reason is that, although the overall penetrant uptake in the film at the start of the sorption is low, the top surface reaches instantaneous saturation. Based on the reaction time scale, the mobility of polymer chains in the film regime near the top of the layer will decrease, and result in a reduction in diffusion coefficient of the incoming penetrant or the penetrant present there. This will limit further transport of penetrant into the polymer film (which only occurs from the top layer) and yield slower uptake and thus a lower diffusion coefficient. We have estimated the diffusion coefficient from short-time data (below 1 s of sorption) and further the diffusivity calculated based on sorption kinetics obtained at 9.5 Torr was 1.24×10^{-14} m^2/s which is only 20% smaller than the value obtained at 1.4 Torr. Thus, it can be concluded that the estimated diffusion coefficient based on short time data (from sorption kinetics at 1.4 Torr) is not significantly different from the value

expected at lower activity. In addition, it was also observed that the equilibrium mass uptake at 1.4 Torr did not follow Henry's law (did not scale linearly with pressure) when compared to equilibrium uptake at 9.5 Torr. The equilibrium uptake at 1.4 Torr was 1.9 wt % which is almost 70 % higher than 1.1 wt%, the expected value based on Henry's law. This deviation for Henry's law could be a result of changes in polymer surface due to reaction with $TiCl_4$.

The measurements suggest that the diffusion coefficient of $TiCl_4$ in PMMA is approximately 2 orders of magnitude higher than that for the isopropoxide precursor. These results indicate that the ratio of diffusion lengths, which scales with square root of D, should be approximately ten. Previously (Chapter 4) we observed that ~200 nm thick films were required in order to prevent nucleation at the polymer-substrate interface during $TiCl_4$-H_2O ALD. From a simple calculation of the ratio of diffusion lengths, nucleation at the interface should be observed at ~20 nm film thickness for the isopropoxide precursor system. However, the isopropoxide precursor displays much lower solubility in PMMA than does $TiCl_4$, which reduces the overall permeability and the concentration that will be observed at the polymer substrate interface. Furthermore, with ultra thin films (25-30 nm), a greater fraction of polymer chains are confined near the substrate than will be the case with a thicker film. This confinement reduces the polymer chain mobility and is manifested into a lower diffusion coefficient in this thickness regime[10, 14]. These two phenomena partially explain why no nucleation was observed for film thickness down to 10 nm in titanium isopropoxide-H_2O ALD. In addition, the absolute value of average diffusion length for both precursors can be estimated by evaluating $(D.t)^{1/2}$. For an exposure time of 2 seconds, this value is 175 nm

and 16 nm for $TiCl_4$ and titanium isopropoxide respectively. The estimated values are reasonably consistent with the required masking layer thickness for both systems.

In addition to the importance of controlling the minimum required thickness of a masking layer for successful ASALD processes, the precursor diffusion coefficient can be important from another perspective. It is beneficial to use a precursor with a low diffusion coefficient because this permits use of a thinner masking layer. However, lower diffusion coefficients also imply that the precursor will desorb at a lower rate during the purge step. If insufficient purge duration is used, the precursor will slowly build up inside the polymer film during subsequent cycles. To assess this possibility, concentration profiles of precursor inside the polymer films were evaluated by solving the 1-D diffusion equation and using a diffusion coefficient of 1.35×10^{-16} m^2/s and exposure and purge times of 2s and 60s, respectively. After only 150 cycles, a concentration of up to 3 % of the equilibrium value could accumulate inside the polymer film. Under the operating conditions of our ALD experiment, titanium isopropoxide exhibits very low equilibrium uptake in PMMA. A concentration of 3% of the equilibrium uptake translates to an absolute value of 1.02×10^{-7} wt. fraction of titanium isopropoxide in the polymer film. Therefore, since the isopropoxide precursor does not react with the polymer and equilibrium uptake of water is low, undetectable nucleation was observed in our experiments. However, for a polymer-precursor system that exhibits a higher level of precursor solubility in the polymer film, a low diffusion coefficient of the precursor molecule can be undesirable since this would require a longer duration purge step to ensure adequate removal of penetrant from the film. This implies that in

addition to the diffusion coefficient, solubility of the precursor in the polymer film is also an important parameter in designing a successful ASALD process.

7.6 CONCLUSIONS

Sorption studies of $TiCl_4$, titanium isopropoxide and water in polymer films using a quartz crystal microbalance technique were performed to estimate diffusion coefficients and equilibrium uptake of the precursors in several polymer films. Under the operating conditions of our ALD experiments, the solubility of water in the polymer films investigated are extremely low ($\sim 10^{-4} - 10^{-5}$ wt% of polymer). The estimated uptake indicates that sorption of water in polymer masking layer is not a significant issue and hence does not pose limitations on the implementation of polymer-based masking approaches for ASALD. In fact, the sorption and transport properties of metal precursors played a greater role in determining the specific parameters needed for selective deposition processes. The estimation of diffusion coefficient data for titanium isopropoxide and titanium tetrachloride in PMMA helped explain the differences observed previously in the required masking layer thicknesses for successful ASALD. Transport studies have indicated that although the use of precursors with lower diffusion coefficients in the polymer films allows the use of thinner masking layers for successful process, such situations also demand longer purge times for complete removal of precursor sorbed during the exposure step. As a result, optimization of polymer/precursor combinations will be needed during process development.

7.7 REFERENCES

1. Crank, J., *The Mathematics of Diffusion*. Second ed.; Oxford University Press: Oxford, 1975; p 414

2. Sauerbrey, G., The use of quartz oscillators for weighing thin layers and for microweighing. *Zeitschrift fuer Physik* 1959, 155, 206-22.

3. Lu, C.; Czanderna, A. W.; Editors, *Methods and Phenomena, Vol. 7: Applications of Piezoelectric Quartz Crystal Microbalances*. 1984; p 393 pp.

4. Berger, C. M.; Henderson, C. L., The effect of humidity on water sorption in photoresist polymer thin films. *Polymer* 2003, 44, (7), 2101-2108.

5. Barrie, J. A.; Machin, D., Diffusion and association of water in some poly(alkyl methacrylates). 2. Transient state diffusion. *Transactions of the Faraday Society* 1971, 67, (Pt. 10), 2970-8.

6. Bueche, F., Diffusion of Water in Polymethyl Methacrylate. *Journal of Polymer Science* 1954, 14, (76), 414-416.

7. Roussis, P. P., Diffusion of Water-Vapor in Poly(Methyl Methacrylate. *Journal of Membrane Science* 1983, 15, (2), 141-155.

8. Smith, L. S. A.; Schmitz, V., The Effect of Water on the Glass-Transition Temperature of Poly(Methyl Methacrylate). *Polymer* 1988, 29, (10), 1871-1878.

9. Barrie, J. A.; Machin, D., Diffusion and Association of Water in Some Polyalkylmethacrylates .1. Equilibrium Sorption and Steady State Permeation. *Transactions of the Faraday Society* 1971, 67, (577), 244-&.

10. Singh, L. Effect of nanoscale confinement on the physical properties of polymer thin films. PhD Dissertation, Georgia Institute of Technology, 2004.

11. Vogt, B. D.; Soles, C. L.; Jones, R. L.; Wang, C. Y.; Lin, E. K.; Wu, W. L.; Satija, S. K.; Goldfarb, D. L.; Angelopoulos, M., Interfacial effects on moisture absorption in thin polymer films. *Langmuir* 2004, 20, (13), 5285-5290.

12. Stannett, V.; Haider, M.; Koros, W. J.; Hopfenberg, H. B., Sorption and Transport of Water-Vapor in Glassy Poly(Acrylonitrile). *Polymer Engineering and Science* 1980, 20, (4), 300-304.

13. Koros, W. J.; Hellums, M. W., Transport properties. In *Encycl. Polym. Sci. Eng.*, Wiley: New York, 1990; Vol. Suppl. Vol., pp 724-802.

14. Singh, L.; Ludovice, P. J.; Henderson, C. L., Effect of nanoscale confinement on the diffusion behavior of photoresist polymer thin films. *Proceedings of SPIE-The International Society for Optical Engineering* 2004, 5376, (Pt. 1, Advances in Resist Technology and Processing XXI), 369-378.

CHAPTER 8

SUMMARY AND RECOMMENDATIONS FOR FUTURE WORK

8.1 SUMMARY

Atomic layer deposition (ALD) has become an important technique for depositing high quality ultra-thin films [1, 2]. During ALD, film growth depends critically on the chemistry of the surface upon which each deposition cycle reaction occurs. Therefore, it should be possible to chemically tailor a surface to achieve area selective deposition. The critical challenge in achieving area selective ALD (ASALD) is devising materials and methods for modifying selected regions of a substrate surface to prevent ALD reactions from occurring and thus preventing film growth. This work investigated a novel masking approach to achieve effective ASALD. Various parameters which are important in establishing a successful process were identified and fundamental limitations investigated. In addition, the ASALD technique has been employed to develop a novel top surface imaging process.

An ALD reactor was designed and fabricated as a part of this thesis; TiO_2 was selected as the material for investigation. Specifically, $TiCl_4$ and DI water were initially chosen as precursors to investigate the area selective ALD of titanium dioxide films. $TiCl_4$ has a very high reactivity towards hydroxyl bonds and thus the $TiCl_4$-H_2O ALD system is a highly sensitive system to evaluate the success of any masking methodology. Initial experiments focused on optimizing the operating conditions of the reactor to deposit high quality films in an ALD mode. It was established that under the identified

operating conditions, the film was deposited in a self saturated growth mode. The resulting films were smooth (RMS roughness 0.18 nm – 0.40 nm) and free of contaminants. The films demonstrated good electrical properties with high dielectric constant (~100).

Self assembled monolayers (SAM) of octadecyltrichlorosilane have been previously investigated to perform selective ALD of HfO2, ZrO_2 and TiO_2. One segment of our initial research investigated similar techniques; results indicated that a defect free well packed monolayer is critical for successfully blocking all nucleation sites. Since it was extremely challenging to obtain such defect free monolayers, the reactive titanium precursor eventually encountered an unprotected reactive silanol site on the silicon surface and reacted to initiate the ALD reaction sequence in that area. In principle, it may be possible to obtain well-packed SAM films by invoking long deposition times for SAM formation. However, such processing challenges, combined with the fact that patterning of SAMs using traditional lithography techniques is not a well-established practice, pose serious limitations on the successful application of SAMs as masking layers for ASALD.

In order to overcome the limitations of SAM-based masking approaches, a new masking approach based on polymer thin films was proposed in this thesis. Unlike SAMs, polymers can be quickly and easily spin coated to obtain defect free thin films. Furthermore, a significant amount of research has been invested in developing a variety of different polymeric materials and processes for the high resolution patterning of polymer films. Thus, if a polymer or class of polymers is identified that can prevent the nucleation and growth of a material on its surface during ALD and these polymers can be patterned lithographically, such a “photoresist-like” process may offer an improved

masking alternative ASALD relative to SAM-based approaches. After ALD is completed, the polymer masking layer should be removable in the same way that resist films are stripped, thus obtaining a direct patterned structure of the desired ALD film.

A number of factors that must be considered in designing a successful ASALD process based on polymer films were identified. These include: reactivity of polymer with ALD precursor, diffusion of ALD precursors through polymer mask and remnant precursor content in the polymer film during ALD cycling. Investigations suggested that ALD nucleation can be successfully blocked on polymer films that do not contain oxygen in their backbone. Inclusion of oxygen led to low levels of nucleation; however, direct –OH sites in the polymer backbone led to increased nucleation. It was observed that remnant water in the polymer film does not pose a serious limitation and its effect can be minimized by using reasonable purge times (1-2 minutes). Metal precursor diffusion through the polymer mask was identified as a critical parameter in determining the minimum required masking layer thickness for a successful ASALD process. Specifically, 180-200 nm thick PMMA films were required to prevent the metal precursor from diffusing through the masking layer and reacting with silanol groups at the polymer-substrate interface. It was encouraging to observe that PMMA demonstrated low reactivity towards $TiCl_4$ and direct pattern deposition on lithographically defined PMMA demonstrated as a proof of concept for the polymer based masking approach for selective ALD.

However, several limitations of this ASALD process were identified which were due to a combination of the intrinsic reactivity of PMMA with $TiCl_4$ and the diffusion of $TiCl_4$ through the PMMA film. For example, a minimum masking layer thickness of

approximately 180-200 nm was required to prevent undesired titania formation beneath the PMMA polymer mask. In addition, the PMMA film was difficult to remove using simple solvent washes after ALD deposition, and this difficulty was attributed to reaction of the $TiCl_4$ precursor with the PMMA film. Intrinsic reactivity of $TiCl_4$ with the C=O group in PMMA results from complexation of the electron deficient Ti center with the electron rich O atom in the carbonyl group. Hence, titanium isopropoxide (TiIP) was investigated as an alternate metal precursor since isopropoxide is not as electronegative as Cl and thus should not easily cause coordination or reaction of Ti with the carbonyl groups in PMMA. Furthermore, the isopropoxide ligand is also significantly larger than the Cl substituents in $TiCl_4$, and thus access of TiIP to C=O groups in PMMA should be more sterically hindered. As expected, no Ti was detected on PMMA samples exposed only to Ti-isopropoxide pulses. Depositions were conducted on different PMMA samples with successive increases in the number of ALD cycles. XPS scans of the PMMA samples showed that no Ti was detectable on the polymer surface after 500 ALD cycles (2s – 25s – 2s – 30s). During the same 500 cycles, a 35nm thick TiO_2 film was deposited on a bare Si substrate. These observations suggested that extreme hydrophobicity (WCA > 109°) of masking layers is not a prerequisite for successfully preventing ALD nucleation as has been previously suggested for SAM surfaces. These results also demonstrated an effective polymer masking based ASALD of titanium dioxide. In addition, the larger size of TiIP slowed its diffusion through the masking layer so that the PMMA film thickness could be reduced to 10 nm without the formation of titania beneath the polymer film.

In order to measure solubilities and diffusion coefficients of different ALD precursors in the polymer masking layer, an experimental apparatus based on the quartz crystal microbalance technique was designed and fabricated. Water showed extremely low solubility in polymer films under our ALD processing conditions; hence it was concluded that sorption of water into the polymer films is not a critical limitation for selective ALD processes. In fact, the sorption and transport properties of metal precursors played a greater role in determining the specific parameters needed for selective deposition processes. The estimation of diffusion coefficient data for titanium isopropoxide and titanium tetrachloride in PMMA helped explain the differences observed previously in the required masking layer thicknesses for successful ASALD. Transport studies have indicated that although the use of precursors with lower diffusion coefficients in the polymer films allows the use of thinner masking layers for successful processes, such situations also demand longer purge times for complete removal of precursors sorbed during the exposure step. As a result, optimization of polymer/precursor combinations will be required during process development.

The experiments discussed above demonstrated that nucleation of titania films produced by ALD can be successfully blocked on polymer materials that do not contain reactive OH groups in their backbone. In addition, during ALD on polymers containing –OH groups in their backbone, a conformal and defect free film can be formed directly on the polymer surface. Such conformal titania layers can serve as effective etch barriers when exposed to oxygen plasmas. This characteristic was utilized to develop a novel ASALD-based top surface imaging (TSI) technique. The ASALD-TSI process has demonstrated sharp contrast (etch barrier deposition vs exposure dose) and therefore

offers the potential to overcome many of the challenges experienced with conventional TSI schemes.

8.2 RECOMMENDATIONS FOR FUTURE WORK

In this work we developed a polymer based masking approach to perform direct pattern deposition of titanium dioxide on Si substrates. It would be interesting to investigate if similar methodology could be implemented for ASALD of other metal oxides such as HfO_2, ZrO_2 etc. These materials are of significant interest due to their potential application as high-k gate dielectrics. $Hf[N(CH_3)_2]_4$-H_2O and $Zr[C(CH_3)_3]_4$-H_2O can be chosen as precursors for initial studies. Based on our observation with TiIP-H_2O-PMMA ASALD, such precursor combinations should not pose challenges due to reactivity with PMMA. However, solubility and diffusion coefficients of metal precursor will play a significant role in establishing the specific process parameters needed for successful processes.

Polymer masking based ASALD could also be extended to metal films. Platinum is a potential capacitor electrode material for dynamic random access memories (DRAMs)[3] and is also being considered as a gate metal for future metal-oxide-semiconductor field effect transistors (MOSFETs) because of its high work function.[4] As a result, ASALD of Pt may offer significant advantages since this approach should obviate the need for metal patterning. ALD of Pt using $CH_3C_5H_4Pt(CH_3)_3$-O_2 has already been demonstrated[3, 5, 6] and ASALD of Pt using the same PMMA as masking layer can be attempted. Success of these studies would allow the fabrication of a complete gate stack ((Si-HfO_2/ZrO_2-Pt)

using a single masking step and two different ASALD processes. One challenge that might be encountered is the fact that ALD of Pt using the precursors mentioned above have only been demonstrated to a minimum temperature of 200 ^{o}C.[5] Continuous heating of PMMA at such high temperatures could lead to hard baking and thus property modification of the polymer and may pose problems during removal of the masking layer after the ASALD process. Initial experiments should thus investigate low temperature ALD of Pt and electrical properties of the films produced.

An ASALD based TSI method was developed in this thesis. Preliminary characterization of the process indicated sharp contrast (amount of material deposited vs exposure dose). A sufficient thickness of TiO_2 (etch barrier) can be deposited in the regions of low exposure dose by subjecting the surface to a higher number of ALD cycles, which represents an improved capability in comparison to conventional TSI methods. In addition, it was observed that regions of low exposure dose required a higher number of ALD cycles to produce a conformal TiO_2 layer. The basic mechanism of ALD indicates that ALD nucleation occurs on active sites on the surface and depending upon concentration of active site, the nucleated islands will merge after a different number of cycles. The islands will merge sooner in case of surfaces with a higher density of active sites than for a surface with a relatively low density of active sites. This phenomenon is illustrated in figure 8-1 where the evolution of film growth on two different surfaces with an increasing number of ALD cycles is presented. The low exposure dose region corresponds to a low density of active sites (surface A) and high dose region corresponds to high density of active sites (surface B). Please note that the

schematic shown below for two different surfaces do not represent the same number of ALD cycles.

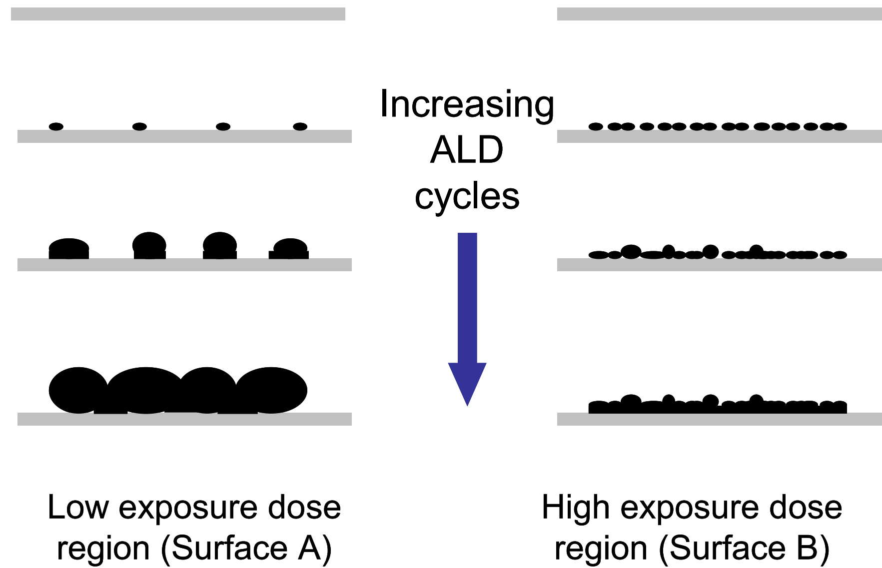

Figure 8-1: ALD growth of film on two different surfaces

On surface A, the nucleated islands will be spaced farther apart than those on surface B owing to a different density of nucleation sites. The growth rate on surface B is smaller and since the nucleated islands are farther apart, they will require a higher number of ALD cycles prior to merging. In addition, the size of the islands on surface A will be larger at the point of merger than will those on surface B. A subsequent ALD cycle would result in continuous film deposition on both the surfaces. As illustrated in figure 8-1, this could translate into an enhanced surface roughness for surface A than for surface B. Whether or not the roughness on surface B will diminish during subsequent ALD cycles or will maintain its original state is unclear. If the roughness is not reduced, the line edge roughness (LER) may increase in the low exposure dose region. Detailed

investigations of this issue will generate insight into the fundamental advantages/limitations of the ASALD-TSI process. One approach to investigate the LER issue would be to deposit TiO_2 (for a different number of ALD cycles) on surfaces exposed to different doses and then subject the structures to a brief plasma etch to remove the polymer film where no deposition had occurred. The resulting surface could then be probed with atomic force microscopy to evaluate roughness and phase difference on the surface. These experiments will verify the growth mechanism at surfaces as a function of exposure dose. Topography/phase image of the scanned surface may also offer insight into approaches to control LER.

The sorption of $TiCl_4$ into PMMA represents a very interesting polymer-penetrant system. Despite the fact that $TiCl_4$ reacts with PMMA, the sorption kinetics shows saturation, which is not common for reactive sorption. This indicates that $TiCl_4$ molecules coordinated/reacted with PMMA contribute to the solubility of the absorbed $TiCl_4$ molecule. This observation suggests that $TiCl_4$ co-ordinates with the C=O bond (in PMMA) in a manner similar to that in which water hydrogen bonds with a variety of hydrophilic polymers. However, unlike hydrogen bonded water, $TiCl_4$ forms a permanent bond with the polymer. Further investigation into sorption kinetics of such system could be of fundamental interest to polymer science and membranes community.

8.3 REFERENCES

1. Ritala, M.; Leskela, M., *Atomic layer deposition*. Academic Press: San Diego, 2002; Vol. 1, p 103-159.

2. Leskela, M.; Ritala, M., Atomic layer deposition chemistry: recent developments and future challenges. *Angewandte Chemie, International Edition* 2003, 42, (45), 5548-5554.

3. Aaltonen, T.; Ritala, M.; Sajavaara, T.; Keinonen, J.; Leskelae, M., Atomic Layer Deposition of Platinum Thin Films. *Chemistry of Materials* 2003, 15, (9), 1924-1928.

4. Wilk, G. D.; Wallace, R. M.; Anthony, J. M., High-kappa gate dielectrics: Current status and materials properties considerations. *Journal of Applied Physics* 2001, 89, (10), 5243-5275.

5. Aaltonen, T.; Ritala, M.; Tung, Y. L.; Chi, Y.; Arstila, K.; Meinander, K.; Leskela, M., Atomic layer deposition of noble metals: Exploration of the low limit of the deposition temperature. *Journal of Materials Research* 2004, 19, (11), 3353-3358.

6. Aaltonen, T.; Rahtu, A.; Ritala, M.; Leskela, M., Reaction Mechanism Studies on Atomic Layer Deposition of Ruthenium and Platinum. *Electrochemical and Solid-State Letters* 2003, 6, (9), C130-C133.